DETERMINING FLOW FIELD SINGULARITIES FROM DRIFTER TRAJECTORIES

HALMAR HALIDE

DETERMINING FLOW FIELD SINGULARITIES FROM DRIFTER TRAJECTORIES

by

© **Halmar Halide**

A Thesis submitted to the School of Graduate Studies
in partial fulfillment of the requirements
for the degree of Master of Science

Department of Physics
Memorial University of Newfoundland
February, 1992

St. John's Newfoundland

ISBN 0-315-73316-0

Abstract

This thesis is concerned with techniques for determining the properties of singularities in the flow field. Okubo and Ebbesmeyer (1976) and Molinari and Kirwan (1975) developed a regression technique that has become a standard for determining velocity gradients of the flow field. Kirwan (1988) has pointed out that this regression technique is fundamentally inadequate because it assumes a paradigm with the flow centre fixed to the centroid of the drifter cluster. Kirwan *et al.*, (1988) formulated a solution to this dilemma by inverting non-linear solutions obtained by Okubo (1970) for motion near a flow field singularity with specified differential kinematic properties (DKP). The DKP are horizontal divergence, vorticity, stretching and shearing deformation rate. We solve the non-linear equations of Kirwan *et al.*, (1988) to obtain DKP and the position and velocity of a flow field singularity from a single drifter trajectory. This solution (henceforth called the OK solution) is mathematically more concise than that presented in Kirwan *et al.*, (1988) and corrects previously undetected algebraic errors in the published literature. It has been successfully tested using artificially generated data. The method is fundamentally limited due to the requirement that DKP are

time invariant. It also has the undesirable feature that it requires fourth order time derivatives of data. A new method, the HS method, that uses regression without artificially setting the flow centre to the cluster centroid is presented. It has also been successfully tested by application to artificially generated data. The DKP are successfully recovered by the HS providing all drifters in the cluster are being moved by the same unique singularity in the flow field.

Applying all three methods to three neighbouring drifter tracks measured on Sable Island Bank clearly indicated the limitations of all three methods. The regression technique of Okubo and Ebbesmeyer (1976), the OE method, 'failed' because the flow centre was not at the cluster centroid position. The OK method gives ambiguous results in that it can not distinguish between solid body rotation about a point and a slab that oscillates. The lack of a single well defined flow centre for all three drifter trajectories was sufficient to ensure the HS method gave meaningless DKP that had large intermittent fluctuations. Nevertheless, given trajectories near a well-defined flow field singularity, we can be assured that both the HS and OK method can be used to obtain the position, velocity and DKP of the singularity. Depending upon the separation scales of the drifters, the HS method can be much less or more

sensitive to noise than the OK method.

Acknowledgements

I am greatly indebted to the following people who assisted me through this study.

1. Dr. B. G. Sanderson, my supervisor, outlined the basic idea of the HS method. Dr. Sanderson also introduced me to the usefulness of computer algebra. His guidance contributed a lot towards shaping my understanding of how to put a piece of evidence into a meaningful picture.

2. Dr. A. E. Hay, Dr. K. Lamb, Dr. J. Helbig, Dr. N. Rich and Dr. M. Morrow, provided some interpretations and constructive suggestions in order to make the thesis clearer and more informative.

3. Prof. Dr. A. D. Kirwan Jr. gave his critical review on the HS method and suggested future studies regarding this method and provided important references. Dr. R. J. Greatbatch helped provide a Eulerian perspective and helped interpret some of the results in terms of the conservation of potential vorticity.

4. Allan Goulding assisted me with the computing system, S. Kioroglou

helped me with some preliminary ideas on how to correct Kirwan's algebra. Cheng He helped me to prepare this thesis. Badal K. Pal provided me with low-pass filtering programs and other software. Timm J. Otterson and Craig Hamm introduced me to the MATLAB software. I thank Joe Craig for assistance in gathering and editing data.

5. The Government of Indonesia provided a generous scholarship and research allowance under the Higher Education Development Project funded by World Bank XXI. The World University Service of Canada managed this scholarship, the research allowance and provided guidance.

6. My family by their continuous encouragement when I get frustrated and bored.

Contents

List of Figures

List of Tables

Chapter 1

Introduction

The objective of this thesis is to analyse flow fields by studying drifter trajectories. A trajectory is a path of a current follower, an object that follows the water movements. We are especially interested in determining Differential Kinematic Properties (DKP) of the fluid flow in the vicinity of velocity singularities, the stationary points (relative to some spatially uniform translation) in the flow field. In two-dimensional flow, these properties can cause some fluid surface to be increased/decreased in area, rotated, stretched or sheared (Saucier, 1953; Molinari and Kirwan, 1975; Sanderson, 1984).

There are several reasons why we analyse drifter trajectories. The distribution of material, eg. biota, can be more directly related to Lagrangian

measurements of velocity than Eulerian measurements. Drifter trajectories can cover broad range of scales including large-scale flows and mesoscale eddies (Poulain and Niiler, 1989) with high spatial resolution. Spatial resolution of Lagrangian techniques is better than most Eulerian techniques with the possible exception of satellite observations. Spatial resolution of Lagrangian observations is adequate for comparison with eddy-resolving numerical models (Kirwan *et al.*, 1990).

The DKP are of interest for a variety of reasons. Flow field properties of drifter data, such as DKP, can be assimilated into eddy-resolving models for purposes of data interpolation/extrapolation and flow field prediction. DKP of the flow field provide a direct link to dynamical forces. For example, by using a group of drifters, Reed (1971) calculated divergence from changes in a cluster's area, and vorticity from changes in a cluster's orientation. This provided a link to dynamical processes in the Alaskan current. Sanderson (1987) inferred dynamics via a vorticity equation and analysis of iceberg trajectories. Bower (1989) examined the dynamics of large-amplitude meanders by estimating potential vorticity from the trajectories of RAFOS floats in the Gulf Stream. These floats follow an isopycnal surface of fluid. Padman and Niiler (1990) deployed ARGOS drifters, satellite-tracked drifting buoys,

in their attempt to investigate the dynamics of a cold-water jet. Finally, Okubo (1978) has shown that DKP can play an important role in determining the distribution of material in the ocean such as an accumulation of zooplankton in parallel rows at the ocean surface (Owen, 1966).

Okubo (1970) investigated the trajectories of particles due to singularity structures in the flow field with various DKP. He particularly looked at how flow field singularities affected dispersion of floatable particles due to turbulence. This work interpreted observations of reversal and suppression of the dispersion of floating objects in Lake Huron (Csanady, 1963) as being caused by convergent singularities called surface confluences.

Regression methods were then developed in order to obtain DKP from observations of drifter clusters. The basic method was developed by Molinari and Kirwan (1975) and Okubo and Ebbesmeyer (1976). Okubo *et al.*, (1976) extended the technique to calculate Lagrangian deformations and eddy diffusivities, kinematic variables that cause a horizontal spreading of the clusters, of the residual motion. Kirwan and Chang (1979) considered the effect of biasing due to sampling frequency. Sanderson *et al.*, (1988) showed how previous investigators had calculated the number of degrees of freedom incorrectly when they calculated eddy-diffusivities from residual motion caused

by small-scale turbulent eddies.

Kirwan (1988) pointed out bias problems with the regression model paradigm in the OE method of Okubo and Ebbesmeyer (1976). Let us consider a cluster of drifters embedded in a stationary anticyclonic eddy as shown in figure 1.1. Here, the initial and later positions of the drifters are denoted by the dashed and solid circles, respectively. l_1 and l_2 are the positions of the flow centre and a drifter with respect to the cluster's centroid. The bias problem in this particular case is due to the fact that the cluster's centroid does not coincide with the flow centre of the eddy. For a small-area cluster ($l_2 \ll l_1$), the OE model would show that the eddy moves with certain velocity that equals to the value of the DKP multiplied by l_1. This is not true since we are dealing with a non-moving eddy. Further, the estimated DKP using this model would also become biased. Enlarging the cluster area by increasing l_2 will not solve the problem because the cluster may encounter another bias factor produced by yet larger-scale shear across the flow. Kirwan (1988) demonstrated that the above regression techniques gave fundamentally unreliable estimates of the DKP of flow field singularities.

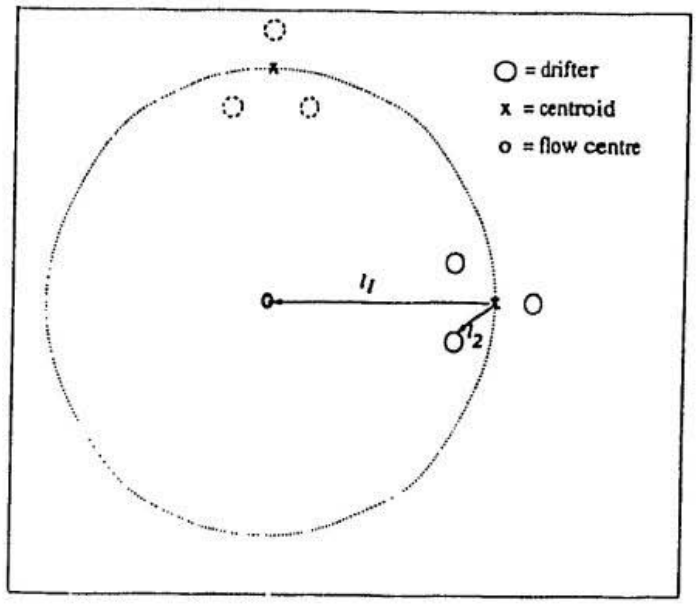

Figure 1.1: The displacement of a cluster of 3-drifters in a stationary anticyclonic eddy.

Kirwan *et al.*, (1984, 1988, 1990) found an alternative method for calculating DKP from drifter trajectories. They assumed that drifters were near a flow field singularity and then inverted the solutions of Okubo (1970) to obtain DKP from the drifter trajectory. This method (subsequently called the OK method) is an elegant way of obtaining flow field singularity properties from one drifter trajectory. However, previous tests, made by Sanderson and Goulding (personal communication) on simulated data, indicated that the solutions reported by Kirwan *et al.*, (1988) had errors. This is not surprising in view of the algebraic complexity of the inversion of the very non-linear

equations of Okubo (1970).

The present work finds and corrects algebraic errors in the solution of Kirwan *et al.*, (1988) and gives more concise expressions for the solutions. Having made these corrections, the OK method is tested by analysing generated data. By adding random motions we evaluate how OK estimates of differential kinematic properties of the flow field might be affected by measurement error. The OK method requires determination of high order time derivatives of the drifter trajectory. Differentiation of experimentally obtained drifter trajectories is an inherently noisy process. Thus considerable smoothing is required.

A new regression method is developed for calculating DKP from drifter clusters. This new regression technique does not suffer from the assumption that the centre of the flow field singularity is coincident with the cluster centroid. Instead it uses one of the assumptions of the OK method, viz. that the velocity of the flow centre is steady, to close the statistical analysis. We subsequently refer this new regression technique as the HS method. Then, we compare the OK, HS and OE methods in an analysis of computer generated and real oceanic data.

Having obtained the tools for determining the flow field parameters, we

want to consider the following question. Since an ocean may consist of eddies at all scales, do two drifters that are nearby measure the same flow field singularity? Our analysis will provide an interesting answer in the case of three drifter trajectories on Sable Island Bank, Scotian Shelf.

Chapter 2

Calculating the Properties of Flow Field Singularities from the Trajectory of a Single Particle: The OK Method

Generally a particle's velocity will be constantly changing as it moves under the influence of a flow field. However, we expect that there might be points in the flow field where, relative to some uniform translation, the components

of particle's velocity would vanish simultaneously (Minorsky, 1962; Okubo, 1970). Such points will be called stationary or singular points in the following work. We will consider that these stationary points define the position of a flow centre (that may be translating). Near the flow centre we assume that the velocity can be expanded as a Taylor series in the distance from the flow centre. Thus, sufficiently close to the flow centre the first order terms in the Taylor expansion dominate and the flow fields kinematic parameters can be described using linear velocity gradients. Flow near singularities can have a variety of kinematic properties so that particle trajectories may be stable or unstable to small perturbations about the singularity position. We will be concerned with two-dimensional velocity fields, which is consistent with the constraints on the motion of most commonly used types of oceanic drifting buoys. However, the methods throughout this thesis could be generalized to 3-D.

Figure 2.1 shows the common types of singularity (Okubo, 1970): (1) points of divergence (convergence) where an infinite number of streamlines meet; (2) lines of divergence (convergence) from which an infinite number of streamlines diverge (converge) asymptotically; (3) neutral or saddle points where a couple of streamlines meet and the others converge and diverge

asymptotically; (4) vortex point about which streamlines form ellipses. Some examples of singularities can be found in the ocean. Line of convergence can be observed parallel to the coast as a result of a horizontal flow toward the coastline (Bjerknes *et al.*, 1911; Neumann and Pierson, 1966). The vortex point or centre can be found as a result of warm/cold core rings (Parker, 1971; Richardson *et al.*, 1978).

In general, flow fields can have a very complicated spatial structure. If we were to describe such a flow field using a Taylor series expansion of velocity as a function of space then many terms with high order spatial derivatives would be required. In the vicinity of the singularity, however, the flow field can be approximated in terms of linear velocity gradients.

A scaling argument on the Navier Stokes equations shows that the difference between velocity at a point $\vec{x}$ and a velocity at a second point a distance ℓ away from $\vec{x}$ scales proportional to $\ell^{1/3}$ (Schertzer and Lovejoy, 1989). Thus velocity gradients will scale as $\ell^{-2/3}$. Kawai (1985) has compiled observations that are consistent with velocity gradients scaling as $\ell^{-2/3}$ for a wide range of oceanic scales. A consequence of this scaling is that as $\ell \rightarrow 0$ the velocity gradients tend to infinity. Ultimately molecular viscosity defines a smallest possible scale ℓ over which velocity can vary substantially, so velocity gradi-

ents do not become infinite in the ocean. But velocity gradients do become larger as ℓ becomes smaller. Furthermore, measurements are seldom able to resolve more than a narrow band of all the possible scales of oceanic motion. Thus a drifter trajectory, for example, is a smoothed version of the real flow. Nevertheless, velocity gradients due to the smaller scale eddies resolved will be greater than those due to the larger scale eddies. We might expect, therefore, to find localized regions in the flow field that have strong gradients. For mostly historical reasons (Okubo, 1970) we call these points flow singularities and expect that it is sensible to describe the flow field near singularities as Taylor series expansion in terms of distance from the singularity.

A search for the frequency of occurrence and properties of oceanic flow field singularities is therefore important for two reasons. First, flow field singularities are likely to be our clearest mathematical window into the highly non-linear dynamical processes that often control fluid flow. Second, the horizontal distribution of particles or floatables can be greatly influenced by properties of any nearby flow field singularities. Third, the concept of flow field singularities can be used to interpret flow field pattern resulting either from the solutions of Navier-Stokes and continuity equations close to the singularities or those obtained from experiments. Classifying singularities

based on local solutions of the Navier-Stokes and continuity equations has been done before (Oswatitsch, 1958; Rott, 1958, 1959; and Perry and Fairlie, 1974). This enabled Perry and Chong (1987) to identify some singularities such as nodes, saddles, foci from the dye patterns on the downwind side of a missile-shape body.

In this section we follow Okubo (1970) and calculate particle trajectories near flow field singularities with known DKP. We then follow Kirwan *et al.*, (1988) to solve the inverse problem, namely to find DKP of a flow field singularity given a particle trajectory in the vicinity of the singularity.

Following Okubo (1970) the linear velocity field near a flow field singularity can be expressed using the Taylor series expansion as

$$u = \frac{dx}{dt} = a^* x + b^* y \tag{2.1}$$

$$v = \frac{dy}{dt} = c^* x + d^* y \tag{2.2}$$

where $a^* = \frac{\partial u}{\partial x}$, $b^* = \frac{\partial u}{\partial y}$, $c^* = \frac{\partial v}{\partial x}$, $d^* = \frac{\partial u}{\partial y}$ are the velocity gradients independent of time (i.e. constants), and x and y are positions relative to the singularity point. Note that we are assuming above that the singularity does not move, i.e. its translation velocity $U_T = V_T = 0$ and we have neglected the higher-order terms in x and y. These velocity gradients can be related

to the DKP a, b, c and d as:

$$\begin{aligned} a^* &= \tfrac{d+a}{2} \\ b^* &= \tfrac{b-c}{2} \\ c^* &= \tfrac{b+c}{2} \\ d^* &= \tfrac{d-a}{2} \end{aligned} \tag{2.3}$$

where the DKP are:

$$\begin{aligned} \textit{stretching deformation rate} &= a = \tfrac{\partial u}{\partial x} - \tfrac{\partial v}{\partial y} \\ \textit{shearing deformation rate} &= b = \tfrac{\partial v}{\partial x} + \tfrac{\partial u}{\partial y} \\ \textit{vorticity} &= c = \tfrac{\partial v}{\partial x} - \tfrac{\partial u}{\partial y} \\ \textit{divergence} &= d = \tfrac{\partial u}{\partial x} + \tfrac{\partial v}{\partial y}. \end{aligned} \tag{2.4}$$

These DKP are often more readily related to our usual formulations of dynamical processes than the velocity gradients. The stretching deformation rate is a measure of change of shape by different rates of stretching along the x and y directions without change of area or orientation. Positive a describes a stretching in the x direction and shrinking in the y direction. The shearing deformation rate can be related to the change of shape and/or distortion of fluid elements as a result the velocity varying in a direction perpendicular to the velocity. The vorticity implies the rate of change in orientation without change in area or shape, so it represents the rotational nature of the singu-

larity. The horizontal divergence is a measure of the fractional rate of area increase (Saucier, 1955; Okubo, 1970; Molinari and Kirwan, 1975; Kirwan, 1975). The above DKP are not independent of the coordinate system and a principal coordinate system can be defined so that the shearing deformation vanishes and the flow is characterized by a, c, d and the orientation of the principal axes (Batchelor, 1967; Saucier, 1953).

The DKP are related to various types of singularity structure as shown in figure 2.1. The choice of axes can be related to the characteristic roots resulting from manipulating (2.1) and (2.2) as will be discussed next. Schematic trajectories near the flow centre are drawn on the Figure. The shape of the trajectory depends upon the relative importance of stretching-shearing deformation and vorticity (plotted on the ordinate) and the divergence (plotted on the absisca).

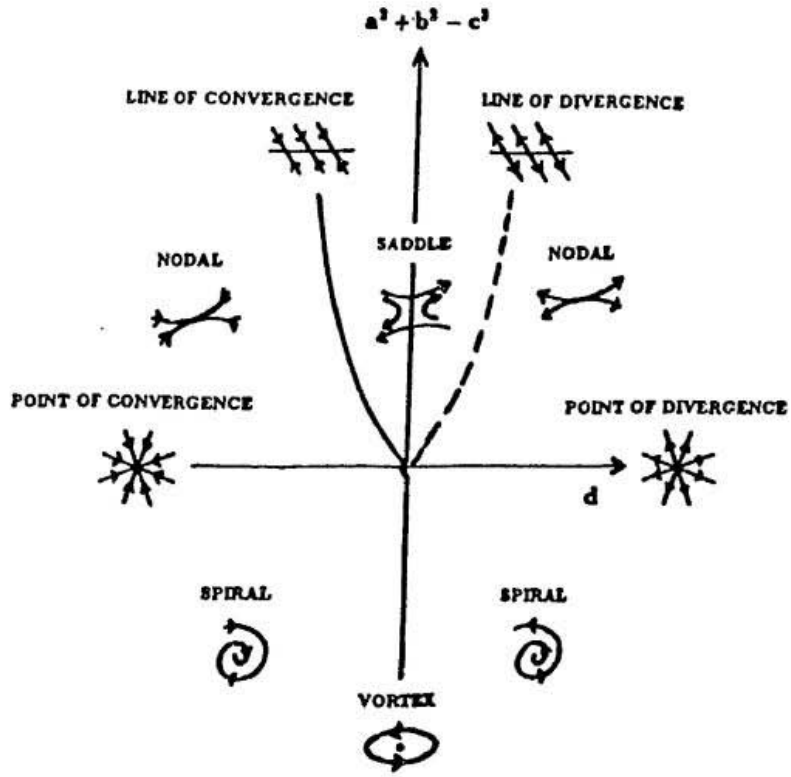

Figure 2.1: Classification of singularities in the parameter space for the linear velocity field. Adapted from Okubo (1970).

Defining the differential operator $D\ (\ \ ) = \frac{d}{dt}\ (\ \ )$ we can rewrite (2.1) and (2.2) as

$$(D - a^*)\ x - b^*\ y = 0 \tag{2.5}$$

$$-c^*\ x + (D - d^*\ )\ y = 0 \tag{2.6}$$

Eliminating x by multiplying (2.5) by c^* and operating on (2.6) with $(D - a^*)$ and adding the resulting equations gives

$$[D^2 - (a^* + c^*)\ D + a^*\ c^* - b^*\ d^*\ ]\ y = 0. \tag{2.7}$$

The characteristic equation of (2.7)

$$r^2 - (a^* + c^*)\, r + a^*\, c^* - b^*\, d^* = 0$$

has the following roots.

$$\begin{aligned} r_1 &= \frac{[\, d+(a^2+b^2-c^2)^{1/2}\,]}{2} \\ r_2 &= \frac{[\, d-(a^2+b^2-c^2)^{1/2}\,]}{2} \end{aligned} \tag{2.8}$$

The roots have been expressed in terms of the DKP a, b, c, d by using (2.3). Providing that the roots r_1, r_2 are distinct, i.e. $a^2 + b^2 - c^2 \neq 0$, the general solution for y is

$$y(t) = C_1 e^{r_1 t} + C_2 e^{r_2 t} \tag{2.9}$$

where C_1 and C_2 are arbitrary constants. We will consider the case $r_1 = r_2$ later in this chapter. Substituting the solution for y as given by (2.9) into (2.6) we obtain the following solution for x.

$$x(t) = \frac{(r_1 - d^*)C_1\, e^{r_1 t} + (r_2 - d^*)\, C_2\, e^{r_2 t}}{c^*}. \tag{2.10}$$

The initial particle position relative to the singularity is:

$$x(t=0) = X_0 \tag{2.11}$$

$$y(t=0) = Y_0. \tag{2.12}$$

Setting $t = 0$ and substituting (2.11) and (2.12) into (2.10) and (2.9) respectively, yields

$$C_1 = \frac{c^* X_0 - Y_0(r_2 - d^*)}{r_1 - r_2} \tag{2.13}$$

$$C_2 = \frac{Y_0 (r_1 - d^*) - c^* X_0}{r_1 - r_2}. \tag{2.14}$$

Substituting (2.13) and (2.14) into (2.9), we get

$$\begin{aligned} y(t) &= \frac{\{(bX_0 + cX_0 - aY_0)q + Y_0\}e^{r_1 t} + \{-(bX_0 + cX_0 - aY_0)q + Y_0\}e^{r_2 t}}{2} \\ &= \frac{q}{2}\{(\frac{1}{q} - a)Y_0 + (b + c)X_0\}e^{r_1 t} + \frac{q}{2}\{(\frac{1}{q} + a)Y_0 - (b + c)X_0\}e^{r_2 t} \\ &= \frac{\{X_0(b + c) + Y_0(p - a)\}e^{r_1 t} + \{Y_0(p + a) - X_0(b + c)\}e^{r_2 t}\}}{2\,p} \end{aligned} \tag{2.15}$$

and substituting (2.13) and (2.14) into (2.10) gives

$$\begin{aligned} x(t) &= \frac{\{X_0 + (aX_0 + bY_0 - cY_0)q\}e^{r_1 t} + \{X_0 - (aX_0 + bY_0 - cY_0)q\}e^{r_2 t}\}}{2} \\ &= \frac{q}{2}\{(\frac{1}{q} + a)X_0 + (b - c)Y_0\}e^{r_1 t} + \frac{q}{2}\{(\frac{1}{q} - a)X_0 - (b - c)Y_0\}e^{r_2 t} \\ &= \frac{\{X_0(p + a) + Y_0(b - c)\}e^{r_1 t} - \{X_0(a - p) + Y_0(b - c)\}e^{r_2 t}\}}{2\,p} \end{aligned} \tag{2.16}$$

where

$$p = \frac{1}{q} = (a^2 + b^2 - c^2)^{1/2}. \tag{2.17}$$

Note that we have expressed (2.15), (2.16) and (2.17) in terms of the DKP rather than velocity gradients.

The value of p^2 together with the divergence d were used by Okubo (1970) to classify the flow field singularity as: inward/outward nodal, saddle, inward/outward spiral, vortex and lines of convergence. Okubo (1970) called p the singularity parameter.

Kirwan *et al.*, (1988) inverted the above solution in their attempt to obtain the kinematic properties of rings from trajectories of drifters in the Gulf of Mexico. They divided the velocity field into translation and swirl components. This kind of treatment can be found in atmospheric studies, e.g. the theory of frontogenesis (Petterssen, 1935). In fact, this is still the Taylor series expansion near the singularity point. Here, Kirwan *et al.*, (1988) allowed the flow field singularity i.e. the ring centre to move.

$$u = U_T + u_s \tag{2.18}$$

$$v = V_T + v_s \tag{2.19}$$

The subscripts T and s denote 'translation' and 'swirl', respectively. The translation component is the translational velocity of the singularity position in the velocity field. The swirl velocity of a particle near the flow centre describes rotation and other motion relative to the translating centre of the flow singularity. The differential kinematic parameters can, therefore, be

related to these swirl velocities as

$$u_s = (d+a)x/2 + (b-c)y/2 \tag{2.20}$$

$$v_s = (b+c)x/2 + (d-a)y/2. \tag{2.21}$$

Substituting (2.20) into (2.18) and (2.21) into (2.19) gives

$$u_k(t) = U_{Tk} + (d_k + a_k)x_k/2 + (b_k - c_k)y_k/2 \tag{2.22}$$

$$v_k(t) = V_{Tk} + (b_k + c_k)x_k/2 + (d_k - a_k)y_k/2 \tag{2.23}$$

where the subscript k indicates values calculated in the time interval $t_k \leq t \leq t_{k+1}$. The expressions for x_k and y_k obtained from (2.15) and (2.16) have the form:

$$\begin{aligned} x_k(t) = \{&[X_k(\ p_k + a_k) + Y_k(b_k - c_k)]e^{[r_{1k}(t-t_k)]} \\ &- [X_k(a_k - p_k) + Y_k(b_k - c_k)]e^{[r_{2k}(t-t_k)]}\}/2\ p_k \end{aligned} \tag{2.24}$$

$$\begin{aligned} y_k(t) = \{&[X_k(b_k + c_k) + Y_k(p_k - a_k)]e^{[r_{1k}(t-t_k)]} \\ &+ [-X_k(b_k + c_k) + Y_k(p_k + a_k)]e^{[r_{2k}(t-t_k)]}\}/2\ p_k. \end{aligned} \tag{2.25}$$

X_k and Y_k are the coordinates of the fluid parcel relative to the singularity point at $t = t_k$. The position of the particle relative to the singularity for

times $t_k \leq t \leq t_{k+1}$ is given by $x_k(t)$ and $y_k(t)$. Similarly $u_k(t)$ and $v_k(t)$ are the total velocities at times $t_k \leq t \leq t_{k+1}$. The variables $u_k(t)$, $v_k(t)$, $x_k(t)$, $y_k(t)$ all vary with t over the interval $t_k \leq t \leq t_{k+1}$. This variation with respect to time occurs as a consequence of Okubo's solutions (equation (2.15) and (2.16)). Translation velocity U_{Tk}, V_{Tk} and the DKP a_k, b_k, c_k, d_k are all taken to be constant over the interval $t_k \leq t \leq t_{k+1}$, although they may change, of course, from interval to interval. In another words, this assumption requires that U_T, V_T, a, b, c, d are slowly changing over the time interval between fixes.

Substituting (2.24) and (2.25) into (2.22) and (2.23) and evaluating them at $t = t_k$, with the subscript k suppressed, gives:

$$\begin{aligned} u &= U_T + \{(d+a)[Xa + Xp - Xa + Xp + Y(b-c) - Y(b-c)] + \\ &\quad (b-c)[X(b+c) - X(b+c) + Yp - Ya + Ya + Yp]\}/4p \\ v &= V_T + \{(b+c)[Xa + Xp - Xa + Xp + Y(b-c) - Y(b-c)] + \\ &\quad (d-a)[X(b+c) - X(b+c) + Yp - Ya + Ya + Yp]\}/4p. \end{aligned}$$

After cancelling and rearranging terms, the above equations reduce to

$$2\,u = 2\,U_T + (a+d)\,X + (b-c)\,Y \tag{2.26}$$

$$2\,v = 2\,V_T + (b+c)\,X + (d-a)\,Y. \tag{2.27}$$

It is clear that we face a problem in which we have eight unknowns U_T, V_T, X, Y, a, b, c, d and only two equations (2.26) and (2.27) presently available to solve for them. We need another six equations. These additional equations can be obtained by differentiating (2.22) and (2.23) with respect to time.

Taking the first derivative with respect to time of (2.22) and (2.23) and assuming as before that a, b, c, d, U_T, V_T are constant gives:

$$\begin{aligned} u' &= \frac{(d+a)x' + (b-c)y'}{2} \\ v' &= \frac{(b+c)x' + (d-a)y'}{2}. \end{aligned}$$

Now, in general we can not expect a, b, c, d, U_T, V_T to be independent of time. But we assume that the time scale for them to change is long compared to the the time scale for x, y to change. This condition must be satisfied for x, y sufficiently small providing a, b, c, d are not all identically zero. Whether or not x, y are sufficiently small for a given data is something that must be checked for as part of the data analysis. Here and subsequently, the prime denotes differentiation with respect to time. Substituting (2.24) and (2.25) into the above equations and evaluating them at $t = t_k$ gives

$$\begin{aligned} u' = {} & \{(d+a)[r_1\{Xp + Xa + Y(b-c)\} - r_2\{Xa - Xp + Y(b-c)\}] + \\ & (b-c)[r_1\{X(b+c) + Yp - Ya\} + r_2\{-X(b+c) + Yp + Ya\}]\}/4p \end{aligned}$$

$$v' = \{(b+c)[r_1\{Xp + Xa + Y(b-c)\} - r_2\{Xa - Xp + Y(b-c)\}] +$$

$$(d-a)[r_1\{X(b+c) + Yp - Ya\} + r_2\{-X(b+c) + Yp + Ya\}]\}/4p.$$

The above equations can be rewritten as:

$$4\ u' = X\ [(a+d)^2 + b^2 - c^2] + 2\ Y\ (b-c)\ d \tag{2.28}$$

$$4\ v' = Y\ [(d-a)^2 + b^2 - c^2] + 2\ X\ (b+c)\ d. \tag{2.29}$$

Taking the second derivative of (2.22) and (2.23) with respect to time of then substituting for x and y using (2.24) and (2.25), and evaluating the resulting equations at $t = t_k$ gives

$$u'' = \frac{(d+a)x'' + (b-c)y''}{2}$$

$$= \{(d+a)[r_1^2\{Xp + Xa - Y(b-c)\} - r_2^2\{Xa - Xp + Y(b-c)\}] +$$

$$[r_1^2\{X(b+c) + Yp - Ya\} + r_2^2\{-X(b+c) + Yp + Ya\}]\}/4\ p$$

$$v'' = \frac{(b+c)x'' + (d-a)y''}{2}$$

$$= \{(b+c)[r_1^2\{Xp + Xa + Y(b-c)\} - r_2^2\{Xa - Xp + Y(b-c)\}] +$$

$$(d-a)[r_1^2\{X(b+c) + Yp - Ya\} +$$

$$r_2^2\{-X(b+c) + Yp + Ya\}]\}/4\ p$$

and, after rearranging terms and using the equalities

$$r_1^2 + r_2^2 = \frac{d^2 + p^2}{2}$$

and

$$r_1^2 - r_2^2 = d\,p,$$

the above equations become

$$8\,u'' = X[(d+a)^3 + (b^2 - c^2)(3d+a)] + Y[(b-c)(3d^2 + a^2 + b^2 - c^2)] \quad (2.30)$$

$$8\,v'' = Y[(d-a)^3 + (b^2 - c^2)(3d-a)] + X[(b+c)(3d^2 + a^2 + b^2 - c^2)]. \quad (2.31)$$

Applying the same procedure for the third derivative with respect to time of equation (2.22) and (2.23) gives

$$u''' = \frac{(d+a)x''' + (b-c)y'''}{2}$$

$$= \{(d+a)[r_1^3\{Xp + Xa - Y(b-c)\} - r_2^3\{Xa - Xp + Y(b-c)\}]$$

$$+ (b-c)[r_1^3\{X(b+c) + Yp - Ya\} +$$

$$r_2^3\{-X(b+c) + Yp + Ya\}]\}/4\,p$$

$$v''' = \frac{(b+c)x''' + (d-a)y'''}{2}$$

$$= \{(b+c)[r_1^3\{Xp + Xa - Y(b-c)\} - r_2^3\{Xa - Xp + Y(b-c)\}]$$

$$+ (d-a)[r_1^3\{X(b+c) + Yp - Ya\} +$$

$$r_2^3\{-X(b+c) + Yp + Ya\}]\}/4\ p.$$

After rearranging terms and using the equalities

$$r_1^3 + r_2^3 = \frac{2\ d^3 + 6\ d\ p^2}{8}$$

and

$$r_1^3 - r_2^3 = \frac{6\ p\ d^2 + 2\ p^3}{8},$$

we get

$$16\ u''' = 4Yd(b-c)(a^2+b^2-c^2+d^2)$$

$$+ X[(a^2+b^2-c^2+d^2)^2$$

$$+ 4ad(a^2+b^2-c^2+d^2)$$

$$+ 4d^2(a^2+b^2-c^2)] \qquad (2.32)$$

$$16\ v''' = 4Xd(b+c)(a^2+b^2-c^2+d^2)$$

$$+ Y[(a^2+b^2-c^2+d^2)^2$$

$$- 4ad(a^2+b^2-c^2+d^2)$$

$$+ 4d^2(a^2+b^2-c^2)]. \qquad (2.33)$$

The above eight equations, from (2.26) through (2.33), are equations (A3) to (A10) of Kirwan *et al.*, (1988).

Putting $\Gamma = a^2 + b^2 - c^2 + d^2$, we can rewrite equations (2.28), (2.29), (2.30), (2.31), (2.32), and (2.33) as

$$2Xda + 2Ydb - 2Ydc = 4u' - X\Gamma \qquad (2.28')$$

$$-2Yda + 2Xdb + 2Xdc = 4v' - Y\Gamma \qquad (2.29')$$

$$X(2d^2 + \Gamma)a + Y(2d^2 + \Gamma)b - Y(2\,d^2 + \Gamma)c = 8u'' + Xd(2d^2 - 3\Gamma) \qquad (2.30')$$

$$-Y(2d^2 + \Gamma)a + X(2d^2 + \Gamma)b + X(2\,d^2 + \Gamma)c = 8v'' + Yd(2d^2 - 3\Gamma) \qquad (2.31')$$

$$4\Gamma Xda + 4\Gamma Ydb - 4\Gamma Ydc = 16u''' + X(4d^4 - 4d^2\Gamma - \Gamma^2) \qquad (2.32')$$

$$-4\Gamma Yda + 4\Gamma Xdb + 4\Gamma Xdc = 16v''' + Y(4d^4 - 4d^2\Gamma - \Gamma^2) \qquad (2.33').$$

We now solve the equations analytically. Using (2.28′) to eliminate Y from (2.30′) gives

$$X\,(2\,d^2 - \Gamma)^2 = 4\,(2\,d^2 + \Gamma)\,u' - 16\,d\,u''. \qquad (2.34)$$

Using (2.29′) to eliminate X from (2.31′) gives

$$Y\,(2\,d^2 - \Gamma)^2 = 4\,(2\,d^2 + \Gamma)\,v' - 16\,d\,v''. \qquad (2.35)$$

Using (2.28′) to eliminate Y from (2.32′) gives

$$X\,(2\,d^2 - \Gamma)^2 = 8\,\Gamma u' - 16\,u'''. \qquad (2.36)$$

Using (2.29′) to eliminate X from (2.33′) gives

$$Y\,(2\,d^2-\Gamma)^2 \;=\; 8\,\Gamma v' - 16\,v'''. \tag{2.37}$$

Using (2.34) to eliminate X from (2.36) gives

$$4\,(2\,d^2-\Gamma)\,u' = 16\,(u''\,d - u''') \tag{2.38}$$

and similarly (2.35) can be used to eliminate Y from (2.37) to give

$$4(2\,d^2-\Gamma)\,v' = 16\,(v''\,d - v'''). \tag{2.39}$$

Using (2.38) to eliminate Γ from (2.39) gives

$$d \;=\; \frac{u'v''' - v'u'''}{u'v'' - v'u''}. \tag{2.40}$$

We note that

$$2\,d^2-\Gamma \;=\; 4\,M^2 = \; d^2 - a^2 - b^2 + c^2 \tag{2.41}$$

where M^2 is the determinant of

$$M \;=\; \begin{pmatrix} (d+a)/2 & (b-c)/2 \\ \\ (b+c)/2 & (d-a)/2 \end{pmatrix} \tag{2.42}$$

Equation (2.41) indicates that M^2 can be substituted for $2\ d^2 - \Gamma$ in both equations (2.38) and (2.39). Eliminating d from the resulting equations gives

$$M^2 = \frac{u''v''' - v''u'''}{u'v'' - v'u''}. \tag{2.43}$$

Thus we have solved for d using equation (2.40) and have another equation (2.43) relating the remaining unknown DKP to d and to the velocity derivatives. Now, we are in a position to solve the equations for the remaining variables X, Y, a, b and c. Note, we can solve this problem without defining M, but do so in order to preserve parallels with Kirwan *et al.*, (1988).

Substituting (2.41) into (2.36) gives

$$X = \frac{(d^2 - 2M^2)u' - u'''}{M^4}. \tag{2.44}$$

Substituting (2.41) into (2.37) gives

$$Y = \frac{(d^2 - 2M^2)v' - v'''}{M^4}. \tag{2.45}$$

We still have three variables a, b, c to solve for. Eliminating a from (2.28′) and (2.29′) to give an expression for b in terms of c as

$$b = \frac{8d(Xv' + Yu') - 4XYd\Gamma - 4d^2(X^2 - Y^2)c}{4d^2(X^2 + Y^2)}. \tag{2.46}$$

Substituting the above value of b into (2.28′) gives

$$a = \{4d^2(X^2+Y^2)(4u' - X\Gamma) - 2dY[8d(Xv' + Yu') - 4XYd\Gamma] + 16d^3X^2Yc\}/\{8d^3X(X^2+Y^2)\}. \quad (2.47)$$

Substituting the above values of a and b into (2.41) gives an equation that is quadratic in c. To simplify the equation and solve for c, we use computer algebra software (i.e. MACSYMA). It turns out that the equation has repeated roots. We then substitute the solution for c into (2.46) and (2.67) to solve for a and b. Using $\Gamma = 2d^2 - 4M^2$, (2.40), (2.44), (2.45), (2.43) we substitute for Γ, d, X, Y, M^2 in the resulting equations to obtain the following solutions in terms of the time derivatives of velocity.

$$a = -\frac{u'v''' - 2u''v'' + u'''v'}{u'v'' - u''v'} \quad (2.48)$$

$$b = -\frac{v'v''' - v''v'' - u'''u' + u''u''}{u'v'' - u''v'} \quad (2.49)$$

$$c = -\frac{v'v''' - v''v'' + u'''u' - u''u''}{u'v'' - u''v'} \quad (2.50)$$

Our solutions for X, Y, a, b, c are all different from those of Kirwan *et al.*, (1988). Only in the case of d does the OK solution give the same expression as Kirwan *et al.*, (1988).

To sum up, we present all solutions for the DKP and positions relative

to the flow centre obtained using the OK method as below

$$
\begin{aligned}
a &= -\frac{u'v''' - 2u''v'' + u'''v'}{u'v'' - u''v'} \\
b &= -\frac{v'v''' - v''v'' - u'''u' + u''u''}{u'v'' - u''v'} \\
c &= -\frac{v'v''' - v''v'' + u'''u' - u''u''}{u'v'' - u''v'} \\
d &= \frac{u'v''' - v'u'''}{u'v'' - v'} \\
X &= \frac{(d^2 - 2M^2)u' - u'''}{M^4} \\
Y &= \frac{(d^2 - 2M^2)v' - v'''}{M^4}.
\end{aligned}
$$

From (2.26) and (2.27) we see that the swirl velocity defined by (2.18) and (2.19) can be written as

$$u_s = \frac{1}{2}(a+d)X + \frac{1}{2}(b-c)Y \tag{2.51}$$

$$v_s = \frac{1}{2}(b+c)X + \frac{1}{2}(d-a)Y \tag{2.52}$$

and the translation velocity of the flow centre is

$$U_T = u - u_s \tag{2.53}$$

$$V_T = v - v_s. \tag{2.54}$$

The above solutions were obtained on the assumptions that $a^2 + b^2 - c^2 \neq 0$, i.e. the charecteristic roots in equation (2.8) are different. Let us now use

continuity to show that the above solutions also hold for the multiple root case, i.e. $a^2 + b^2 - c^2 = 0$. A point of divergence/convergence is an example of such a case. Let a, b, c be such that $a^2 + b^2 - c^2 = 0$. If we perturb the parameters so that $\hat{a} = a, \hat{b} = b + \epsilon, \hat{c} = c, \hat{d} = d$, the velocity field becomes

$$\hat{u} = u + \epsilon\, y/2 \tag{2.55}$$

$$\hat{v} = v + \epsilon\, x/2, \tag{2.56}$$

then, equations (2.48, 2.49, 2.50) still hold since $\hat{a}^2 + \hat{b}^2 - \hat{c}^2 \neq 0$. This allows us to calculate for $\hat{a}, \hat{b}, \hat{c}$ using equations (2.48, 2.49, 2.50). Note that here we have to calculate up to third order time derivatives from the perturbed flow fields (equation (2.55) and equation (2.56)). The results are

$$a = -\frac{u'v''' - 2u''v'' + u'''v'}{u'v'' - u''v'} + O(\epsilon) \tag{2.57}$$

$$b = -\frac{v'v''' - v''v'' - u'''u' + u''u''}{u'v'' - u''v'} + O(\epsilon) \tag{2.58}$$

$$c = -\frac{v'v''' - v''v'' + u'''u' - u''u''}{u'v'' - u''v'} + O(\epsilon). \tag{2.59}$$

If we let $\epsilon \to 0$ into the above equations, we find that these equations will reduce to (2.48, 2.49, 2.50). Similarly, these results are also obtained by perturbing a and c. From this, we deduce that the OK solutions still hold for both the unrepeated and multiple root cases.

Chapter 3

Testing Our OK Solutions

In the previous chapter we showed how a single particle trajectory would be used to calculate: the position X, Y of the particle relative to the flow centre using (2.44) and (2.45), the translation velocity U_T and V_T of the flow centre using (2.53) and (2.54) and the DKP a, b, c, d of the flow centre using (2.48), (2.49), (2.50) and (2.40), respectively. We will now test these solutions using artificially generated data that has known flow properties. Several artificially generated data sets covering cases of pure stretching and pure shearing without translation velocity and pure rotation with uniform translation velocity are used. We construct the simulated trajectory of a particle from its initial position relative to the flow centre X_0, Y_0; the translation velocity of the flow

centre U_T, V_T; and the DKP a, b, c, d of the flow field. The OK method is then used to calculate the kinematic parameters of these artificially generated trajectories. Kirwan's solutions (Kirwan *et al.*, 1988) will be used to calculate kinematic parameters from the same data sets. From now on we will refer to the solution given by equations (A3), (A4), (A12), (A13), (A14), (A15), (A16), and (A17) of Kirwan *et al.*, (1988) as the Kirwan solution. This solution is incorrect, but has been used by others (Lewis and Kirwan, 1987; Lewis *et al.*,, 1989; Indest *et al.*, 1989; Kirwan *et al.*, 1990) to calculate DKP of drifter data. They therefore merit some study to interpret these drifter analyses.

The OK method requires taking high order derivatives of the particle trajectory. High order derivatives are unstable to both measurement errors and trajectory fluctuations caused by small scale eddies. We will, therefore, analyse the robustness of the OK method by applying it to an artificially generated trajectory to which a known amount of random noise has been added.

3.1 Pure Stretching

We now consider the case of an eddy with pure stretching and no translation velocity. The streamlines for such a flow are sketched in Appendix B. In this case, the absolute position $(\tilde{x}, \tilde{y})$ of the particle is the same as its position relative to the flow centre and is obtained from (2.15) and (2.16) with x, y replaced by $\tilde{x}, \tilde{y}$.

To calculate the time derivatives numerically, we use a forward differencing scheme for the first three points (Mathews, 1987)

$$u(t) = \frac{-3\tilde{x}(t) + 4\tilde{x}(t+\Delta) - \tilde{x}(t+2\Delta)}{2\ \Delta} \tag{3.1}$$

$$v(t) = \frac{-3\tilde{y}(t) + 4\tilde{y}(t+\Delta) - \tilde{y}(t+2\Delta)}{2\ \Delta}, \tag{3.2}$$

centered differencing at the middle points

$$u(t) = \frac{-\tilde{x}(t+2\Delta) + 8\ \tilde{x}(t+\Delta) - 8\ \tilde{x}(t-\Delta) + \tilde{x}(t-2\Delta)}{12\ \Delta} \tag{3.3}$$

$$v(t) = \frac{-\tilde{y}(t+2\Delta) + 8\ \tilde{y}(t+\Delta) - 8\ \tilde{y}(t-\Delta) + \tilde{y}(t-2\Delta)}{12\ \Delta}, \tag{3.4}$$

and a backward differencing at the last three points

$$u(t) = \frac{3\ \tilde{x}(t) - 4\ \tilde{x}(t-\Delta) + \tilde{x}(t-2\Delta)}{2\ \Delta} \tag{3.5}$$

$$v(t) = \frac{3\ \tilde{y}(t) - 4\ \tilde{y}(t-\Delta) + \tilde{y}(t-2\Delta)}{2\ \Delta}. \tag{3.6}$$

Here, Δ denotes the time interval between two consecutive points in the time series. Throughout the thesis the above numerical differencing schemes will be used to obtain up to the fourth order time derivatives of positions. Tests were also done using time derivatives obtained analytically from (2.15) and (2.16), but these are not reported here. These tests gave, of course, the same results as obtained using numerically calculated time derivatives.

We set the stretching deformation rate at $a = 0.1$, and the other DKP at $b = c = d = 0$. Let the initial position with respect to the flow centre (which is also the absolute initial position in this case) be $X_0 = 0.003$ and $Y_0 = 0.4$. The DKP and the position have a unit of $time^{-1}$ and unit distance, respectively. The time interval between successive positions is chosen to be 2 units. Substituting these values for X_0, Y_0, a, b, c, d into equations (2.15) and (2.16), we can obtain a time series of positions. The same data set is used to evaluate Kirwan's solutions (Kirwan *et al.*, 1988). From now on, the numerically calculated results of the generated data using our solutions to the OK problem will be labelled 'OK'. Values obtained from the generated data using solutions given by Kirwan *at al.*, (1988) will be labelled as 'KIRWAN'.

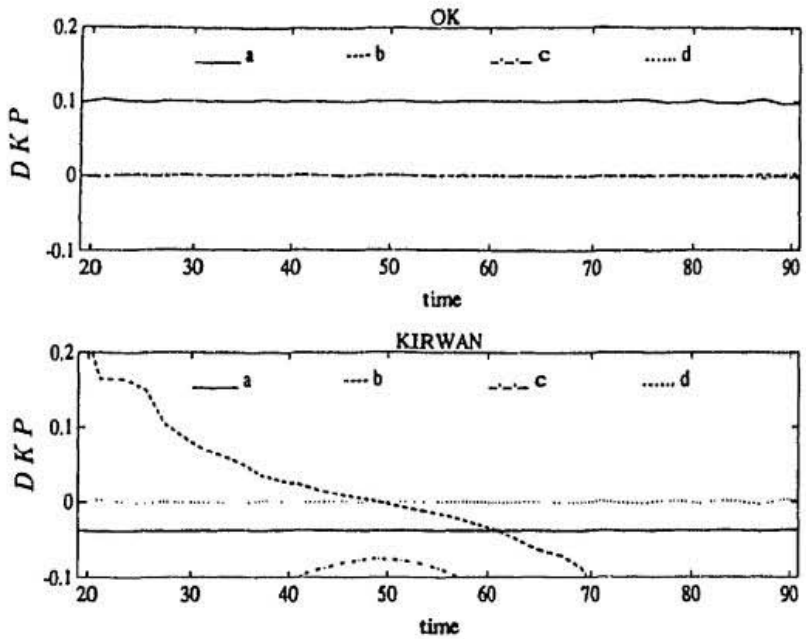

Figure 3.1: The DKP calculated, using OK (above) and KIRWAN (below) solutions, from trajectories with pure stretching deformation.

Figure 3.1 shows time series of the DKP calculated from the simulated trajectory with pure stretching motion. The upper diagram is obtained by using the OK solutions ((2.40), (2.48), (2.49), (2.50)) and gives the expected values of all parameters, e.g. $a = 0.1$, $b = c = d = 0$ in units of $time^{-1}$. These parameters are constant and in accordance with those used to generate the trajectory. The lower diagram, on the other hand, is produced by KIRWAN solutions. It shows that only the divergence is calculated correctly. The other

three parameters do not conform with those used to generate the simulated trajectories.

Note that in both the upper and lower diagrams, we do not include some results at the beginning and at the end of the time series since it contains spurious features. This is caused by the numerical differentiation process that is being used. In figure 3.2 we show the position of the particle at intervals Δ. Clearly, at small and large times the particle moves quickly in one direction and slowly in the other direction. This leads to numerical errors at small and large times. We do not have this problem when making use of the analytically computed time derivatives of equations (2.15) and (2.16).

Having calculated the DKP, we calculate the position of the particle relative to the flow centre using (2.44) and (2.45). The position of the flow centre is calculated by subtracting the position of particle relative to the flow centre from the absolute particle position generated using (2.15) and (2.16). The result is shown in figure 3.2. In this figure, the '*' symbol denotes the particle's trajectory and the 'o' symbol corresponds to the flow centre. We find that the OK solution gives the flow centre at the origin (0,0) where it should be.

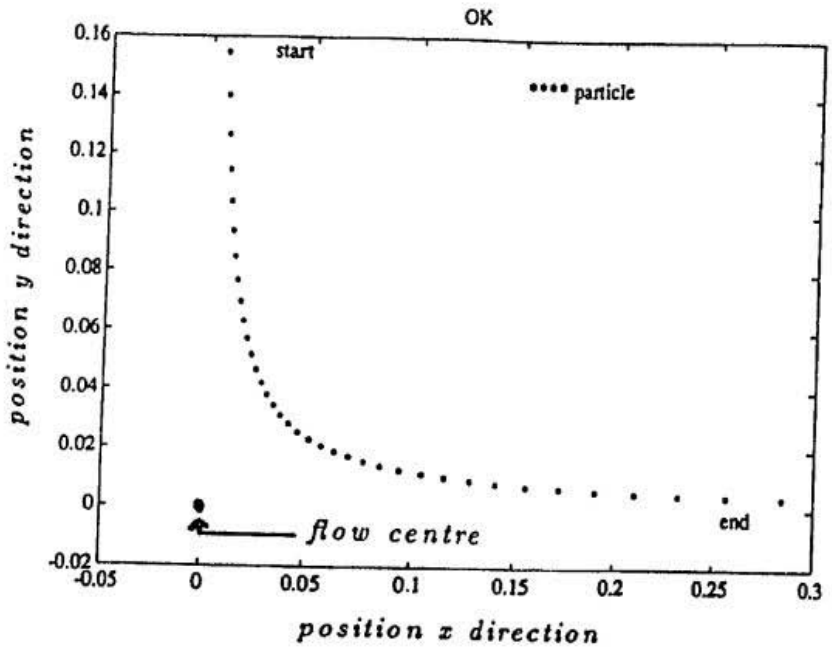

Figure 3.2: The particle's trajectory and the calculated position of the flow centre for the pure stretching case using OK.

The above procedures are used again to locate the flow centre from the KIRWAN solutions, i.e. subtracting (A.13) and (A.14) of Kirwan *et al.*, (1988) from the particle position. The result is presented in figure 3.3. In this figure, the flow centre moves far from the origin, whereas it should be stationary at the origin.

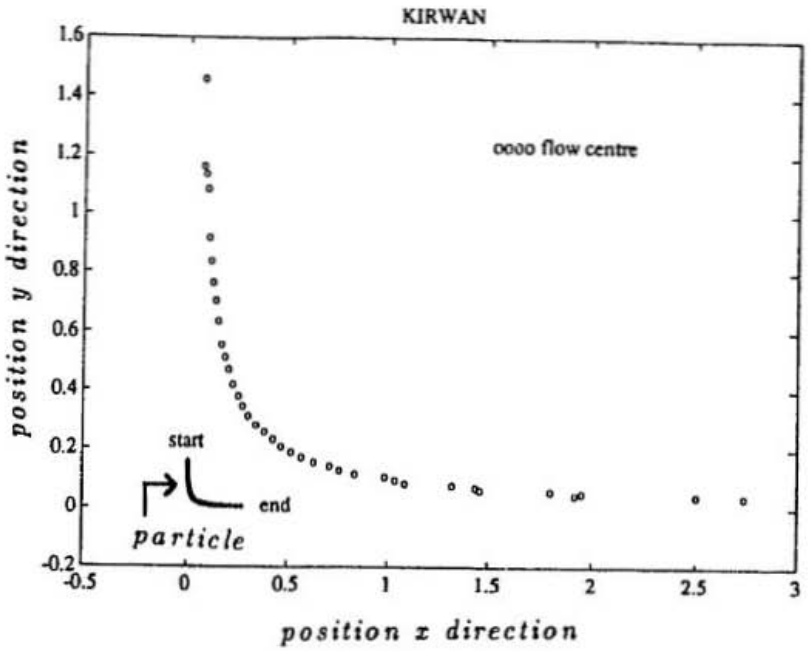

Figure 3.3: The particle's trajectory and the calculated position of the flow centre for the pure stretching case using KIRWAN.

Having obtained the DKP and the position relative to the flow centre, we proceed to calculate the swirl and flow centre velocities. To do this, we make use of equations (2.51), (2.52), (2.53) and (2.54). The result is presented in figure 3.4 in which we plot the time series of translation velocities, U_T and V_T, together with the swirl velocities, u_s and v_s. The top diagram is the result given by the OK solution. Here, we find that the translation velocity (U_T, V_T) is zero. This is correct since our simulated eddy has no translation velocity.

The swirl velocity describes the particle velocity relative to the velocity of the flow centre. A particle placed in this type of flow with pure stretching having a positive stretching deformation rate, a, will move toward the x-axis and away from the y-axis (see figure 3.2). As a consequence, the eastward component of velocity, u_s, increases. On the other hand, the northward component of velocity, v_s, will decrease. These features are obtained by the OK solutions.

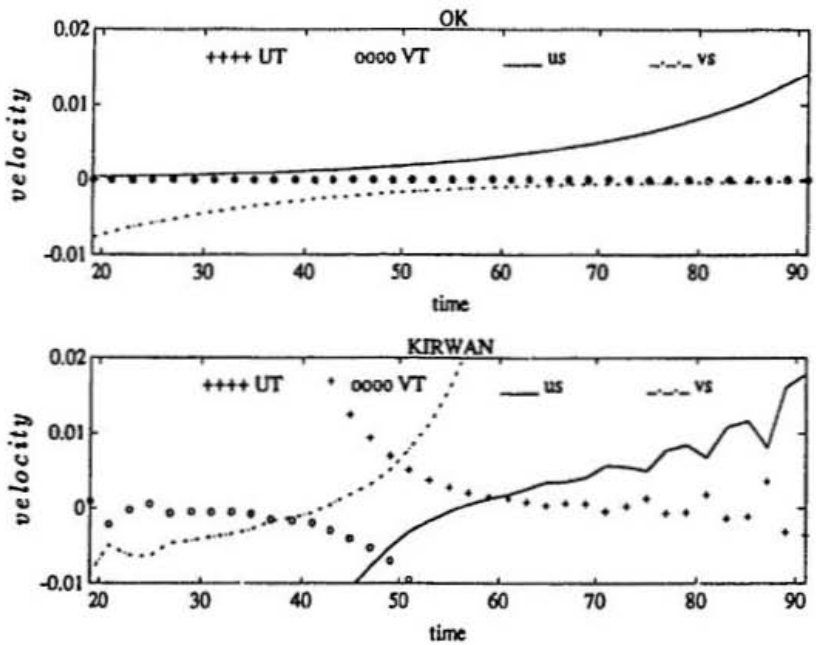

Figure 3.4: Swirl and translational velocities calculated from trajectories with pure stretching. The upper/lower plot shows values obtained using the OK/KIRWAN solution.

The bottom diagram is obtained using KIRWAN's solutions. It shows us that the eddy has translation velocities that are inconsistent with the parameters used to simulate the trajectory. Also, we see that both components of the swirl velocity increase. This is inconsistent with a pure stretching flow field singularity.

In the case of pure stretching, we find that the OK solution correctly obtains all the kinematic parameters. On the other hand, KIRWAN solutions give incorrect values for all the kinematic parameters except divergence.

3.2 Pure Shearing

Equations (2.15) and (2.16) are now used to simulate trajectories resulting from a stationary eddy with pure shearing. The streamlines for such a flow are sketched in Appendix B. In this case the DKP values and initial position are: $b = 0.1,\ a = c = d = 0,\ X_0 = 0.003,\ Y_0 = 0.4$. The time interval between two successive points is chosen to be 2 units. The resulting trajectory was analysed by both the OK and KIRWAN methods and the resulting DKP are presented in figure 3.5.

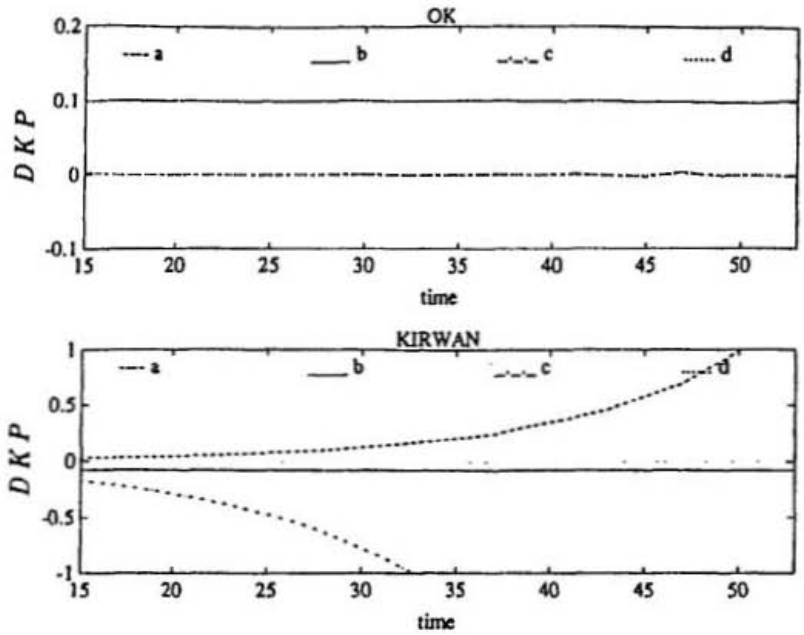

Figure 3.5: The DKP calculated, using OK (above) and KIRWAN (below) solutions, from trajectories with pure shear deformation.

The diagram at the top of figure 3.5 is obtained by using the OK solutions and gives the correct values of all parameters, e.g. $b = 0.1$, $a = c = d = 0$ in units of $time^{-1}$ which are are independent of time. The bottom diagram shows DKP obtained using the KIRWAN solutions. It shows that only the divergence is calculated correctly. The shearing b has the correct magnitude, but the wrong sign. The other two parameters are inconsistent with those used to generate the simulated trajectory.

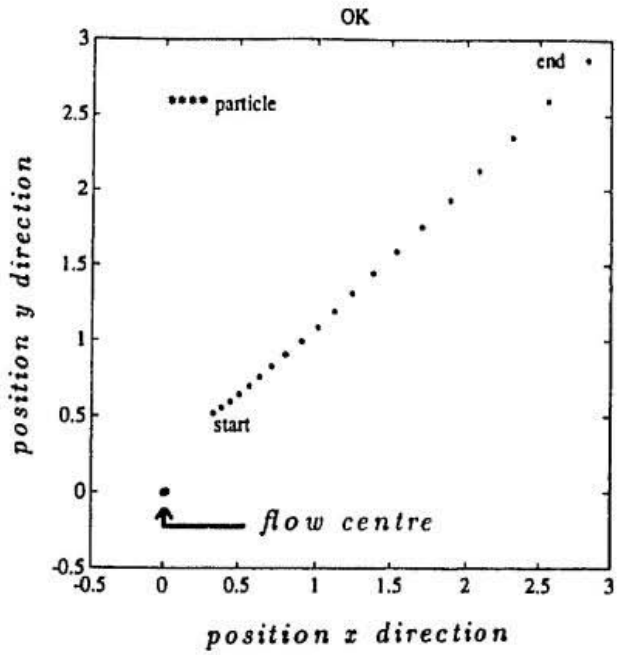

Figure 3.6: The OK solution for particle trajectory and position of the flow centre from a trajectory with pure shearing.

Having obtained the DKP, we calculate the position of the particle relative to the flow centre using (2.44) and (2.45). As for the previous case, the position of the flow centre is computed by subtracting the position of particle relative to the flow centre above from the trajectory generated using (2.15) and (2.16). The positions obtained from the OK solutions are presented in figure 3.6. The OK solutions show that the flow centre lies at the origin (0,0)

as it should.

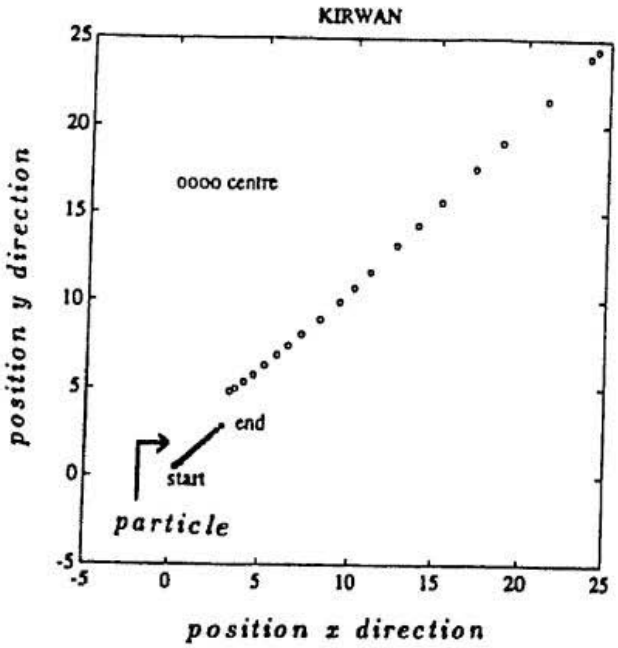

Figure 3.7: The KIRWAN solution for particle trajectory and position of the flow centre calculated from a trajectory with pure shearing.

Using Kirwan's solution for the particle position relative to the flow centre position, i.e. (A13) and (A14) of Kirwan *et al.*, (1988), and subtracting them from the trajectory generated using (2.15) and (2.16) we obtain the plot of flow centre trajectory 'o' in figure 3.7. The particle trajectory obtained from (2.15) and (2.16) is plotted with '*'. It shows that the flow centre moves rapidly, whereas it should be stationary.

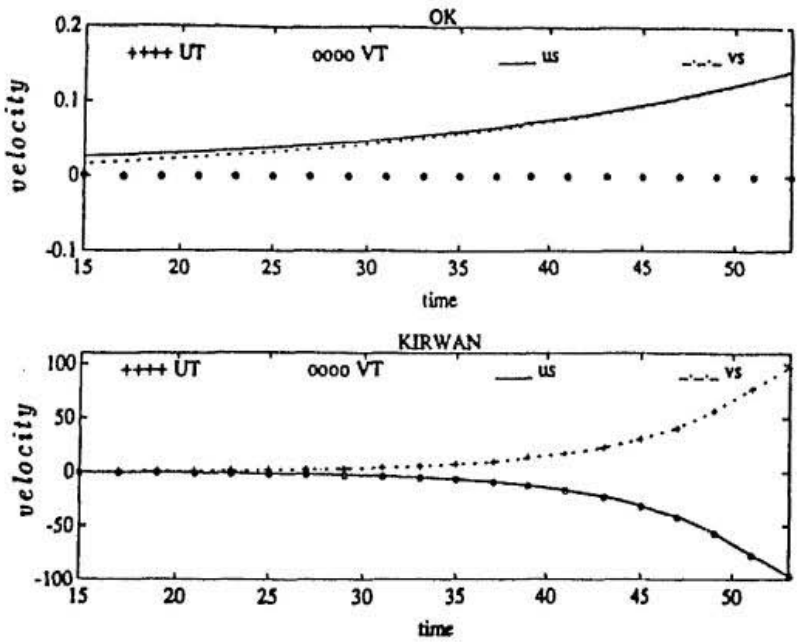

Figure 3.8: Swirl and translational velocities calculated from trajectories with pure shearing, using OK (above) and KIRWAN (below) solutions.

Having obtained the DKP and the position relative to the flow centre, we proceed further to calculating the translation and swirl velocities. In this regard, we make use of (2.51), (2.52), (2.53) and (2.54). The result is presented in figure 3.8 in which we plot the translation velocities, U_T and V_T, together with the swirl velocities, u_s and v_s. The upper diagram are results given by the OK solutions. Here, we find that there is no translation

velocity as shown by the both values of U_T and V_T being equal to zero. This is correct since our simulated eddy has no translation velocities. The trajectory of a particle in this type of pure shearing flow with a positive shearing deformation rate, b, has an asymptote of $x = y$ (see figure 3.6). As a result, both components of swirl velocity (u_s, v_s) enlarge. These features are properly described by the OK solutions.

The lower diagram is obtained using KIRWAN's solutions. It shows that the eddy has translation velocities which are not consistent with the values used to generate the trajectory. We also see that the u_s decreases whereas v_s increases. These values are inconsistent with the trajectory being analyzed.

We have tested the OK and KIRWAN solutions by analysing trajectories with pure shearing. The OK solutions give a correct representation of the flow field. On the other hand, KIRWAN solutions fail to give correct estimates for all kinematic parameters except the divergence.

3.3 Pure Rotation with Translation Velocity

The artificial trajectory for the case of pure rotation is generated using the following expressions:

$$\tilde{x}(t) = U_T\, t + 3\, cos(\omega t) \tag{3.7}$$

$$\tilde{y}(t) = V_T\, t + 3\, sin(\omega t) \tag{3.8}$$

where $\omega = \frac{\pi}{100}$. Here the 3 indicates that the particle moves in a circular trajectory of radius 3 about the flow centre which translates at velocity U_T, V_T.

Putting the angular velocity $\omega = 3.14 \times 10^{-2}$, $U_T = V_T = 0.01$ into (3.7) and (3.8), we get a trajectory for pure rotation about a translating flow centre. The time interval between two successive points is chosen to be 8 units. The OK and KIRWAN solutions are used to analyse the generated trajectory. Note that equations (3.7) and (3.8) could equally well describe a flow field that moves as a sheet so that all points on the sheet have the same (but displaced) circular trajectories relative to a uniform translation U_T, V_T. An inertial oscillation superposed on uniform translation is one example of this type of motion.

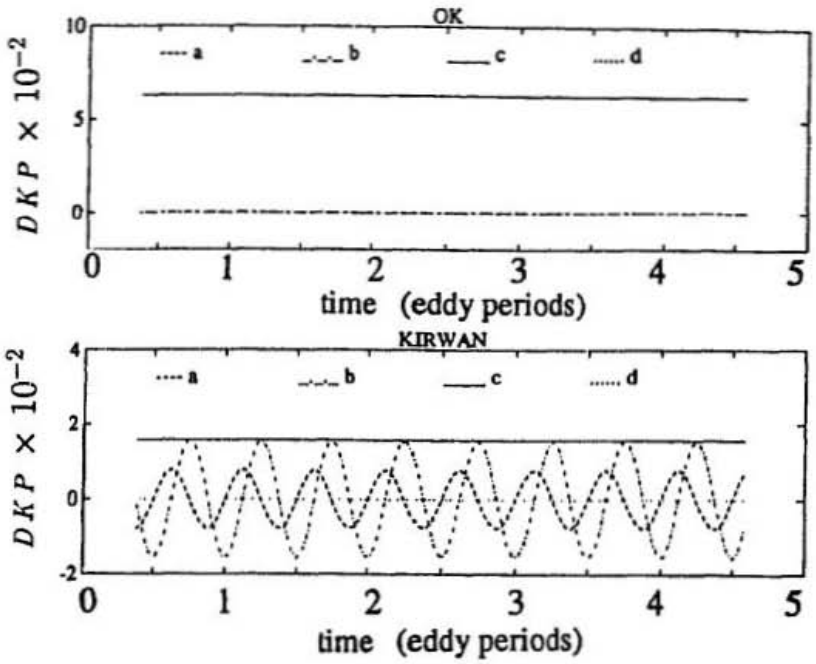

Figure 3.9: The numerically calculated DKP for pure rotation with translation case using OK and KIRWAN.

Figure 3.9 shows the time series of calculated DKP for pure rotation and translation. The upper diagram is obtained by using the OK solutions. It shows a single line at $c = 6.28 \times 10^{-2}$ and three overlapping lines showing $a = b = d = 0$. These values are identical to those used to generate the trajectory.

The lower diagram produced by KIRWAN shows that only the divergence, d, is calculated correctly. This finding is similar to those of the pure stretching

and pure shearing shown earlier. The vorticity, c, is only one fourth of the true value but it is constant. The stretching b and shear c oscillate at twice the rotational frequency of the eddy.

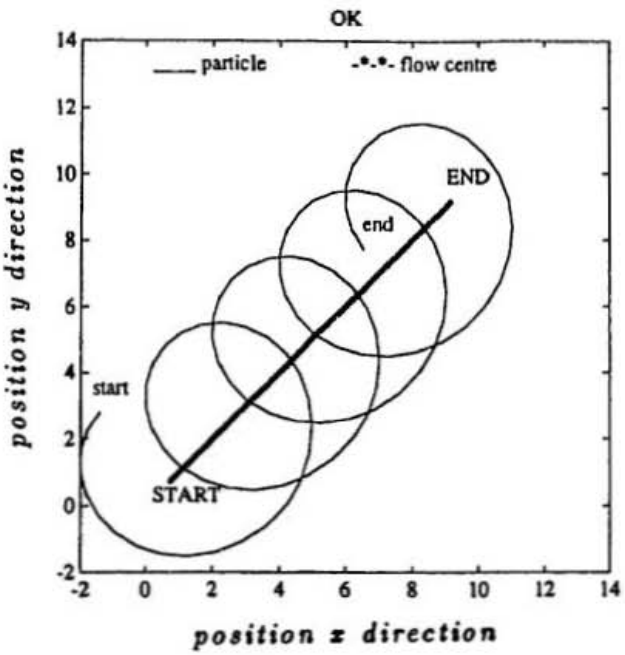

Figure 3.10: The OK solution for particle trajectory and position of the flow centre calculated from a trajectory that rotates around the translating flow centre.

Having obtained the above DKP, we calculate the position of a particle relative to the flow centre using (2.44) and (2.45). The position of the flow centre is obtained by subtracting the position of particle relative to the flow

centre from the trajectory generated using (3.7) and (3.8). The positions obtained from the OK solution are shown in figure 3.10. In this diagram, the '-*-' symbol denotes the flow centre trajectory and the '—' symbol corresponds to the particle's trajectory. Using the OK solution, we find that the flow centre translates northeastward consistent with the flow velocity used to generate the simulated data. The translation velocity will be presented later on.

Using Kirwan's solution for particle position relative to the flow centre, i.e. (A13) and (A14) of Kirwan *et al.*, (1988), and subtracting them from the position of particle generated using (3.7) and (3.8) we obtain the plot of flow centre trajectory '-*-' in figure 3.11. The particle trajectory obtained from (3.7) and (3.8) is plotted with '—'. Figure 3.11 shows that the flow centre moves northeastward while rotating. The radius of its circle is greater than the actual trajectory. This feature shows that KIRWAN gives another incorrect result.

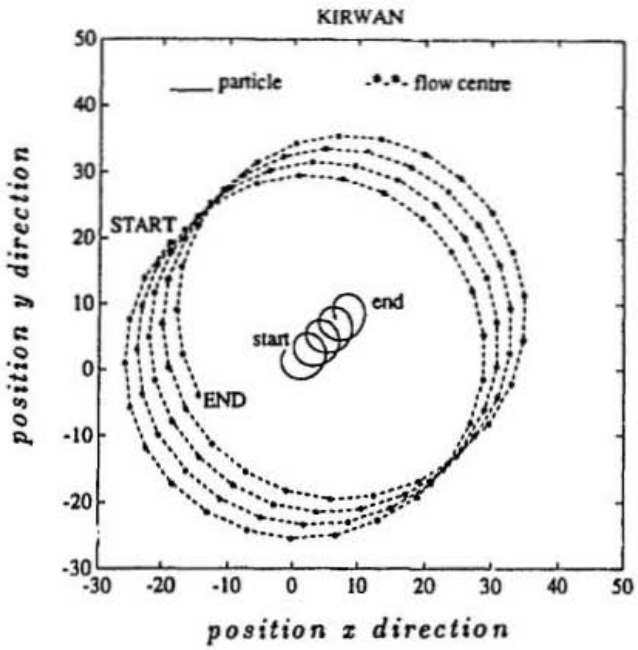

Figure 3.11: The KIRWAN solution for particle trajectory and position of the flow centre calculated from a trajectory that rotates around the translating flow centre.

Having found the DKP and the position relative to the flow centre, we proceed to calculate the flow centre and swirl velocities. In order to get these, we make use of equations (2.51), (2.52), (2.53) and (2.54). In figure 3.12 we plot a time series of the translation velocities, U_T and V_T, together with the swirl velocities, u_s and v_s. The top diagram shows results given by the OK solutions. Here, we find that the particle has a translation velocity with both U_T and V_T equal to 0.01 (the lines are overlapping on the plot). This is exactly

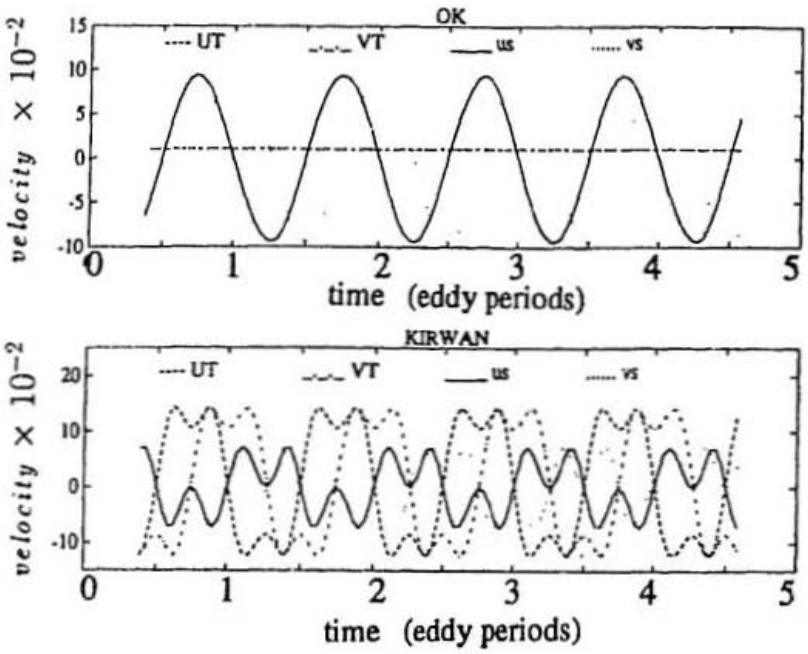

Figure 3.12: Swirl and translation velocities calculated from a trajectory that rotates around a translating flow centre. The top plot is from OK solution and the lower plot is from Kirwan solution.

as same as the values used to simulate the trajectory. The swirl velocity is also obtained correctly. The components of swirl velocity, u, and v, have an amplitude of 9.42×10^{-2} and oscillate at the eddy rotation frequency. The actual amplitude of the swirl velocity is equal to $\omega \times r = \pi \times 10^{-2} \times 3 = 9.42 \times 10^{-2}$. Here, r denotes the distance to the flow centre which is set to 3 in equations (3.7) and (3.8).

The bottom diagram is obtained using KIRWAN's solutions. It shows that the eddy has an oscillating translation velocity which is not consistent with the value used to generate the trajectory. Further, we see that both components of the swirl velocity oscillate but with an incorrect pattern. Again, KIRWAN's results are not in agreement with the parameters used to generate the simulated data.

Parameters	TRUE	OK	KIRWAN
$a\ (\times 10^{-2})$	0	0	-0.78 to 0.78
$b\ (\times 10^{-2})$	0	0	-1.57 to 1.57
$c\ (\times 10^{-2})$	6.28	6.28	1.57
$d\ (\times 10^{-2})$	0	0	0
$U_T\ (\times 10^{-2})$	1	1	-12.33 to 14.33
$V_T\ (\times 10^{-2})$	1	1	-12.33 to 14.33
$u_s\ (\times 10^{-2})$	-9.42 to 9.42	-9.42 to 9.42	-7.25 to 7.25
$v_s\ (\times 10^{-2})$	-9.42 to 9.42	-9.42 to 9.42	-7.25 to 7.25

Table 3.1: Tabulated kinematic properties obtained using OK and KIRWAN and the TRUE values for the pure rotation with translation case

All findings resulting from pure rotation about a translating flow centre are summarized in Table 3.1. The calculated kinematic parameters obtained from the OK solution and the Kirwan *et al.*, (1988) solution are in the columns labelled 'OK' and 'KIRWAN', respectively. The column labelled 'TRUE' shows values used to generate the trajectories. The OK method ob

tains all kinematic parameters correctly. Thus, the OK is able to give a reliable estimation of the flow field for pure rotation with translation. With the exception of divergence d the KIRWAN solution gives kinematic parameters that differ from the true value. There is no doubt that Kirwan's solution (Kirwan *et al.*, 1988) contains errors. The vorticity e obtained from the KIRWAN solution is at least steady (whereas a and b fluctuate). Previous investigators (Lewis and Kirwan, 1987; Kirwan *et al.*, 1988; Indest *et al.*, 1989; Lewis *et al.*, 1989; Kirwan *et al.*, 1990) have applied their solution to drifter tracks in a large rotating eddy. The KIRWAN solution probably gives reasonable looking divergence and vorticity when it is used to look at such rotating eddies, but the vorticity will be too small by a factor of 4.

We have tested both the OK and KIRWAN solutions using several generated trajectories with kinematic properties ranging from pure stretching and deformation without translation to pure rotation with translation. In all cases, the OK solution successfully obtains all kinematic properties from the trajectories. As a result, the OK method is able to describe the flow field characteristics quite well. On the other hand, only divergence can be found correctly using the KIRWAN solution. The other parameters and the kinematic properties of the flow field are not in agreement with values used to

generate the trajectories. This is not surprising since only the divergence has a common expression in both the OK and KIRWAN solutions (see equation (2.40) in Chapter 2 of this thesis and (A.12) of Kirwan *et al.*, (1988)).

Special attention will be given to Kirwan's solutions. Having read his laboratory notes which demonstrate his elegant procedure for deriving the solutions, we have located the points at which algebraic errors have been made. The errors are caused by wrongly expressing the value of $a^2 + b^2 - c^2 - d^2$ in terms of parameter M^2, the determinant matrix of the DKP (Kirwan's laboratory notes). Instead of using $a^2 + b^2 - c^2 - d^2 = -1M^2$, he probably used $a^2 + b^2 - c^2 - d^2 = -M^2$ when solving for X and Y. Also, he used $a^2 + b^2 - c^2 - d^2 = -2M^2$ instead of using $a^2 + b^2 - c^2 - d^2 = -1M^2$ when solving for M^2. If we correct the above substitutions in Kirwan's laboratory notes then we have shown that the parameters M^2, X, Y would be calculated correctly and would be the same as our OK solutions. We did not check whether or not this would be sufficient to correct his solutions for a, b and c. Now, we are promoting the OK solutions for correctly determining the flow field singularities from a single drifter trajectory. Let us be clear on one matter, however, it was the work of Kirwan *et al.*, (1988) that provided the method of solution, whereas we have merely corrected the algebra. Of

course Kirwan *et al.*, (1988) was really inverting Okubo's (1970) study for flow around a flow field singularity. Hence we label the OK solutions in honour of the people principally responsible for obtaining them.

3.4 The Effect of Random Noise on the OK Method

This section will focus on how the OK method is affected by noise. The noise added to the trajectory has also a normal distribution. This kind of distribution is commonly encountered in nature. The amount of noise is given in terms of the S/N ratio, which measures the strength of signal relative to the noise. This noise is added to the trajectory of pure rotation given by (3.7) and (3.8). The OK solution is then used to obtain the DKP from the noisy trajectory.

The following steps will be employed to create the normally distributed noise. We generate a uniformly distributed noise by using the IMSL subroutine called 'RNUNF'. This subroutine is a multiplicative congruential generator and it produces a random number between 0 and 1 (Neelamkavil, 1987).

It has an iteration relation

$$rnum_i = K\ rnum_{i-1}\ mod(2^{31}-1)$$

where $rnum_{i-1}$ is the initial value, the seed, and K is a constant which has a value of $7^5 = 16,807$ (Law and Kelton, 1982). Next, this uniformly distributed noise is transformed to a normally distributed noise. To produce this kind of noise, we use the so-called 'polar method' (Marsaglia and Bray, 1964). The method will generate random numbers which have a mean of 0 and a variance of 1 (Morgan, 1984; Press *et al.*, 1986).

The normally distributed random numbers $R(t)$ produced by the above method are added to the trajectories

$$\tilde{x}(t) = U_T\ t + 3\cos\omega\ t + A\ R(t) \tag{3.9}$$

$$\tilde{y}(t) = V_T\ t + 3\sin\omega\ t + A\ R(t) \tag{3.10}$$

where $\omega = \frac{\pi}{100}$ and A is the noise amplitude. The time interval between successive positions is chosen to be 8 units. We will use the translation velocities, $U_T = V_T = 0.01$ for the following work. Without the noise, the DKP are $a = b = d = 0$, $c = 2\ \omega = 6.28 \times 10^{-2}$. Three different trajectories will be created corresponding to values of $A = 10^{-3}, 10^{-2}, 10^{-1}$. These trajectories will have different S/N ratios according to the noise amplitude. The

amplitudes, A, of $10^{-3}, 10^{-2}, 10^{-1}$ will correspond to S/N ratios of 530, 53, 5.3, respectively. These S/N ratios are obtained by dividing the root mean square value of the velocity obtained from (3.27) and (3.28) with $A = 0$ by the root mean square value of the noise velocity. Having obtained these noise contaminated trajectories, the OK method will be used to analyse each trajectory in turn.

Effects of the random noise on the DKP are shown in figure 3.13. The lower diagram shows that if the signal is relatively strong compared to the noise (i.e. S/N of 530), we may still obtain DKP which are close to the values without noise, i.e. $A = 0$. The middle plot in figure 3.13 shows a S/N of 53 and the upper plot shows a S/N of 5.3. As the noise level increases, the random variability dominates the calculated DKP. A relatively small amount of noise in the trajectory causes a large amount of noise in the calculated DKP. For example, when the signal to noise ratio for the trajectory velocity is 53 the signal to noise ratio of the vorticity calculated by the OK method is only $\frac{6.28}{4.5} = 1.4$.

The trajectory and calculated positions of the flow centre are shown in figure 3.14. In the lower diagram, we see that for very weak noise the position of the flow centre is close to the position without noise. With a S/N of 5.3

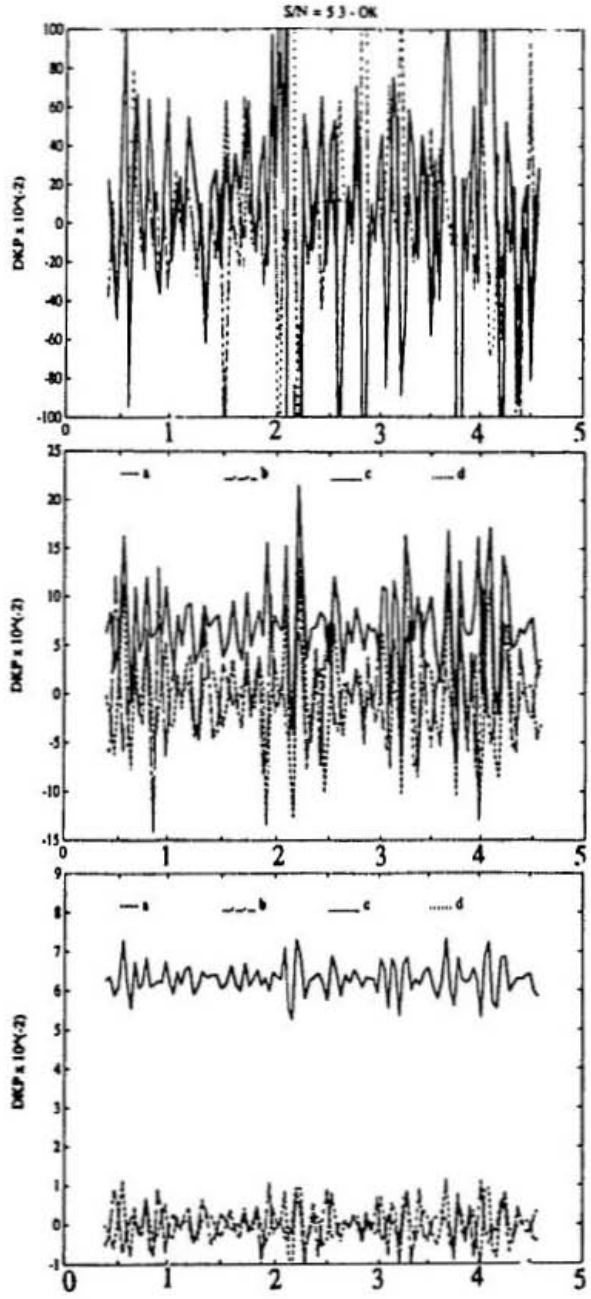

Figure 3.13: The DKP calculated using the OK method with S/N ratios of 5.3 (top), 53 (middle) and 530 (bottom).

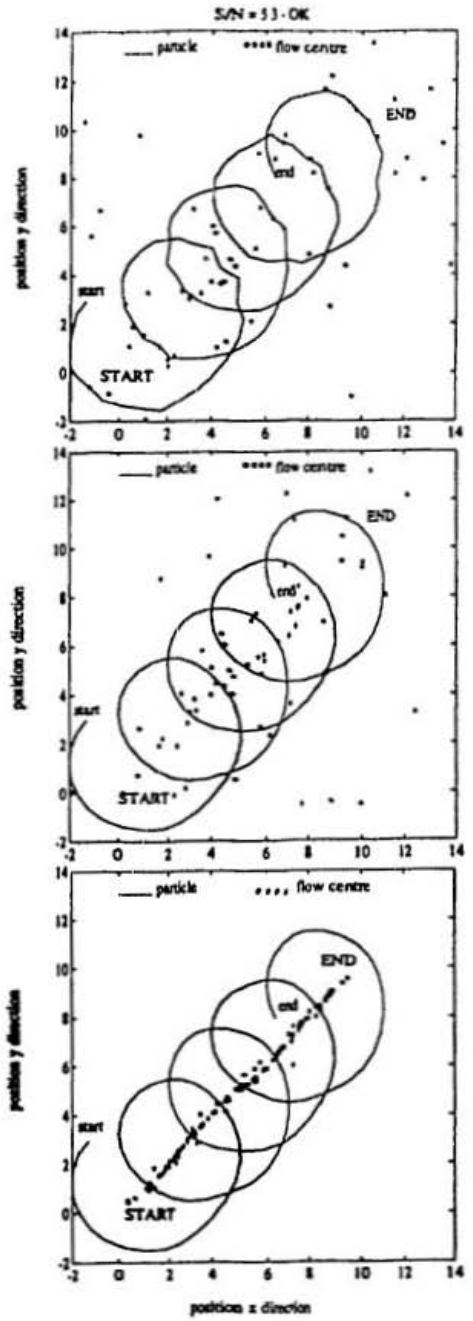

Figure 3.14: The particle's trajectory and calculated positions of the flow centre using the OK method with S/N ratios of 5.3 (top), 53 (middle) and 530 (bottom).

Estimated	*S/N ratio*		
parameters	5.3	53	530
$a \times 10^{-2}$	-12 ± 17	0.0 ± 0.5	0.00 ± 0.05
$b \times 10^{-2}$	3 ± 8	0.0 ± 0.5	0.00 ± 0.05
$c \times 10^{-2}$	-13 ± 18	7.2 ± 0.4	6.28 ± 0.01
$d \times 10^{-2}$	-1.1 ± 6	0.0 ± 0.4	0.00 ± 0.04

Table 3.2: Average values of DKP obtained from noisy data. The averaging was done over 106 points. The signal to noise ratio of the raw data was 5.3, 53, 530 for the three cases considered.

(upper diagram) or 53 (middle diagram), the positions of the flow centre scatter all over the place. These scattered positions are caused by the large variability in the calculated DKP.

We expect that averaging will reduce the noise induced fluctuations in the DKP. However, such averaging will also eliminate real high frequency signals in the DKP. This is not at issue for the present case since we are considering DKP that are constant.

Table 3.2 shows the effect of noise on estimating the DKP using the OK method. Three different noise levels, characterized by the S/N ratios of the raw generated data are examined. The generated data had S/N ratios of 5.3, 53, 530 and the corresponding columns in Table 3.2 are labelled '5.3', '53', '530'. These values of DKP are calculated for a trajectory comprising

106 drifter positions, thus giving 106 estimates of each DKP parameter from which the mean value and standard deviation of this mean are obtained.

Averaging over 106 independent estimates is sufficient to yield a useful estimate of c for the data that has a S/N of 53, however, it is not enough when S/N is 5.3.

It is clear that the OK method is very sensitive to noise. A similar finding has been presented earlier by Kirwan *et al.*, (1990). The source of noise may be the experimental error in fixing the drifter position, the small scale variations in the flow field and the up to fourth order numerical differentiation scheme inherently possessed by the OK method. Smoothing the trajectories by filtering can greatly improve the performance of the OK method. But such filtering also eliminates high frequency information. A new cluster method that does not involve so many higher order differentiations will be presented in the next chapter.

Chapter 4

A New Regression Method for Calculating DKP from a Cluster of Drifters: the HS Method

Velocity gradients can be calculated from a single trajectory under the assumption that the Eulerian flow field is stationary and the flow field centre (i.e. singularity position) is fixed (Kirwan *et al.*, 1988). However, this has

the disadvantage that the fourth time derivative of drifter position must be calculated. A small amount of measurement error can lead to such higher order derivatives being very unreliable.

Okubo and Ebbesmeyer (1976) use a linear regression method to calculate velocity gradients from the position and velocity of many drifters. This method assumes the flow centre is fixed to the cluster centroid and that the velocity gradient is common to all drifters. Kirwan (1988) shows that fixing the flow centre to the cluster centroid can cause serious biasing whereby energy might be transferred from the swirl velocity to the translation velocity for example.

Let us now develop a way to calculate velocity gradients from a cluster of drifters. We will not fix the flow singularity centre to the cluster centroid. However, we will assume that the same velocity gradient applies to all drifters in a cluster occupying a local region of space. Our new method will only require up to the second time derivative of drifter position. It is still based upon a linear regression but we will be doing a best fit to a different model from that of Okubo and Ebbesmeyer (1976).

Okubo and Ebbesmeyer (1976) did a least squares fit for a model that consisted of motion being described by a mean flow equal to the centroid

velocity and linear velocity gradients causing velocities proportional to the displacement from the centroid position. Our new approach fits the data to a model where the flow centre does not accelerate and linear velocity gradients cause velocities proportional to the displacement from the position of the flow centre. The position and velocity of the flow centre are variables that are regressed for, in addition to the velocity gradients. Okubo and Ebbesmeyer (1976) use a regression to solve for the centroid velocity and velocity gradients. Our stipulation of zero flow centre acceleration gives further regression equations so that we can also solve for flow centre position and velocity.

Consider a cluster with n drogues in it. The velocity of the i^{th} drogue can be expressed as:

$$u_i = U_T + a^*(\tilde{x}_i - X_T) + b^*(\tilde{y}_i - Y_T) + u_i^r \qquad (4.1)$$

$$v_i = V_T + c^*(\tilde{x}_i - X_T) + d^*(\tilde{y}_i - Y_T) + v_i^r \qquad (4.2)$$

where $a^* = \frac{\partial u}{\partial x}$, $b^* = \frac{\partial u}{\partial y}$, $c^* = \frac{\partial v}{\partial x}$, and $d^* = \frac{\partial v}{\partial y}$ are the velocity gradients, U_T, V_T are the velocities of the flow centre, X_T, Y_T are the position of the flow centre, $\tilde{x}_i$, $\tilde{y}_i$ is the position of the i^{th} drifter (i = 1, 2, ..., n), and u_i^r, v_i^r are the residual velocities. Note that the DKP can be determined from

the above velocity gradients by making use of (2.4). Differentiating (4.1) and (4.2) with respect to time (indicated by a prime) gives

$$u_i' = a^* u_i - a^* U_T + b^* v_i - b^* V_T + u_i^{r\prime} \tag{4.3}$$

$$v_i' = c^* u_i - c^* U_T + d^* v_i - d^* V_T + v_i^{r\prime} \tag{4.4}$$

where the flow center is assumed not to accelerate ($\frac{d}{dt}U_T = \frac{d}{dt}V_T = 0$) and a^*, b^*, c^*, d^* are taken to be constant over a time interval. Equations (4.3) and (4.4) can be rewritten into a standard form for a linear regression model

$$u_i' = \alpha + a^* u_i + b^* v_i + u_i^{r\prime} \tag{4.5}$$

$$v_i' = \beta + c^* u_i + d^* v_i + v_i^{r\prime} \tag{4.6}$$

where

$$\alpha = -a^* U_T - b^* V_T \tag{4.7}$$

$$\beta = -c^* U_T - d^* V_T. \tag{4.8}$$

Expressing (4.5) and (4.6) as a matrix equation:

$$A = UG + R \tag{4.9}$$

where

$$A = \begin{pmatrix} a'_1 & c'_1 \\ \cdot & \cdot \\ \cdot & \cdot \\ \cdot & \cdot \\ a'_n & c'_n \end{pmatrix}$$

$$U = \begin{pmatrix} 1 & a_1 & c_1 \\ \cdot & \cdot & \cdot \\ \cdot & \cdot & \cdot \\ \cdot & \cdot & \cdot \\ 1 & a_n & c_n \end{pmatrix}$$

$$G = \begin{pmatrix} \alpha & \beta \\ a^* & c^* \\ b^* & d^* \end{pmatrix}$$

$$R = \begin{pmatrix} u_1^{r'} & v_1^{r'} \\ . & . \\ . & . \\ . & . \\ u_n^{r'} & v_n^{r'} \end{pmatrix}$$

Standard linear regression (Draper and Smith, 1966; Okubo and Ebbesmeyer, 1976; Okubo *et al.*, 1976) yields the following solution for $\alpha, \beta, a^*, b^*, c^*, d^*$

$$G = [U^T U]^{-1} U^T A \tag{4.10}$$

and residual accelerations $u_i^{r'}, v_i^{r'}$

$$R = [1 - U(U^T U)^{-1} U^T] A. \tag{4.11}$$

Note that this regression technique will produce biased estimates of the coefficients caused by uncertainties in both the independent and dependent variables (Kirwan and Chang, 1979). Having obtained α, β, a^*, b^*, c^*, and d^* from (4.10), we use (4.7) and (4.8) to solve for U_T and V_T. The expressions for U_T and V_T are

$$U_T = \frac{d^*\alpha - b^*\beta}{b^*c^* - a^*d^*} \tag{4.12}$$

$$V_T = \frac{a^*\beta - c^*\alpha}{b^*c^* - a^*d^*}. \tag{4.13}$$

We are now in a position to solve for X_T and Y_T. We rewrite (4.1) and (4.2) as

$$u_i = \varphi + a^* \tilde{x}_i + b^* \tilde{y}_i + u_i' \tag{4.14}$$

$$v_i = \phi + c^* \tilde{x}_i + d^* \tilde{y}_i + v_i' \tag{4.15}$$

where

$$\varphi = U_T - a^* X_T - b^* Y_T \tag{4.16}$$

$$\phi = V_T - c^* X_T - d^* Y_T. \tag{4.17}$$

To find ϕ and φ (and thereby X_T, Y_T) we do a least squares regression on equations (4.14) and (4.15). The sum of the squares of the residuals in (4.14) and (4.15) are

$$S_1 = \sum_{i=1}^{n} (u_i')^2 = \sum_{i=1}^{n} (u_i - a^* \tilde{x}_i - b^* \tilde{y}_i - \varphi)^2$$
$$S_2 = \sum_{i=1}^{n} (v_i')^2 = \sum_{i=1}^{n} (v_i - c^* \tilde{x}_i - d^* \tilde{y}_i - \phi)^2.$$

The following normal equations are found by minimizing the sum of the squares of the residuals

$$\frac{\partial S_1}{\partial \varphi} = 0 \Longrightarrow -2 \sum_{i=1}^{n} (u_i - a^* \tilde{x}_i - b^* \tilde{y}_i - \varphi) = 0$$
$$\frac{\partial S_2}{\partial \phi} = 0 \Longrightarrow -2 \sum_{i=1}^{n} (v_i - c^* \tilde{x}_i - d^* \tilde{y}_i - \phi) = 0$$

and, thereby, we solve for ϕ and φ.

$$\varphi = \frac{\sum_{i=1}^{n} u_i - a^* \sum_{i=1}^{n} \tilde{x}_i - b^* \sum_{i=1}^{n} \tilde{y}_i}{n} \tag{4.18}$$

$$\phi = \frac{\sum_{i=1}^{n} v_i - c^* \sum_{i=1}^{n} \tilde{x}_i - d^* \sum_{i=1}^{n} \tilde{y}_i}{n} \tag{4.19}$$

Note that equations (4.18) and (4.19) can be equivalently obtained by averaging (4.14) and (4.15) over all drifters and requiring that $\sum_{i=1}^{n} u_i^r = 0$ and $\sum_{i=1}^{n} v_i^r = 0$. Now, the expressions for the position of the flow centre, X_T and Y_T, can be obtained by substituting (4.18) and (4.19) into (4.16) and (4.17) respectively.

$$X_T = \frac{(V_T - \phi)b^* - (U_T - \varphi)d^*}{b^*c^* - a^*d^*} \tag{4.20}$$

$$Y_T = \frac{(U_T - \varphi)c^* - (V_T - \phi)a^*}{b^*c^* - a^*d^*} \tag{4.21}$$

Having located the flow centre and velocity gradients, we can write the swirl velocity of the i^{th} drifter as

$$u_{si} = a^*(\tilde{x}_i - X_T) + b^*(\tilde{y}_i - Y_T) \tag{4.22}$$

$$v_{si} = c^*(\tilde{x}_i - X_T) + d^*(\tilde{y}_i - Y_T) \tag{4.23}$$

and the residual velocity of the i^{th} drifter becomes

$$u_i^r = u_i - U_T - u_{si} \tag{4.24}$$

$$v_i^r = v_i - V_T - v_{si} \tag{4.25}$$

The velocity of the the i^{th} drifter in (4.1) and (4.2) has been divided into translation of the flow centre (4.12), (4.13); a swirl velocity (4.22), (4.23); and a residual velocity (4.21), (4.25). Thus (4.10), (4.12), (4.13), (4.20) and (4.21) constitute a complete set of equations for a^*, b^*, c^*, d^*, U_F, V_F, , X_I, Y_F. The swirl velocities are given by (4.22) and (4.23) and are different for each drifter, depending upon where the drifter is relative to the flow centre. The application of this system of equations to obtain DKP will subsequently be referred to as the HS method and the equations will be referred to as the HS equations. The magnitude of the residual velocity compared to the magnitude of the total drifter velocity indicates how much of the variance is accounted for by the model.

Chapter 5

Testing and Comparing Techniques for Obtaining DKP from Drifter Trajectories

The HS method can be used to calculate velocity gradients, the flow centre position, and the flow centre translation velocity from the motion of a cluster of drifters. In the following sections, the HS method will be applied to data and will be compared with Okubo and Ebbesmeyer's (1976) cluster method and the OK solution obtained in Chapter 2. First we will analyse

artificially generated data that has known DKP. Subsequently we analyse drifter measurements made in the spring of 1991 on Sable Island Bank on the Scotian Shelf.

5.1 Artificially Generated Data

In this section, three trajectories are generated analytically. These trajectories simulate an eddy with pure rotation and a translating flow centre, as in subsection (3.3) of Chapter 3. The Okubo and Ebbesmeyer (1976), OK and HS methods are applied to obtain the kinematic properties of this artificial data. Subsequently the method of Okubo and Ebbesmeyer will be referred as the 'OE' method. To calculate the kinematic parameters and the position and the velocity of the flow centre using HS method, one has to calculate the velocities and the accelerations of each drifter in a cluster. On the other hand, one does not need to compute accelerations when using the OE method (Okubo and Ebbesmeyer, 1976) to obtain the DKP and the mean velocity of the cluster. The OE method gives information about the centroid velocity/position rather than the flow centre velocity/position. The OE method is, therefore, fundamentally different from the HS and the OK

methods. We only expect the OE method to be equivalent to the OK and the HS methods in the special circumstance that the flow centre position and velocity coincide with the cluster centroid position and velocity.

The three artificial drifter trajectories are denoted by subscripts 1, 2, 3 indicating the drifter's number.

$$\tilde{x}_1(t) = U_T\, t + 2.9\, cos(\omega(t-2)) \tag{5.1}$$

$$\tilde{y}_1(t) = V_T\, t + 2.9\, sin(\omega(t-2)) \tag{5.2}$$

$$\tilde{x}_2(t) = U_T\, t + 3.0\, cos(\omega t) \tag{5.3}$$

$$\tilde{y}_2(t) = V_T\, t + 3.0\, sin(\omega t) \tag{5.4}$$

$$\tilde{x}_3(t) = U_T\, t + 3.1\, cos(\omega(t-1)) \tag{5.5}$$

$$\tilde{y}_3(t) = V_T\, t + 3.1\, sin(\omega(t-1)) \tag{5.6}$$

where $\omega = \frac{\pi}{100}$, $U_T = V_T = 0.01$. The time interval between two consecutive data points is taken to be 8 units as before. The artificially generated data can be seen in figure 5.2. In the OE method, one has to calculate the centroid position, x_c and y_c. This position can be obtained by using

$$x_c(t) = \frac{\tilde{x}_1(t) + \tilde{x}_2(t) + \tilde{x}_3(t)}{3} \tag{5.7}$$

$$y_c(t) = \frac{\tilde{y}_1(t) + \tilde{y}_2(t) + \tilde{y}_3(t)}{3}. \tag{5.8}$$

The velocity and acceleration of each drifter are numerically calculated as in chapter 3.

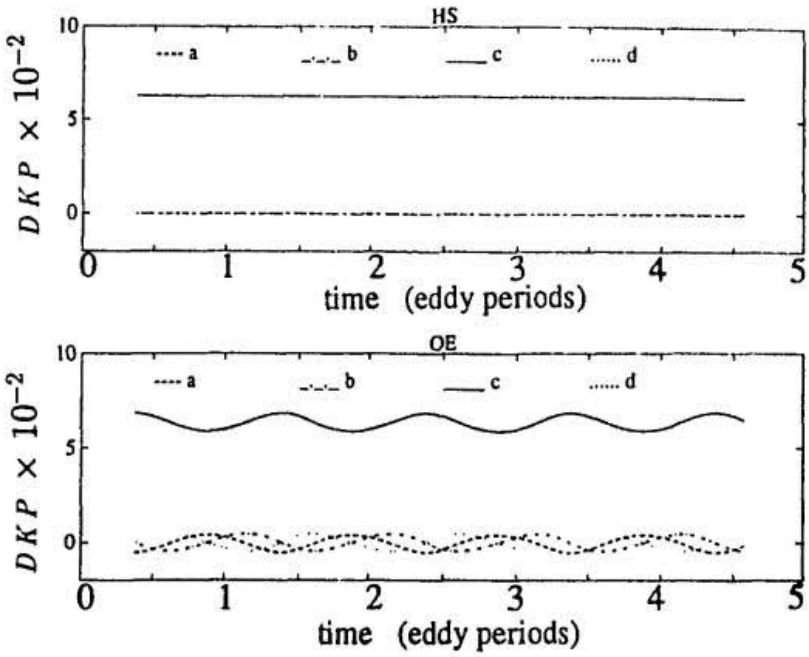

Figure 5.1: The numerically calculated DKP of pure rotation with translation case using the HS and the OE.

Figure 5.1 shows the time series of calculated DKP for the simulated trajectories with pure rotation and translation. The diagram at the top is obtained by using the HS solutions and gives the correct values for all parameters, e.g. $c = 2\,\omega = 6.28 \times 10^{-2}, b = c = d = 0$. These are shown by one line at 6.28×10^{-2} and three overlapping lines merge into a single

line at 0.0. Note also that these values are independent of time. The same result has been reported in the earlier analysis using the OK solutions (refer to figure 3.9). It means that both the HS and OK successfully obtain the DKP from simulated data.

The bottom diagram in figure 5.1 shows DKP obtained by using the OE method. All the DKP a, b, c, d oscillate about their true value. This oscillation is at the frequency of rotation. These oscillations result from the so-called biasing problem discussed by Kirwan (1988). The biasing can be viewed as energy from the swirl velocity contributing to both the velocity gradients, i.e. the DKP, and the translation velocity of the flow field.

The position of the flow centre is obtained from the HS method by using (4.20) and (4.21). This position is plotted in figure 5.2, along with the three simulated drifter tracks. In this diagram, the '*****' denotes the flow centre position and the drifter's positions are represented by three different types of lines, i.e. dash, solid, dot and dash lines. Using the HS method, we find that the flow centre translates northeastward consistent with values of U_T, V_T used to generate the trajectories. This result is also obtained from the OK method as shown in figure 3.10. Here, we can not compare the HS and OK methods with the OE since the latter does not solve for the flow centre

position.

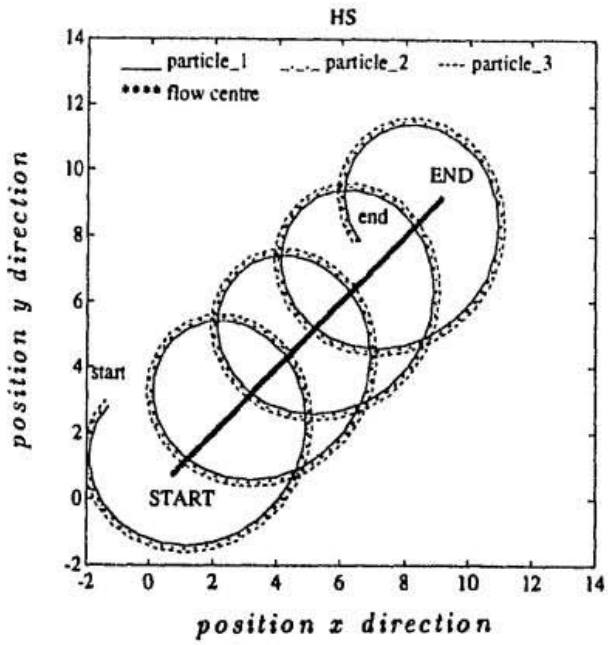

Figure 5.2: Trajectories of three particles with pure rotation about a translating flow centre. The flow centre trajectory has been calculated using the HS method.

In the case of the HS method, translation velocities of the above flow centre can be calculated from (4.12) and (4.13). Also, having obtained the DKP and the position of the flow centre, we use (4.22) and (4.23) to calculate the swirl velocity. The results of the HS method are given on a diagram at the top of figure 5.3. In this diagram, we plot both the translation velocities

denoted by 'UT' and 'VT' as well as the swirl velocities, 'us' and 'vs'. We see that the translation velocities represented by two overlapping lines at 1.0×10^{-2} which is exactly the value used to generate the data. The components of swirl velocity are shown by two oscillating lines at the frequency of rotation and with an amplitude of 9.42×10^{-2} which are in accordance with the amplitude and frequency of the oscillating functions used to generate the data. These results are the same as the OK analysis described earlier (refer to figure 3.12). Again, we can see that both the HS and OK methods produce the same result.

In the lower diagram, however, we find quite different results. It shows the cluster centroid velocity denoted by 'U_BAR' and 'V_BAR'calculated by the OE method. The amplitude and the frequency of oscillation are almost the same as for the swirl velocities obtained by the HS and OK methods. The only difference is that the components of centroid velocity are shifted upward by 1.0×10^{-2}. This amount of shifting is equal to the translation velocity of the flow centre.

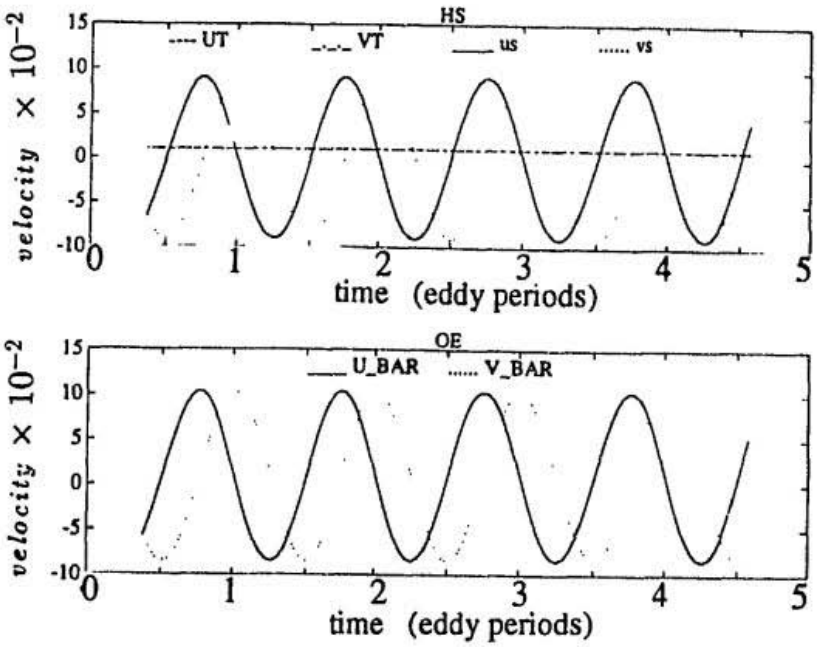

Figure 5.3: The numerically calculated velocities for the pure rotation with translation case using the HS and the OE.

The results of the three different methods are summarized in the columns labelled 'OK', 'HS', and 'OE' along with the 'TRUE' value in table 2. It is clear that both the OK and HS methods give the same result for all of the calculated parameters and they are in agreement with the true values used to generate the simulation data. The OE solution shows the biasing problem that has been elucidated by Kirwan (1988). We have put the centroid velocity for the OE method in the rows showing swirl velocity for the OK and HS

methods. The centroid velocity is the sum of the swirl velocity plus the velocity of the translating flow centre. We have also tested the HS method

Parameters	TRUE	OK	HS	OE
a $(\times 10^{-2})$	0	0	0	-0.39 to 0.31
b $(\times 10^{-2})$	0	0	0	-0.35 to 0.35
c $(\times 10^{-2})$	6.28	6.28	6.28	5.97 to 6.67
d $(\times 10^{-2})$	0	0	0	-0.35 to 0.35
U_T $(\times 10^{-2})$	1.0	1.0	1.0	-
V_T $(\times 10^{-2})$	1.0	1.0	1.0	-
u_s $(\times 10^{-2})$	-9.42 to 9.42	-9.42 to 9.42	-9.42 to 9.42	-8.42 to 10.42
v_s $(\times 10^{-2})$	-9.42 to 9.42	-9.42 to 9.42	-9.42 to 9.42	-8.42 to 10.42

Table 5.1: Kinematic parameters calculated by the three different methods for the case of pure rotation with translating flow centre.

on three generated trajectories for case of pure stretching. The results are the same as those obtained using the OK method and are consistent with parameters used to generate the trajectories. This means that both the OK and the HS are able to determine the flow field properties correctly.

Summarizing, we have found two methods that can correctly calculate the flow field properties from drifter trajectories for the case of pure stretching and rotation with translating flow centre that have only one flow field singularity. These are the OK or the HS methods. The OK method requires that we calculate up to fourth order derivatives of position, whereas the HS

method only requires up to second order derivatives. Numerical instabilities can occur when we take high order derivatives. We expect, therefore, that in this regard the HS method has an advantage over the OK method. The HS method has the disadvantage, however, in that it requires more drifters than the OK method. We still need to perform one more test to examine the sensitivity of the HS method to noise. This is a similar test to that used in the OK method before.

5.2 The Effect of Noise on the HS method

In this section, the effect of noise will be evaluated. The noise $AR(t)$ has the same characteristics as that used in Chapter 3, e.g. normally distributed noise with mean of zero and variance of A^2. The noise is added to the trajectories with the same kinematic properties that were used in subsection 5.1

$$\tilde{x}_1(t) = U_T\,(t-) + 2.9\,cos\,(\omega(t-2\Delta)) + A\,R(t) \tag{5.9}$$

$$\tilde{y}_1(t) = V_T\,(t) + 2.9\,sin\,(\omega(t-2\Delta)) + A\,R(t) \tag{5.10}$$

$$\tilde{x}_2(t) = U_T\,(t) + 3.0\,cos\,(\omega t) + A\,R(t) \tag{5.11}$$

$$\tilde{y}_2(t) = V_T\,(t) + 3.0\,sin\,(\omega t) + A\,R(t) \tag{5.12}$$

$$\tilde{x}_3(t) = U_T\ (t) + 3.1\ cos\ (\omega(t-\Delta)) + A\ R(t) \qquad (5.13)$$

$$\tilde{y}_3(t) = V_T\ (t) + 3.1\ sin\ (\omega(t-\Delta)) + A\ R(t) \qquad (5.14)$$

where $\omega = \frac{\pi}{100}$, $AR(t)$ is the Gaussian noise with a root mean square amplitude A, and Δ is the time interval between two successive points and it is chosen to be 8 units. We still use the translation velocities $U_T = V_T = 0.01$ as before. Without the noise, the DKP are $a = b = d = 0$, $c = 2\,\omega = 6.28 \times 10^{-2}$. Three trajectories will be generated using these values for each given noise amplitude. The noise amplitudes, A, of 10^{-3}, 10^{-2}, 10^{-1} will correspond to S/N ratios of 530, 53, 5.3, respectively. Having obtained these noise-contaminated trajectories, the IIS method will be used to analyse trajectories of three particles in a cluster for each noise level.

Effects of the random noise on the DKP are shown in figure 5.4. The lower diagram shows that if the signal is relatively strong compared to the noise, (i.e. S/N of 530), we may still obtain DKP which are close to the values without noise, i.e. $A = 0$. The middle plot in figure 5.4 shows a S/N of 53 and the upper plot shows a S/N of 5.3. As the noise level increases, the random variability dominates the calculated DKP. A relatively small amount of noise in the signal brings about a large amount of noise in the calculated

DKP. For example, when the signal to noise ratio for the trajectory is 53 the signal to noise ratio of the vorticity calculated by the HS method is only $\frac{6.3}{10.1} = 0.62$. This is a factor of 2 lower than the signal to noise ratio for DKP that was calculated earlier using the OK method.

The trajectory and calculated positions of the flow centre are shown in figure 5.5. In the lower diagram, we see that for very weak noise the position of the flow centre is close to the position without noise. With a S/N of 5.3 (upper diagram) or 53 (middle diagram), the positions of the flow centre scatter all over the place. These scattered positions are caused by the large variability in the calculated DKP.

The generated data had S/N ratios of 5.3, 53, 530 and the corresponding columns in Table 5.2 give the mean DKP and their standard deviation. These values are calculated for a trajectory comprising 106 drifter positions. Averaging over 106 independent estimates is sufficient to yield a useful estimate of c for the data that has a S/N of 53, however, it is not enough when S/N is 5.3. We see that the HS method is very sensitive to noise.

We have shown one example where the HS method is more sensitive to noise than the OK method. This is interesting since the former contains only first-order derivatives whereas the latter method has up to third-order

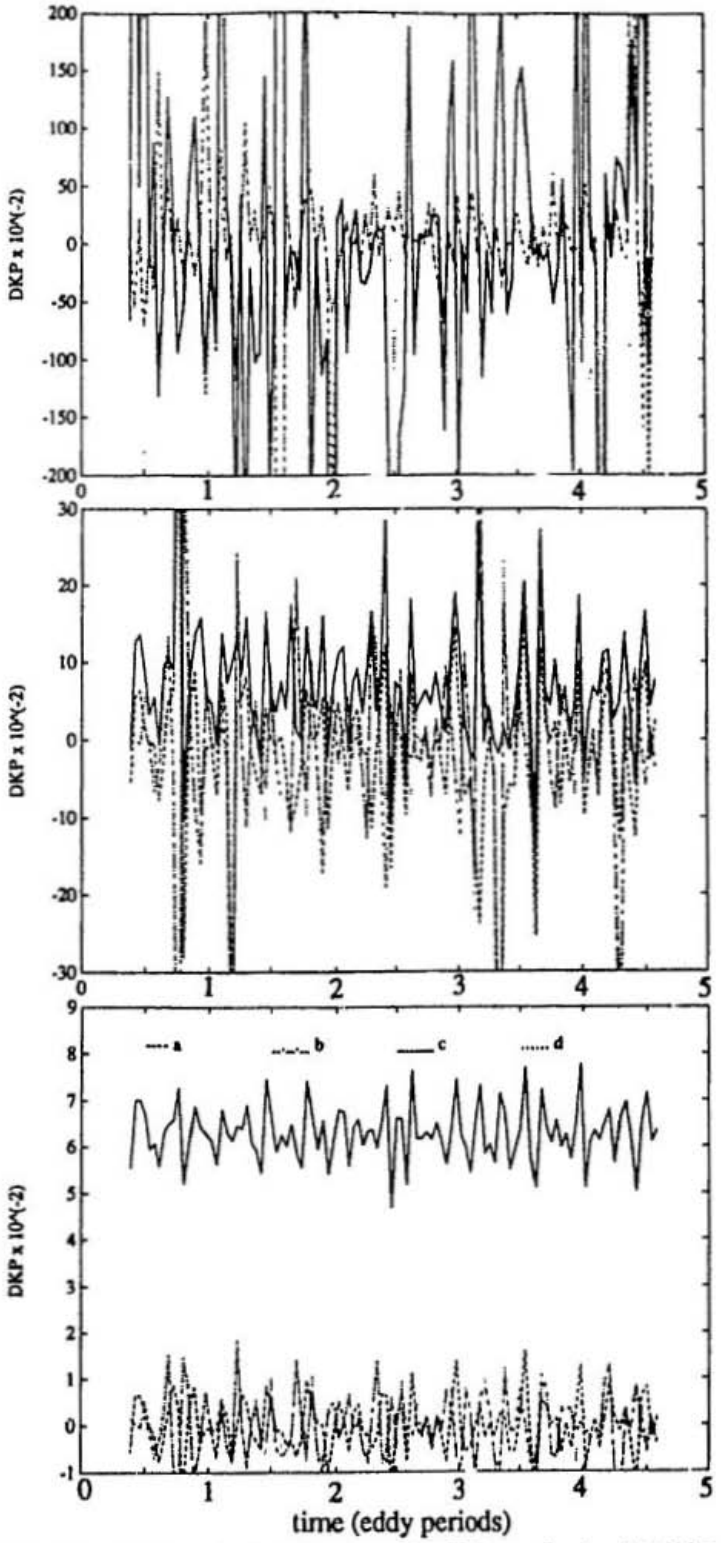

Figure 5.4: The DKP calculated using the HS method with S/N ratios of 5.3 (top), 53 (middle) and 530 (bottom).

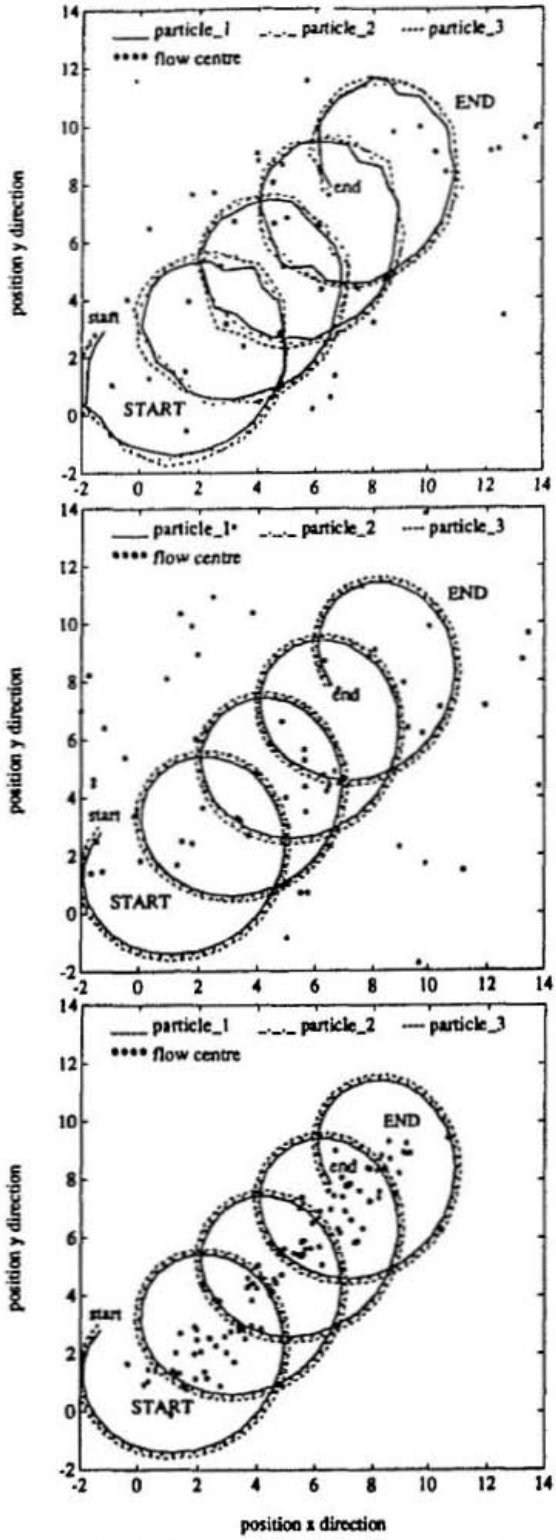

Figure 5.5: The particle's trajectory and calculated positions of the flow centre using the HS method with S/N ratios of 5.3 (top), 53 (middle) and 530 (bottom).

Estimated	*S/N ratio*		
parameters	5.3	53	530
$a \times 10^{-2}$	47 ± 50	-1.7 ± 1.1	0.0 ± 0.1
$b \times 10^{-2}$	-12 ± 19	-1.4 ± 1.5	0.0 ± 0.1
$c \times 10^{-2}$	48 ± 51	7.4 ± 1.0	6.3 ± 0.1
$d \times 10^{-2}$	-0 ± 15	-1.4 ± 1.7	0.0 ± 0.1

Table 5.2: Average values of DKP, analysed using the HS method, obtained from noisy data. The averaging was done over 106 points. The signal to noise ratio of the raw data was 5.3, 53, 530 for the three cases considered.

time derivatives of velocity. That noise obtained from the higher-order time derivatives upon doing the numerical differentiation may affect the estimation was recently shown by Kirwan *et al.*, (1990). Using spectral analysis, they found that the higher-order contribution of the random noise enlarges as the order of the derivatives increases. In such a case, the OK method should suffer from noise more than the HS method. However, our simulation shows that the opposite situation occurs. We argue that the noise problem encountered in the HS method is caused by the matrix operations inherently involved in the method. These operations are matrix inversion and matrix multiplication with its transpose. In the former operation, a small perturbation in the elements of a matrix may cause a large effect on the inverted matrix (Westlake, 1968; Stewart, 1973). In our case, the perturbation is due

to the normally random noise added to the trajectories together with the noise that comes from the first and second-order time derivatives of drifter's position. This, in turn, will produce errors in the solution since that are proportional to the fluctuation of the matrix coefficients (von Neumann and Goldstein, 1947; Wilkinson, 1963). As we can see from the above simulations, the estimation of the kinematic parameters gets poorer as the noise level increases. A measure of this effect is called 'condition number' and a matrix that suffers from this phenomenon is called an 'ill-conditioned' matrix (Forsythe and Moler, 1967; Ralston and Rabinowitz, 1978). The situation is made worse when we multiply a matrix with its transpose since this operation produces a more 'ill-conditioned' matrix (Taussky, 1950).

Physically we might think of the HS method being dependent upon both spatial and time derivatives of the Lagrangian velocity, whereas the OK method depends on the higher order time derivatives but not spatial derivatives. It is, therefore, the spatial derivatives implicit in the HS method that caused the HS method to be even more sensitive to noise than the OK method in the example above. However, if the drifters are initially separated by a greater distance then the DKP calculated using the HS method are far less sensitive to noise than those from the OK method. This result is shown in

figure 5.6. For an example where the drifters were separated by $\sqrt{3}r$, where r is the radius of the eddy, the DKP fluctuate relative to their true values of $a = b = d = 0$, $c = 6.28 \times 10^{-2}$. Averaging over 106 points, we obtain the value of 6.50×10^{-2} and 0.05×10^{-2} for vorticity and the other parameters, respectively. These estimations are much closer to the true values than those given by the OK method for the same S/N ratio of 5.3 (see figure 3.13 and table 3.2). Clearly, the more reliable estimates of the DKP can be obtained by the HS method by enlarging the separation distance among drifters. Increasing the separation distance reduces the error that is introduced by the noise to the spatial velocity gradients. Increasing the separation between drifters can, however, increase the likelihood that the different drifters will be near different flow field singularities.

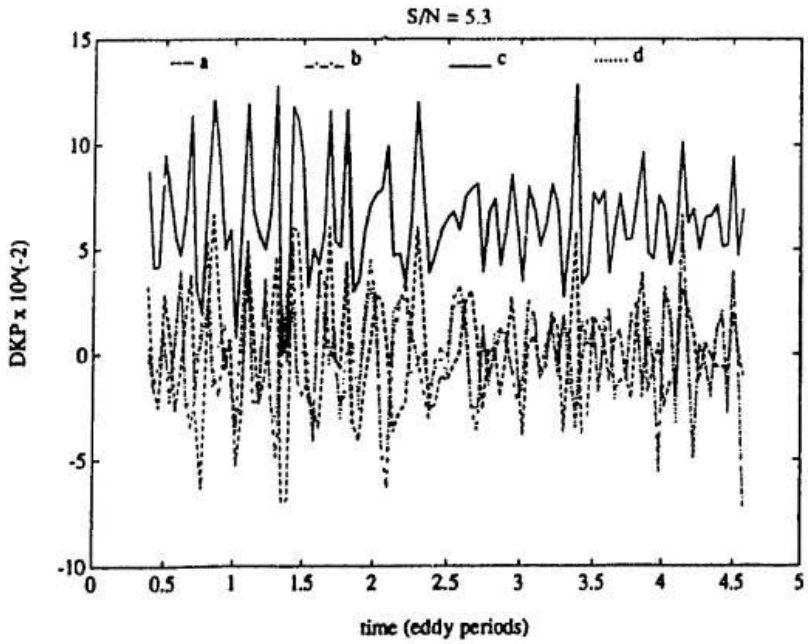

Figure 5.6: The DKP calculated using the HS method with S/N ratios of 5.3. The drifters are separated in a larger distance than those generated using before.

5.3 Oceanic Data

In this section, we will present the analysis of drifter trajectories measured on the Scotian Shelf. Three drifter trajectories are used in the following analysis. These trajectories are presented in figure 5.7. The trajectories consist of positions at 15-minute intervals spanning a total period of about

95 hours. The position is measured with a nominal accuracy of ±20 m. Three methods of analysis will be performed i.e. the OK, HS and OE methods. The results obtained from each method will be compared.

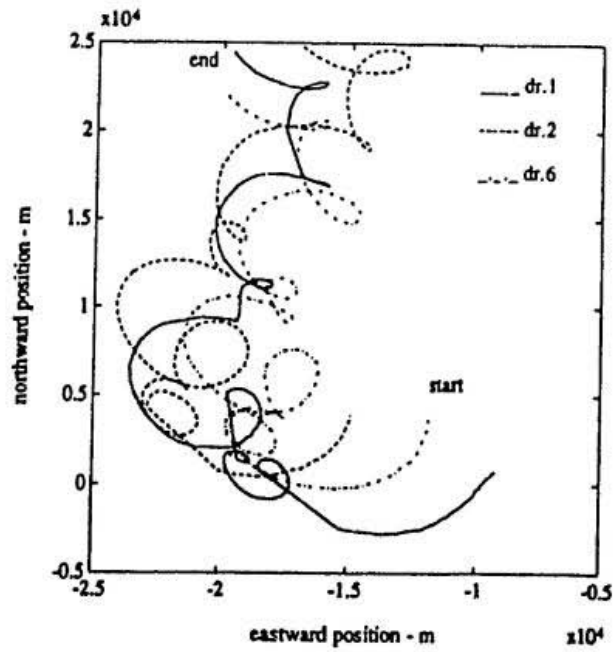

Figure 5.7: The trajectories of three drifters deployed in the Scotian Shelf.

As mentioned in the previous sections, both the OK and HS methods are sensitive to noise. To reduce the noise, we use a low-pass digital filter. A 10^{th} order Butterworth filter was chosen because of its flat frequency response. This high order is needed to have a sharp slope at its cut-off frequency, the

frequency at which the gain has the value of -3 dB. Having set the order of the filter, we do some experiments to drifter 6 denoted by 'dr.6' to examine the effects of different cut-off frequencies on the DKP obtained from the OK method.

The experiment involves several steps. We low-pass filter the trajectory. We use 10^{th} order Butterworth filter with a cut-off frequency of $\frac{1}{2}$ cycles/hour. This filter is available in MATLAB subroutines. We also use a subroutine called 'filtfilt'. Firstly, this subroutine filters the signal, then, the filtered sequence is reversed and run back through the filter. As a result, there is no phase shift in the filtered signal (Little and Shue, 1988). We calculate the velocity numerically and filter this velocity the same way. These velocities are subsequently differentiated numerically and filtered and the process repeated until we have up to third order derivatives of the drifter velocity. Having obtained all these derivatives, we use the OK formulae to obtain the kinematic parameters. These procedures are performed with each of these cut-off frequencies $\frac{1}{3}, \frac{1}{4}, \frac{1}{5}$ and $\frac{1}{6}$ cycles/hour. Some of the results obtained after filtering with these different cut-off frequencies are shown in figure 5.8 and figure 5.9.

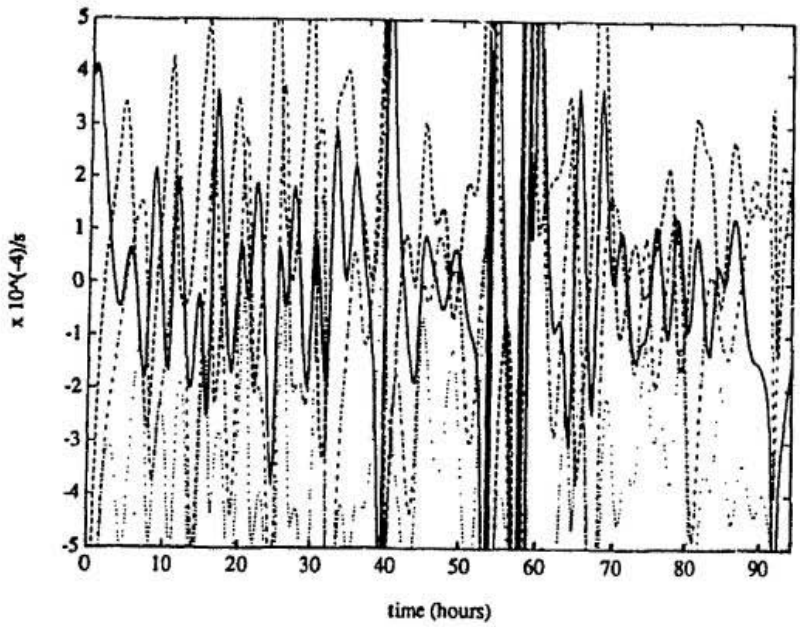

Figure 5.8: The DKP calculated using the OK method with a 10^{th} order filter having a cut-off frequency of $\frac{1}{3}$ cycles/hour.

Figure 5.8 shows that the calculated DKP fluctuate wildly when the cut-off frequency is $\frac{1}{3}$ cycles/hour. Here '- - - -', '_ _ _', '.....', '——' denotes stretching deformation rate, shearing deformation rate, vorticity, divergence respectively. The order of magnitude takes the value of 10^{-4}. Setting the cut-off frequency at $\frac{1}{6}$ cycles/hour, we get a clear feature of each parameter (see figure 5.9).

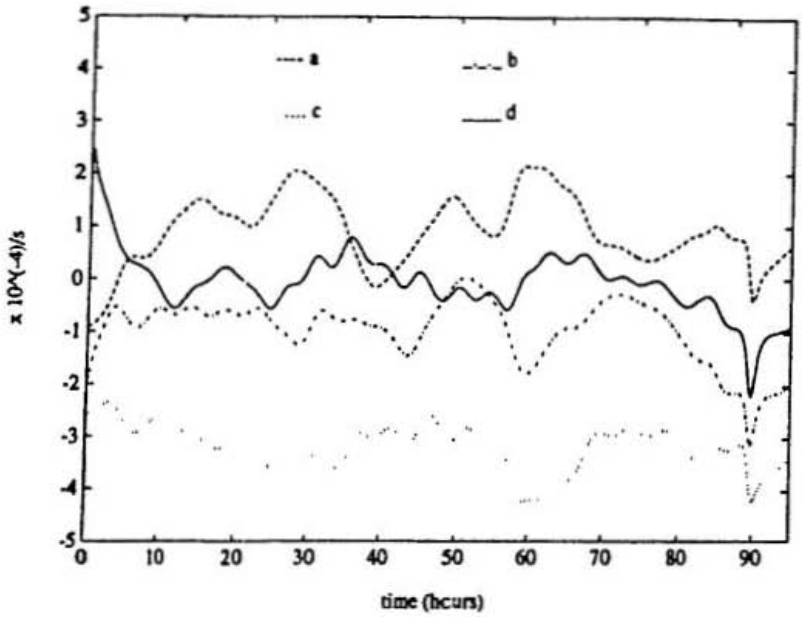

Figure 5.9: The DKP calculated using the OK method with a 10^{th} order filter having a cut-off frequency of $\frac{1}{6}$ cycles/hour.

From the above experiments, an appropriate cut-off frequency should be used in order to increase the signal to noise ratio. We could use the cut-off frequency at $\frac{1}{6}$ cycles/hour, but this is a harmonic frequency of the semi diurnal tide that may contain some information. In order to keep some of this information, we choose the cut-off frequency of $\frac{1}{5}$ cycles/hour for the following work. Typical drifter speeds are 0.10 m/s, so this cut-off frequency

results in displacements of $0.10 \times 5 \times 60 \times 60 = 1800$ m in the 5 hour period between positions. The position uncertainty due to measurement error is 20 m. Thus the signal to noise ratio is 90.

The frequency response of the 10^{th} order filter is shown in figure 5.10. The higher-order low-pass filter being used might have an effect on the filtered signal, causing ringing at the beginning and at the end of a time series (Hellbig, personal communication). To examine this we plot the filtered and unfiltered position versus time in figure 5.11. We see that the ringing has an effect at the end of the time series of both the filtered positions. Here, the unfiltered positions are plotted using the solid lines and the filtered positions of x and y are shown in '- - - -' , '_ _ _' lines, respectively. Note that the 'filtfilt' subroutine produces zero phase shift between unfiltered and filtered signal but fails to reduce the ringing effect caused by the high order filter that is used. In the following work, therefore, we should regard the last 10 hours of the time series to be spurious.

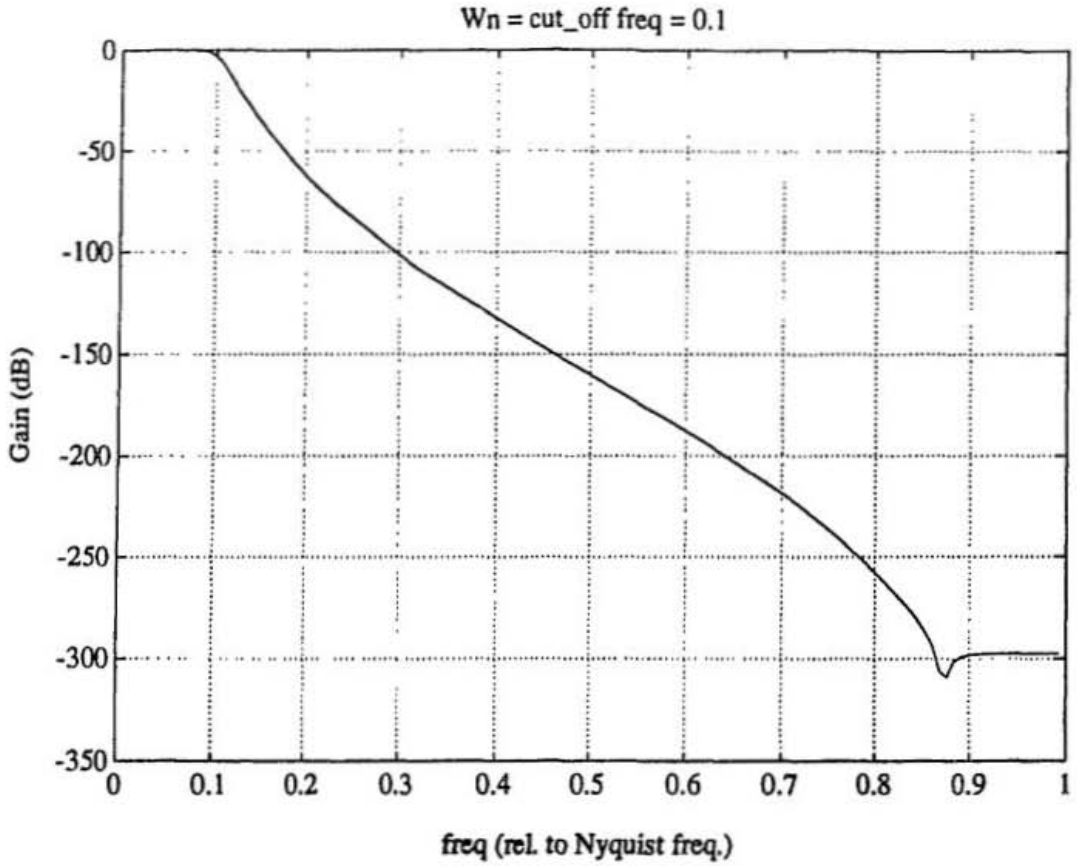

Figure 5.10: The frequency response of the 10^{th} order low-pass filter with a cut-off frequency of $\frac{1}{5}$ cycles/hour.

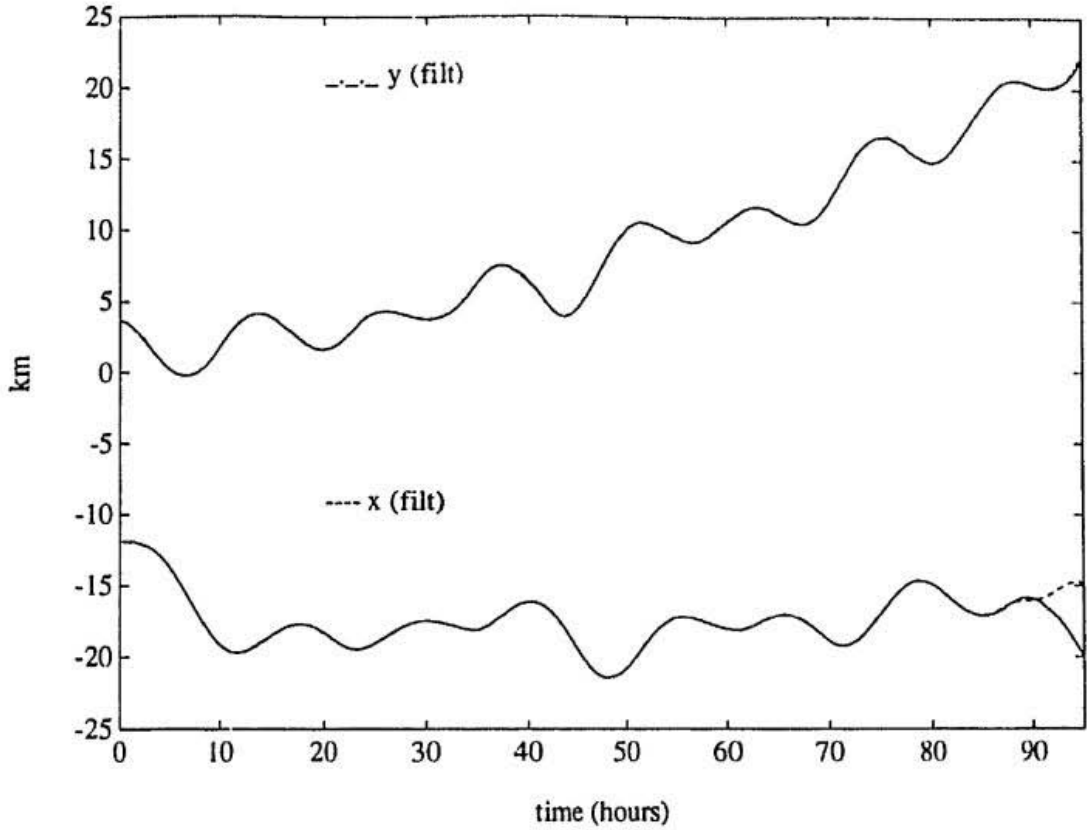

Figure 5.11: The ringing effect on the filtered positions as a result of performing the 10^{th} order low-pass with a cut-off frequency of $\frac{1}{5}$ cycles/hour.

5.3.1 The OK method results

We now use the OK method to analyse the drifter trajectories. We follow the above procedures i.e. numerical differentiation and low-pass filtering after each time differentiation. We use the 10^{th} order low-pass filter with cut-off frequency of $\frac{1}{5}$ cycles/hour. We do the analysis on all three drifters in order to calculate the kinematic parameters, i.e. the DKP, translation and swirl velocities as well as the flow centre's position.

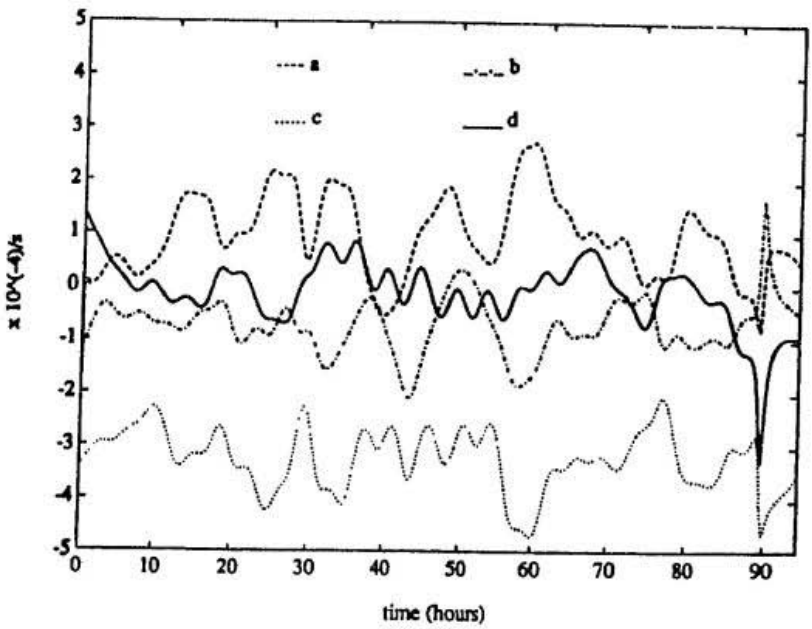

Figure 5.12: The DKP resulting from the OK analysis on the trajectory of 'dr.6'.

Figure 5.12 shows the calculated DKP from 'dr.6'. The parameters show the same trends as in figure 5.8 and have an order of magnitude of $10^{-4}s^{-1}$. These values lie within the range of those that had been reported by previous investigators (of the order of 10^{-5} to 10^{-4}) (Chew and Berberian, 1971; Reed, 1971; Molinari and Kirwan, 1975; Kirwan, 1975; Kawai, 1985). Note that in spite of differences in location and method of analyses, the present result is in agreement with earlier findings. Owing to the fact that all of these measurements were obtained for similar scales of the order of kilometers, the agreement is expected (Kawai, 1985). We see that of all the parameters, the vorticity takes the largest absolute value. It means that the motion is dominated by a rotating feature. Further, we notice that a negative value of vorticity is associated with anticyclonic or clockwise rotation as can be shown from the drifter trajectory in figure 5.13.

The position of the flow centre denoted by '***' is plotted along with the corresponding trajectory in figure 5.13. For most of the time, the flow centre moves with the drifter and is within 1 km of the drifter. It also shows that the flow centre performs mostly a translation and few small amplitude looping motions. The drifter, meanwhile, makes bigger looping motions about the flow centre. Note that near the end of the drifter's trajectory, the ringing

effect caused by the use of the high order filter mentioned leads to a spurious counter-clockwise loop. This counter-clockwise is spurious as can be seen by comparing figure 5.13 with figure 5.7.

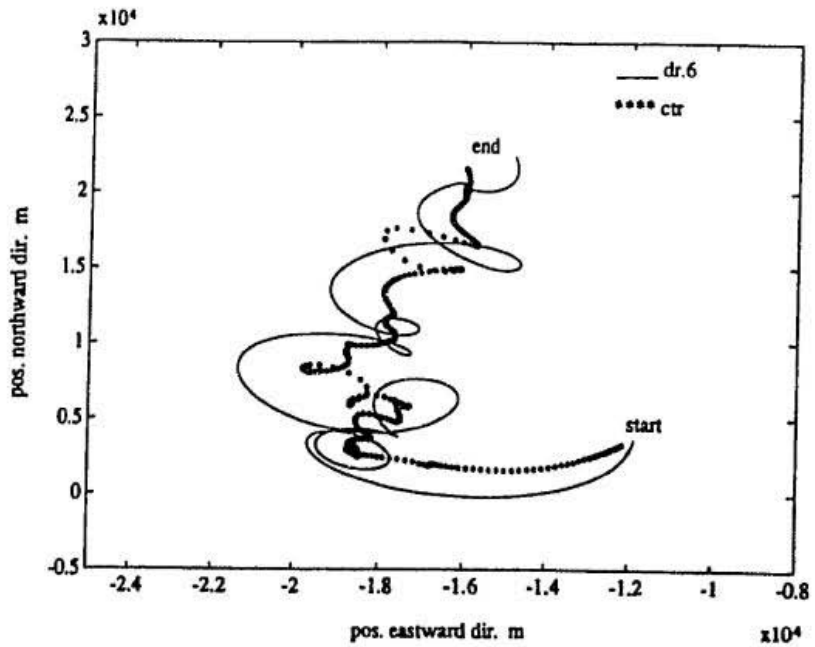

Figure 5.13: The particle's trajectory and flow centre resulting from the OK analysis on the trajectory of 'dr.6'.

The translation velocity of the flow centre of 'dr.6' is shown in figure 5.14. The long time-scale trends in U_T and V_T are consistent with the trajectory of the flow centre plotted in figure 5.13. Both components of the flow centre translation velocity show strong fluctuations with a period of about 6.1 hours.

This is approximately half the semi-diurnal period of the tide.

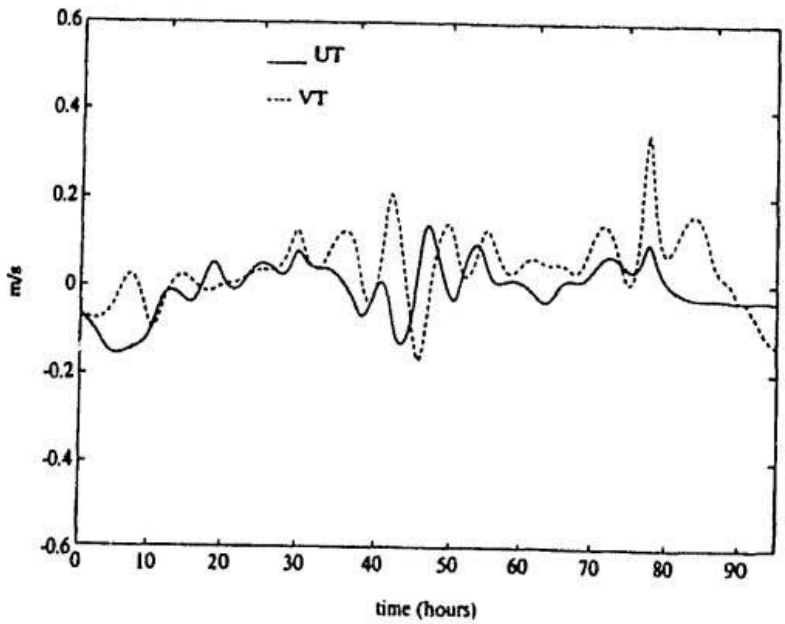

Figure 5.14: The translation velocities resulting from the OK analysis on the trajectory of 'dr.6'.

The motion of the drifter relative to the flow centre is described by the swirl velocity. Components of swirl velocity are plotted in figure 5.15 as a function of time. Figure 5.15 shows a periodic motion with the period between peaks of about 12.5 hours. It is the semi-diurnal tide. We also see that the amplitude of the velocities are not uniform. We try to further investigate this non-uniformity in the velocities by presenting the position of

the drifter relative to its flow centre.

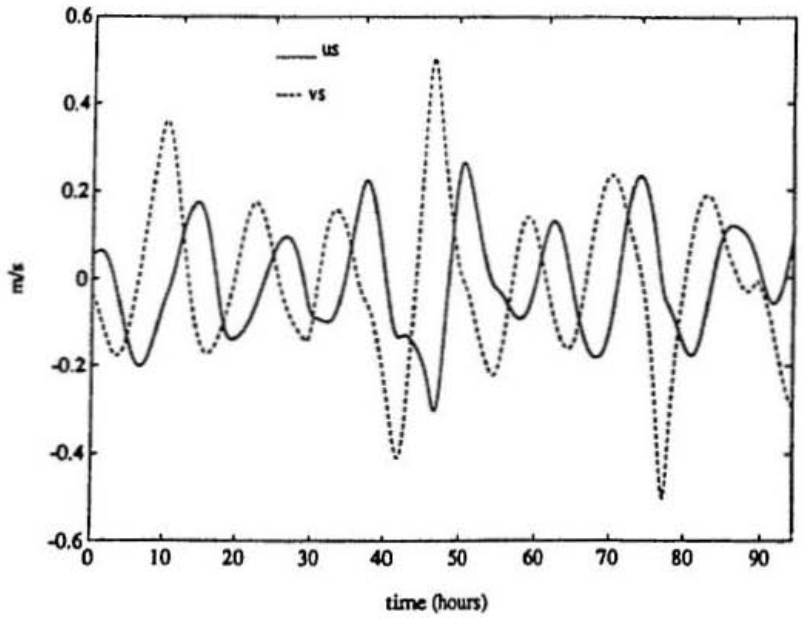

Figure 5.15: The swirl velocities resulting from the OK analysis on the trajectory of 'dr.6'.

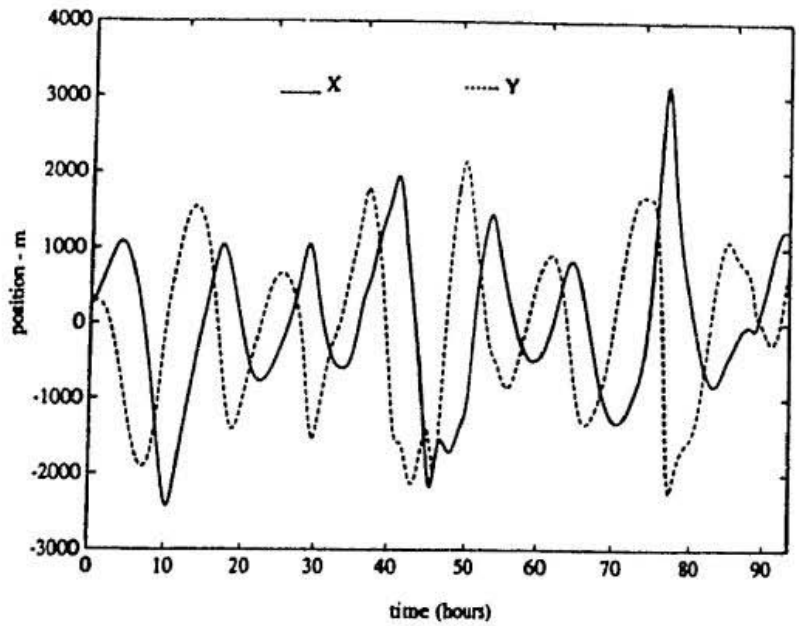

Figure 5.16: The position of the drifter relative to the flow centre resulting from the OK analysis on the trajectory of 'dr.6'.

Figure 5.16 shows the time series of the drifter position relative to the flow centre. The eastward position is denoted by 'X' and the northward direction by 'Y'. It resembles the swirl velocities (figure 5.15). The distance from the drifter to the flow centre is $\sqrt{X^2+Y^2}$. Thus we obtain a time series of this distance to compare with the time series of vorticity plotted in figure 5.12. Fluctuations of $\sqrt{X^2+Y^2}$ about the mean value are then correlated with fluctuations of vorticity about its mean value. We get a

cross-correlation coefficient of -0.84. Similarly we can calculate the speed of the drifter using $\sqrt{u_s^2 + v_s^2}$ and correlate it with vorticity and obtain a coefficient of -0.85. These coefficients tell us that both the distance and speed of the drifter relative to the flow centre are negatively correlated. It means that as the relative distance of the drifter to its centre decreases, the magnitude of the vorticity gets larger. This is consistent with the idea of conservation of angular momentum. The closer the drifter to its flow centre, the greater its angular frequency. This kind of argument was used to explain five cyclonic features of a trajectory in the North Equatorial Current (Kirwan, 1984; Kirwan *et al.*, 1984). We can also think of another way of interpreting the result in terms of potential vorticity $Q = (f + c)/H$. Here, f is the planetary vorticity and is assumed to be constant along the drifter's path, c is the local vorticity and H is the water column. Stretching and shrinking of the water column can be associated with a convergent and divergent motions, respectively (see Gill, 1982 p. 232-233). In the former case, as the drifter moves close to the centre, it rotates faster. Stretching the water column (increasing H) causes c to increase is compensated by gaining positive vorticity (increased cyclonic motion) in order to conserve the potential vorticity. On the other hand, as the drifter moves away from

the centre (corresponding to divergence) then c gets smaller and the drifter rotates slower around the flow centre.

Similar results are found for the other two drifters denoted by 'dr.1' and 'dr.2'. Their DKP have the some order of magnitude of $10^{-4}s^{-1}$ except for peaks at certain time intervals associated with times when we had to use interpolated positions because of instrument failures. These trajectories also show that angular momentum about the flow centre and potential vorticity are conserved.

Table 5.3 shows the cross correlation coefficient between the kinematic parameters obtained from neighbouring drifters. The correlation coefficients obtained by cross correlating parameters related to drifter 1 and drifter 2 are put under a column labelled '*dr.1 and dr.2*', and similarly for the columns labelled '*dr.1 and dr.6*' and '*dr.2 and dr.6*'. The left column is provided for the pararaeters. Note that the position of the flow centre is denoted as 'X_T' and 'Y_T'. As can be seen from the table that the DKP of *dr.*1 are uncorrelated to those of *dr.*2 and *dr.*6. But *dr.*2 and *dr.*6 have well correlated DKP. This suggests that both *dr.*2 and *dr.*6 may be responding to the same singularity in the flow field, whereas *dr.*1 appears to be responding to a different flow field singularity. Figure 5.7 shows the relative positions of the three drifters.

Kinematic parameters	*Correlation coefficients between*		
	dr.1 and dr.2	*dr.1 and dr.6*	*dr.2 and dr.6*
a	0.19	0.12	0.63
b	0.05	-0.07	0.50
c	0.19	0.17	0.96
d	0.16	0.06	0.61
U_T	0.28	0.26	0.44
V_T	0.15	0.17	0.19
u_s	0.46	0.54	0.64
v_s	0.31	0.39	0.47
X_T	0.94	0.97	0.97
Y_T	0.49	0.64	0.76

Table 5.3: Correlation coefficients of the kinematic parameters between pairs of drifters from the OK analysis

Drifters 2 and 6 start adjacent but end up separated with drifter 1 between them. In a fluid flow which has singularities of different scales embedded one within the other, it is not simple to equate proximity with similarity in flow structure. Another interesting finding is that the east-west component of the swirl velocities gives a higher correlation coefficient than that of the north-south component. A similar result is obtained for the translation velocities. It seems the singularity is more coherent in its east-west component than in the north-south component of motion.

The trajectories of the flow centres are presented in figure 5.17. Here '(1)', '(2)', '(6)' corresponds to flow centre of drifters *dr.*1, *dr.*2, *dr.*6, respec-

tively. We see that each drifter seems to have a different flow centre position, typically separated about 2 km. The flow centre position for drifter 1 seems to fluctuate in a noisy manner. This may account for the poor correlation between drifter 1 and other drifters. It is clear from the present analysis that these drifter tracks are not strongly dominated by a single coherent flow field singularity.

From the above discussions, we have presented the OK analysis on a particular trajectory embedded on the Scotian Shelf. The results reveal some interesting features. First of all, the magnitude of the DKP are within the range obtained by previous investigators. One of the parameters, the vorticity, shows that the trajectory will be dominated by anti-cyclonic motion which is in agreement with casual observation of the data. We also find a result that agree with conservation of angular momentum shown by the drifters. The motion of the particle about the flow centre has a dominant period of 12.5 hours whereas the motion of the flow centre has a 6.1 hour period. We have also shown that even though each trajectory has its own singularity or flow centre, the kinematic parameters of two of the drifters are somewhat related. There are similarities between the trajectories of the three drifters plotted in figure 5.7. It is clear, however, that the three drifter

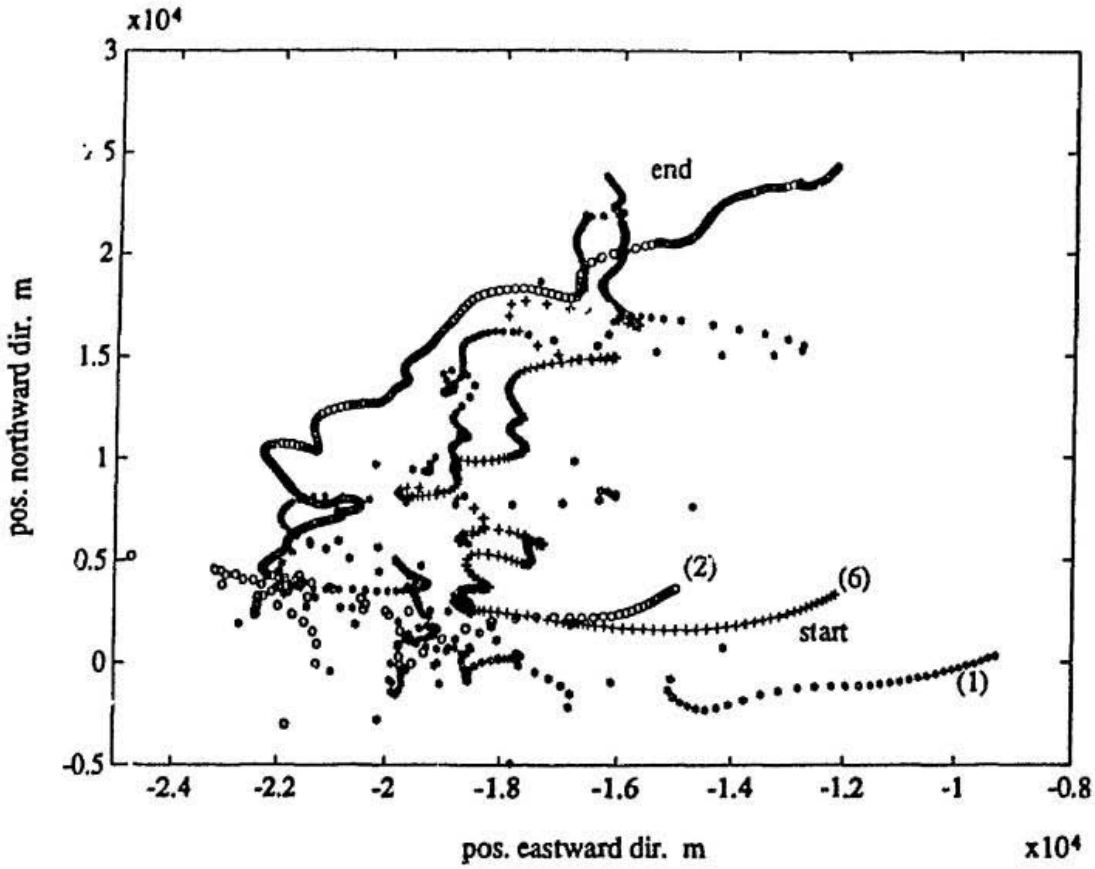

Figure 5.17: The positions of the three flow centres resulting from the OK analysis on the trajectory of 'dr.1', 'dr.2', 'dr.6'.

trajectories do not all result from a common flow field singularity. We expect, therefore, that the HS analysis of this data will break down since there is not one unambiguous singularity common to all three drifters.

5.3.2 The HS method results

In this section, we will use the HS method to analyse the drifter measurements on the Scotian Shelf. This method is also sensitive to noise. To remove the noise, we use a low-pass filter which has the same characteristics as that mentioned earlier, i.e. 10^{th} order Butterworth filter with a cut-off frequency of $\frac{1}{5}$ cycles/hour. The HS method also explicitly assumes that all drifters in the cluster are moving in response to the same flow centre. For the present data set this assumption is unjustified. It is therefore of interest to see whether or not the HS method breaks down totally, or just gives a slightly different looking answer from the OK analysis. To make a comparison between methods, we will calculate the time derivatives and filter the data, in the same fashion as we did for the OK analysis.

Figure 5.18 and figure 5.19 show the calculated DKP. The stretching and shearing deformation rate, vorticity and divergence are denoted by the lines

'- - - -', '-.-.-', '.....', '——' respectively. All parameters have large amplitude swings. Bear in mind that we have used the same low-pass filtering to smooth the data as was used in the OK method.

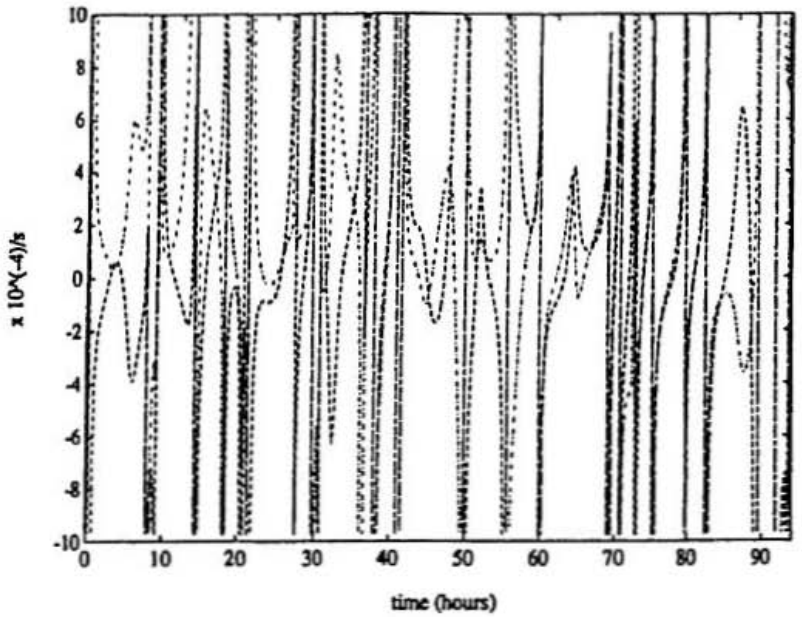

Figure 5.18: The stretching and shearing deformation rate calculated using the HS analysis on the three drifters.

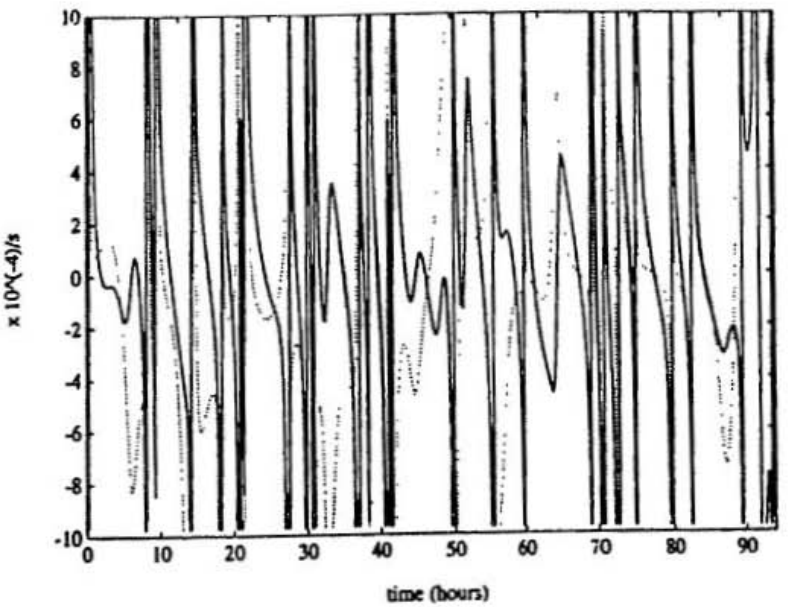

Figure 5.19: The vorticity and divergence calculated using the HS analysis on the three drifters.

The position of the flow centre calculated using the HS method is plotted in figure 5.20 along with the trajectories of the three drifters. In this plot, the '****' denotes the flow centre position and the '(1)', '(2)', '(3)' corresponds to the trajectory of each particle. We see that the flow centre position fluctuates greatly from one time interval to the next. It is clear that the HS method does not identify either the position of the flow centre or the DKP of the flow.

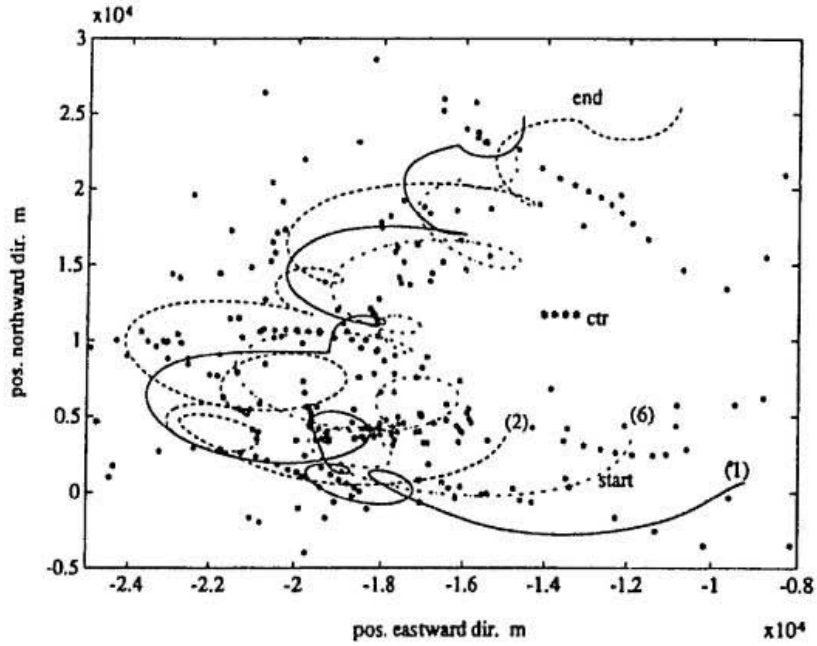

Figure 5.20: The particles' trajectories and flow centre position resulting from the HS analysis.

This probably results from the lack of a well-defined singularity in the flow field to control the motion of all three drifters. The tide dominates the flow on Sable Island bank and the tidal currents generally have large spatial scales compared to the separations between $dr.1$, $dr.2$ and $dr.6$. In view of this situation, we can think of an oscillating sheet of fluid. A drifter embedded in a fluid that is oscillating as a sheet will move around in an elliptic path. There

is no flow field singularity. We are asking the HS method to tell us where the flow centre is and what its properties are. But there is no well defined flow centre, so the HS method responds by giving ridiculous results. The OK method, on the other hand, gives DKP consistent with motion around a vortex - because it is unable to discriminate between motion around a vortex and an oscillating sheet. We will investigate this issue later on. For the time being, we will use the OE method to analyse the data set.

5.3.3 The OE method results

This part of the section will present the results obtained using the OE method. We also low-pass filter the positions and velocities of each drifter. Note that, the OE method does not require the calculation of acceleration terms. However, we need to compute the centroid position of the cluster.

Figure 5.21 shows the DKP obtained using the OE method. The parameters have a magnitude of order $10^{-4}s^{-1}$. We see that the DKP are oscillating about zero. This might not be true. Let us take a look at the vorticity. We notice that in some time intervals, its value becomes positive. This means that at some particular time the trajectory changes its sense of rotation. This

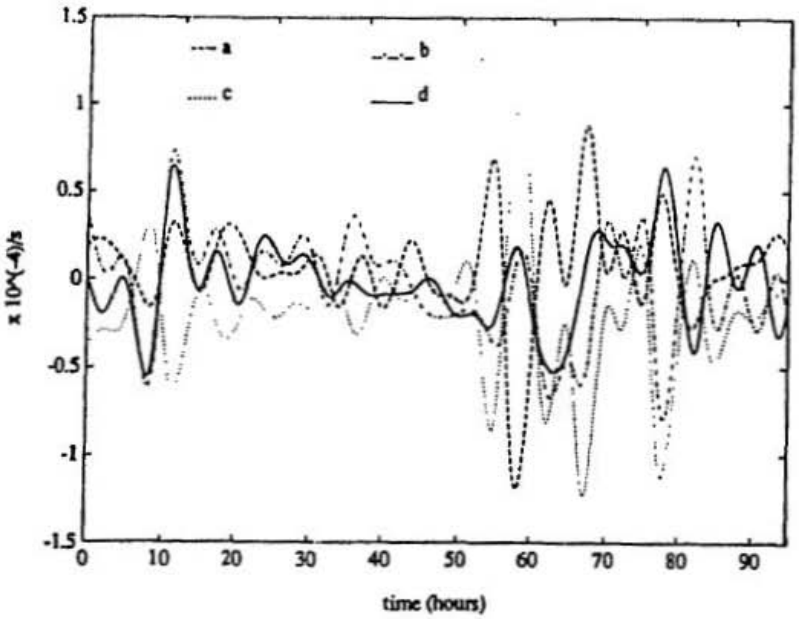

Figure 5.21: The DKP resulting from the OE analysis on the cluster of drifters.

is not realistic since the trajectory always rotates in a clockwise direction, anti-cyclonic. Similarly, the other DKP are probably unrealistic as discussed by Kirwan (1984).

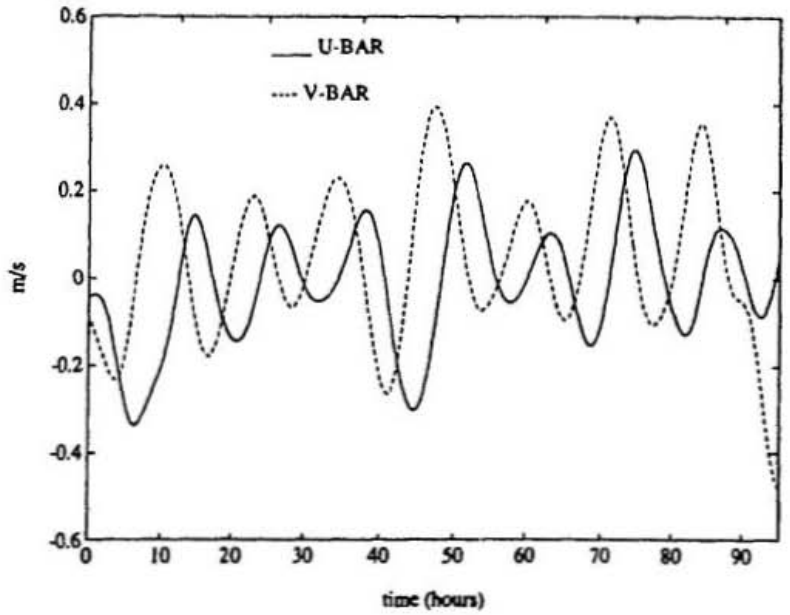

Figure 5.22: The centroid velocities resulting from the OE analysis on the cluster of drifters.

Both eastward and northward components of the centroid velocity oscillate with a period of 12.5 hours in figure 5.22. This means that the centroid is influenced by a semi-diurnal tide. We see that the centroid velocity in figure 5.22 is strongly correlated to the swirl velocity obtained from the OK

analysis in figure 5.15. This is consistent with our earlier interpretation that most of the flow moves elliptically as a spatially coherent sheet.

5.3.4 Data simulation using DKP obtained from the OK

We have presented the results of three methods i.e. the OK, HS and OE. From the analysis, the results obtained by using the HS method give no useful information about the kinematic parameters. Thus, we can not properly describe the flow field. We suspect that the failure is caused by the absence of well-defined singularities which are common to all drifters. We will perform another simulation in which the drifters share the same singularities. We take the DKP and the flow centre's position calculated from dr.6 using the OK method. These DKP are then used to calculate trajectories for three drifters by substituting them into a forward differencing formulae for the first time step

$$\begin{aligned} \tilde{x}_i(t+\Delta) &= \tilde{x}_i(t) + 0.5\Delta[(a(t)+d(t))(\tilde{x}_i(t) - X_T(t))] \\ &\quad +0.5\Delta(b(t)-c(t))(\tilde{y}_i(t) - Y_T(t))] + U_T(t)\Delta \qquad (5.15) \\ \tilde{y}_i(t+\Delta) &= \tilde{y}_i(t) + 0.5\Delta[(b(t)+c(t))(\tilde{x}_i(t) - X_T(t))] \end{aligned}$$

$$+0.5\Delta[(d(t)-a(t))(\tilde{y}_i(t)-Y_T(t))]+V_T(t)\Delta \quad (5.16)$$

and a centred differencing scheme for later time steps.

$$\begin{aligned}\tilde{x}_i(t+\Delta) &= \tilde{x}_i(t-\Delta)+\Delta[(a(t)+d(t))(\tilde{x}_i(t)-X_T(t))] \\ &\quad +\Delta[(b(t)-c(t))(\tilde{y}_i(t)-Y_T(t))]+2U_T(t)\Delta \quad (5.17)\\ \tilde{y}_i(t+\Delta) &= \tilde{y}_i(t-\Delta)+\Delta[(b(t)+c(t))(\tilde{x}_i(t)-X_T(t)) \\ &\quad +\Delta[(d(t)-a(t))(\tilde{y}_i(t)-Y_T(t))]+2V_T(t)\Delta. \quad (5.18)\end{aligned}$$

Here, the subscript 'i' with $i=1,2,3$ denotes the i^{th} drifter. Δ is the time interval between positions. The DKP $a(t), b(i), c(t), d(t)$, translation velocity U_T, V_T, flow centre position X_T, Y_T are all functions of time determined from the OK analysis of *dr*.6. Initially, we locate our simulated drifters at each corner of an equilateral triangle with the singularity at its centre. Thus we expect that the OE method should work for this data. The simulated trajectories of the three drifters are given in figure 5.23.

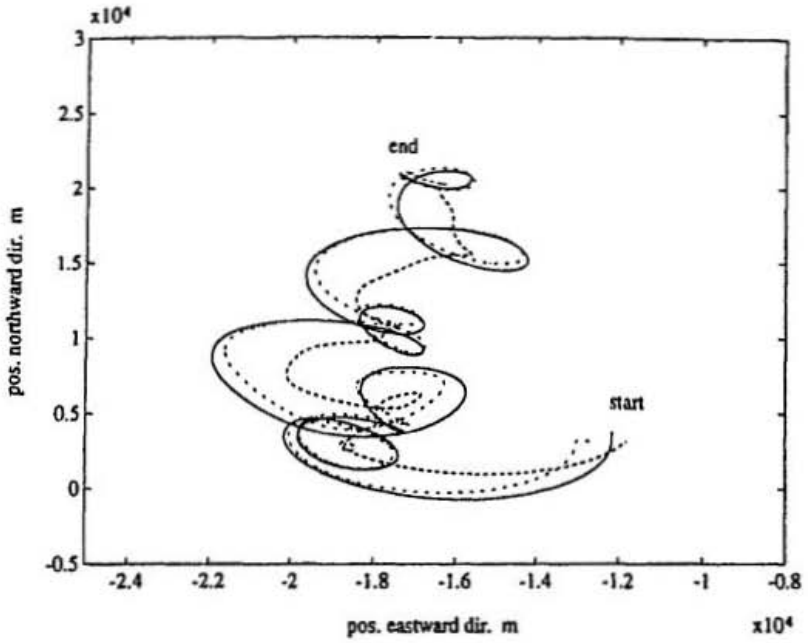

Figure 5.23: The simulated trajectories calculated from the kinematic parameters of 'dr.6'.

The positions of the three simulated drifters are shown in figure 5.23. The three drifters are represented by different lines, i.e. '——', '- - - -' and '_ _ _'. Having generated the trajectories, we proceed further by calculating successive time derivatives of the trajectories and performing low-pass filtering after each differentiation. Then, we apply the OK, HS and OE methods to the simulated data to obtain the kinematic parameters.

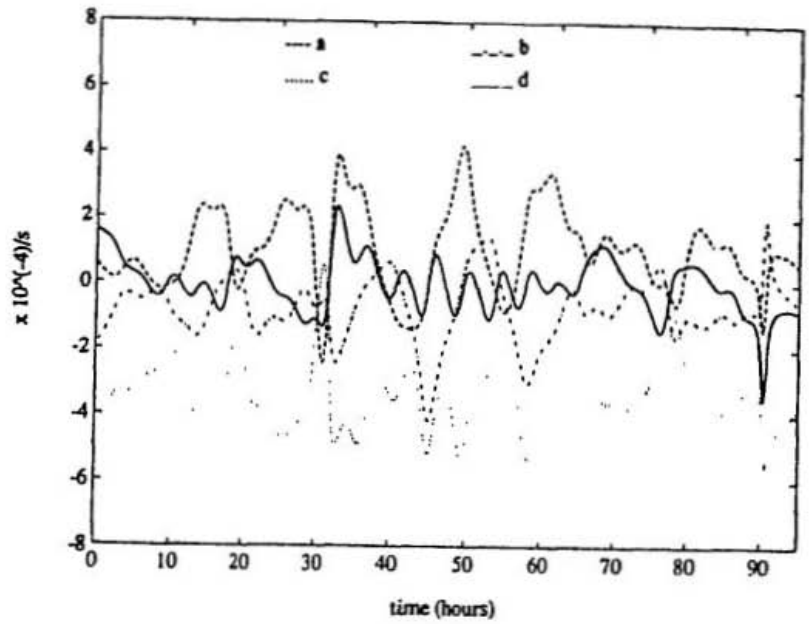

Figure 5.24: The DKP resulting from the OK analysis on the simulated trajectory.

Figure 5.24 shows the DKP calculated by applying the OK method to the simulated data. Here, we choose one of the trajectories plotted in figure 5.13. The DKP used to generate the simulated data are plotted in figure 5.12. The DKP in figure 5.24 are very similar to those in figure 5.13, but they are not identical. The DKP obtained from the simulated data by applying the HS method are shown in figure 5.25. The details of these time series in figures 5.23 and 5.24 are different, but both methods do give strongly correlated

results.

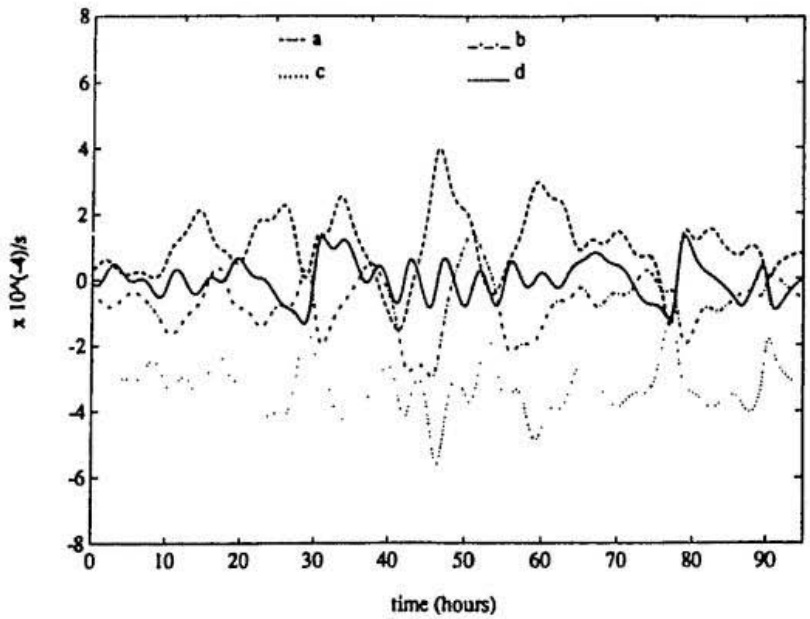

Figure 5.25: The DKP resulting from the HS analysis on the three simulated trajectories.

The results shown in figure 5.26 are obtained from the OE method. They most strongly resemble the DKP, plotted in figure 5.12, which were used to to generate the data. This means that the OE method provides us with a better estimation of the kinematic parameters of the simulated data than those of the OK and HS methods. This is not surprising that the OE gives a nice result since the centroid is no other than the flow centre itself. Hence,

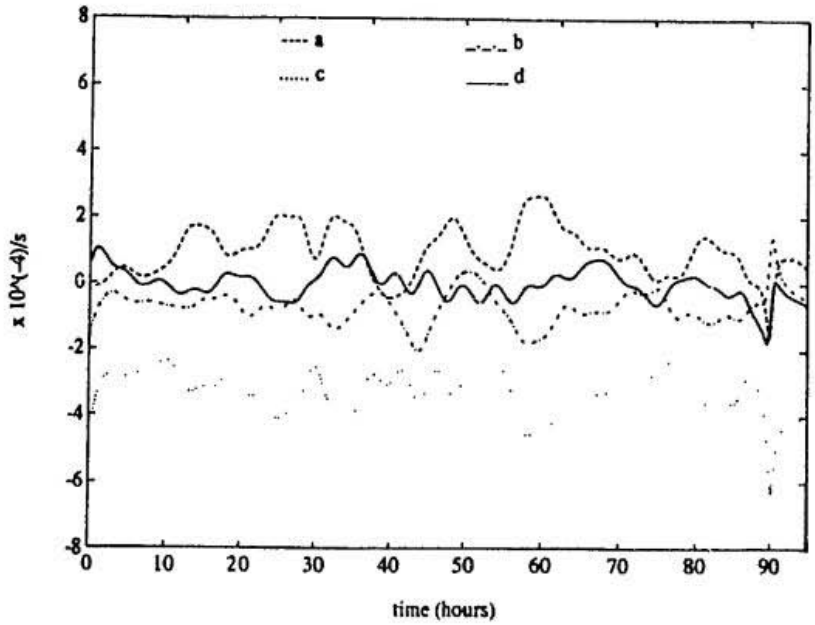

Figure 5.26: The DKP resulting from the OE analysis on the three simulated trajectories.

the results show no biasing problem. If, however, we move the centroid away from the flow centre, then the OE method gives very poor results. Now, we will present the results of performing a cross-correlation analysis between the DKP used to generate the trajectory and the DKP obtained from each of the three methods.

Table 5.4 shows the correlation coefficients obtained by cross-correlating the DKP used to simulate trajectories (symbolized as 'SIM') to the DKP

Kinematic parameters	*Correlation coefficients between*		
	SIM and OK	SIM and HS	SIM and OE
a	0.88	0.91	0.996
b	0.88	0.87	0.996
c	0.98	0.98	0.996
d	0.79	0.55	0.85

Table 5.4: Correlation coefficients of the kinematic parameters between simulated values and the values calculated from the three methods: OK, HS, OE.

calculated from each method. Strongest correlations are obtained between the simulation DKP and those from the OE method. The other two columns obtained by correlating the simulation DKP with from OK and HS analysis give lower correlation coefficients. Despite its higher order derivatives, the DKP obtained using the OK method are more closely correlated to the simulation DKP than the DKP obtained using the HS method. However, the HS method still gives quite a good estimate of the DKP. Clearly, the HS method can provide useful information about DKP if the drifter cluster is moved by only one well defined flow centre. The fact that it breaks down so badly when this condition is not satisfied, suggests that it might be a good indicator for the existence of well defined flow field singularities.

In circumstances where there is no well defined flow centre (such as the

Sable Island bank) the OK method gives plausible DKP and also gives a solution for the flow centre position. But the OK method indicates that a neighbouring drifter might give a different flow centre position in such a flow field. The OK method is essentially unable to use only one trajectory to resolve the difference between a flow field that rotates about a stationary point and a flow field which moves as a sheet so that all points on the sheet have the same (but displaced) circular trajectories. To resolve these cases the OK method requires two drifters. In view of the ambiguity and inaccuracy inherent in all the methods of obtaining DKP from drifter trajectories, it is prudent to consider all techniques available since they are all likely to have their own particular strengths and weaknesses. For example DKP might be much better obtained from the HS method than the OK method if drifter trajectories are distributed at the scale of a dominant eddy and the time series of positions is short. In this case the HS method is less affected by noise than the OK method.

Chapter 6

Summary

Our problem has been to find ways of inverting a drifter trajectory to find kinematic properties of the flow field. In particular we search for structures in the flow field that can be identified as singularities. Two approaches have been developed. First we have corrected algebraic errors made by Kirwan *et al.*, (1988) when they inverted Okubo's (1970) solution for the motion of a drifter near a flow field singularity. Next we generalized the regression technique of Okubo and Ebbesmeyer (1976) so that the flow centre was no longer fixed to the drifter cluster centroid.

Our solutions as manifested in the OK method, have been tested in two ways. First, by substituting the solutions into the nonlinear equations that

they are supposed to solve and using the MACSYMA program to check that the equations are identically satisfied. Second, by generating sets of data ranging from pure stretching and shearing with no translation to pure rotation with translation velocity. The OK method obtained the correct DKP from these simulated trajectories. The solutions by Kirwan *et al.*, (1988) are also examined by the same tests but generally fail to give the correct DKP except for the divergence.

The cluster method of Okubo and Ebbesmeyer (1976), OE, was used to analyse artificially generated trajectories with pure rotation and a constant translation velocity. This OE method failed whenever the position of the flow field singularity was different from that of the cluster centroid. This so-called biasing problem has been pointed out by Kirwan (1988). A new HS cluster method has been developed in order to overcome this problem. The HS method explicitly solves for both the position and velocity of the flow centre. The biasing problem in which the DKP oscillate in accordance with the angular frequency of the eddy, has been successfully overcome by the HS method. Note, however, that the OE method can still be useful for studying the elongation or distortion of a patch of drifters with respect to the patch centroid (Okubo *et al.*, 1976; Okubo *et al.*, 1983).

Both OK and HS methods are capable of determining the flow field parameters of the generated data. Some assumptions have been posed to both methods, i.e. the kinematic parameters are constant or slowly changing relative to the time interval between fixes, a well-defined flow field singularity and the singularity does not accelerate. We can name a translating ring as an example that may fulfill the requirement. The OK method has the advantage of allowing DKP to be determined from a single trajectory. But we can not be sure that a second neighbouring drifter would give the same DKP. This uncertainty arises out of the possibility that the flow field sampled by a drifter may not always consist of unambiguous isolated singularities. The HS method has the disadvantage of requiring more drifters. The HS method seems to break down in a very obvious fashion if all three drifters are not being moved by the same flow field singularity. This might be considered either an advantage or disadvantage; depending upon your point of view.

Putting noise in a trajectory affects both the OK and HS methods. The up to 4^{th} order time derivatives of trajectories make the OK method sensitive to noise. In the case of the HS method only second order time derivatives of the trajectory are used. However, the HS method implicitly relies on spatial derivatives of the trajectories as well. Thus the HS method can be either

more or less sensitive to noise than the OK method; depending upon the separation distance between drogues. To reduce the effect of noise, we could perform a low-pass filter to both the OK and HS methods and enlarge the separation distance between drifters deployed in the flow when applying the HS method. However, we have to ensure that the separation between drifters does not become so great that different drifters are responding to different singularities. The use of low-pass filter has the disadvantage of filtering out any high frequency variability of the DKP. Increasing the distance between drifters to the order of the eddy might become impractical since the size of an eddy has an order of several kilometers or greater.

Some interesting results are obtained by using these methods of analysing the drifter trajectories on the Scotian Shelf. Using the OK method, we can obtain the DKP for each drifter. We find that the DKP are in a range between -5 $\times 10^{-4} s^{-1}$ to 3 $\times 10^{-4} s^{-1}$. It also shows that the trajectory moves in a clockwise direction which is in agreement with observation. The drifter rotates faster around its flow centre when it gets closer to the the flow centre, consistent with conservation of potential vorticity. Further, there is a 12.5 h period of oscillation, the semi-diurnal tide, observed in the swirl velocity with a peak of about 0.5 m/s. The position of the flow centre of each drifter

and its corresponding translation velocity had a dominant 6.1 h periodicity. We do not have an explanation for the fact that certain tidal constituent will affect certain velocity component and not the other component.

It turns out that the three drifters deployed on the Scotian Shelf experienced different flow field singularities. Under this circumstance, the HS method gives wildly fluctuating DKP. The break down of the HS method is caused by the lack of a well-defined flow field singularity which is common to all three drifters. To justify this argument, we do another simulation in which we set a common flow field singularity using DKP obtained from one drifter track by using the OK method. Upon analysing this simulated data, we find that the results obtained from the OK and HS methods return the correct values for the kinematic properties of the flow field. We see that the HS method can be used to identify a flow field singularity provided that all the drifters in the cluster are responding to only the one singularity.

The Scotian Shelf data analysis indicates a dominant semi-diurnal tide that has large spatial scales so that each trajectory has its own flow centre and all drifters do not respond to a single well-defined singularity. We can think of the motion as an oscillating sheet of fluid rather than rotation about a vortex. Each drifter deployed in this type of flow will move in an elliptic

trajectory that is displaced from other drifters. This is supported by the centroid velocity obtained by the OE method being strongly correlated with the swirl velocity attained using the OK method. That explains why each drifter seems to have its own flow centre in this kind of flow.

Bibliography

Batchelor, G. K. 1967. *An Introduction to fluid mechanics.* Cambridge Univ. Press, London, 615 pp.

Bjerknes, V. F. K.; T. Hesselberg and O. Devik. 1911. *Dynamic Meteorology and Hydrography. Part II. Kinematics.* Publication no. 88, Carnegie Institution, Washington D.C.

Bower, A. S. 1989. Potential vorticity balances and horizontal divergence along particle trajectories in Gulf Stream meanders east of Cape Hatteras. *J. Phys. Oceanogr.* 19: 1669 - 1681.

Cramer, H. 1966. *Mathematical methods of statistics.* Princeton Univ. Press, eleventh ed., 575 pp.

Csanady, G.T. 1963. Turbulent diffusion in Lake Huron. *J. Fluid Mech.,* 17: 360 - 384.

Draper, N. R. and H. Smith. 1966. *Applied regression analysis.* John Wiley, 407 pp.

Fahrbach, E.; C. Brockmann and J. Meincke. 1986. Horizontal Mixing in the Atlantic Equatorial Undercurrent estimated from drifting buoy clusters. *J. Geophys. Res.* 91, C9: 10557 - 10565.

Forsythe, G. and C. B. Moler. 1967. *Computer solution of linear algebraic systems.* Prentice-Hall, Inc. New Jersey, 148 pp.

Gill, A. E. 1982. *Atmosphere-ocean dynamics.* Academic Press, Inc. San Diego, 662 pp.

Indest, A. W. Jr.; A. D. Kirwan Jr.; J. K. Lewis and P. Reinersman. 1990. A synopsis of mesoscale eddies in the Gulf of Mexico, in *Mesoscale/Synoptic and Coherent Structures in Geophysical Turbulence*, edited by J. C. J. Nihoul and B. M. Jamart. Elsevier, New York, 485 - 500 pp.

Kawai, H., 1985. Scale dependence of Divergence and Vorticity of near-surface flows in the Sea. *J. Oceanogr. Soc. Japan*, 41: 157 - 175.

Kirwan, A. D. Jr. 1975. Oceanic velocity gradients. *J. Phys. Oceanogr.* 5: 729 - 735.

Kirwan, A. D. Jr. 1984. On the utilization and interpretation of drifter data, in *Ocean Hydrodynamics of the Japan and East China Seas*, edited by T. Ichiye. Elsevier Science Pub., New York, 239 - 251 pp.

Kirwan, A. D. Jr. 1988. Notes on the cluster method for interpreting relative motions. *J. Geophys. Res.* 93: C8, 9337 - 9339.

Kirwan, A. D. Jr.; A. W. Indest; J. Liu and N. Clark. 1990. Ring evolution in General Circulation Models from path analysis. *J. Geophys. Res.* 95, C10: 18057 - 18073.

Kirwan, A. D. Jr.; J. K. Lewis; A. W. Indest; P. Reinersman and I. Quintero. 1988. Observed and simulated kinematic properties of loop current rings. *J. Geophys. Res.* 93, C2: 1189 - 1198.

Kirwan, A. D. Jr.; W. J. Merrel; J. K. Lewis; R. E. Whitaker and R. Legeckis. 1984. A model for analysis of drifter data with an application to a Warm Core Ring in the Gulf of Mexico. *J. Geophys. Res.* 89, C3: 3425 - 3438.

Kirwan, A. D. Jr. and M. S. Chang. 1979. Effect of sampling rate and random position error on analysis of drifter data. *J. Phys. Oceanogr.* 9: 382 - 387.

Law, A. M. and W. D. Kelton. 1982. *Simulation modelling and analysis.* McGraw-Hill, Inc. New York, 400 pp.

Lewis, J. K. and A. D. Kirwan Jr. 1987. Genesis of a Gulf Mexico Ring as determined from Kinematic analyses. *J. Geophys. Res.* 92, C11: 11727 - 11740.

Lewis, J. K.; A. D. Kirwan Jr. and G. Z. Forristall. 1989. Evolution of Warm-Core Ring in the Gulf of Mexico: Lagrangian observations. *J. Geophys. Res.* 94, C6: 8163 - 8178.

Little, J. N. and L. Shure. 1988. *Signal Processing Toolbox.* The MathWorks, Inc. Massachusetts.

Marsaglia, G. and T. A. Bray. 1964. A convenient method for generating normal variables. *SIAM Rev.* 6: 260 - 264.

Mathews, J. H. 1987. *Numerical methods for Computer Science, Engineering and Mathematics.* Prentice-Hall, Inc. Englewood Cliffs, New Jersey, 507 pp.

Molinari, R. and A. D. Kirwan, Jr. 1975. Calculation of differential kinematic properties of the Yucatan Current from Lagrangian observations. *J. Phys. Oceanogr.* 5: 361 - 368.

Morgan, Byron J. T. 1984. *Elements of simulation.* Chapman and Hall, New York, 351 pp.

Neelamkavil, Francis. 1987. *Computer simulation and modelling.* John Wiley & Sons, New York, 307 pp.

Neumann, G. and W. J. Pierson. 1966. *Principles of Physical Oceanography.* Prentice-Hall, New Jersey, 545 pp.

Okubo, A. 1970. Horizontal dispersion of floatable particles in the vicinity of velocity singularities such as convergences. *Deep-Sea Res.*, 17: 445 - 454.

Okubo, A. 1978. Advection - Diffusion in the presence of surface convergence. In: *Oceanic Fronts in Coastal Processes.* Edited by M. J. Bowman and W. E. Esaias. Springer Verlag, Berlin, 23 - 28.

Okubo, A. and C. C. Ebbesmeyer. 1976. Determination of vorticity, divergence and deformation rates from analysis of drogue observations. *Deep-Sea Res.* 23: 349 - 352.

Okubo, A.; C. C. Ebbesmeyer and B. G. Sanderson. 1983. Lagrangian diffusion equation and its application to oceanic diffusion. *J. Oceanogr. Soc. Japan*, 39: 259 - 266.

Okubo, A.; C. C. Ebbesmeyer and J. M. Helseth. 1976. Determination of Lagrangian deformation from analysis of current followers.*J. Phys. Oceanogr.*: 6: 524 - 527.

Oswatitsch, K. 1958. In: *Die Ablongsungbedingung von Grenzschihten. Grenzschiht Forschung.* Edited by H. Goertler. Springer-Verlag, Berlin. 357-367.

Owen, R. W. Jr. 1966. Small-scale, horizontal vortices in the surface layer of the Sea. *J. Mar. Res.* 24: 56 - 66.

Paduan, J. D. and P. P. Niiler. 1990. A Lagrangian description of motion in Northern California Coastal Transition filaments. *J. Geophys. Res.* 95, C3: 18095 - 18109.

Parker, C. E. 1990. Gulf Stream rings in the Sargasso sea. *Deep-Sea Res.* 18: 981 - 993.

Perry, A. E. and B. D. Fairlie. 1974. Critical points in flow patterns. *Adv. Geophys.*, 18 B, 299 - 315.

Perry, A. E. and M. S. Chong. 1987. A description of eddying motions and flow pattern using critical-point concepts. *Ann. Rev. Fluid Mech.*, 19, 125 - 155.

Poulain, P. and P. P. Niiler. 1989. Statistical analysis of the surface circulation in the California Current system using Satellite-Tracked drifters. *J. Phys. Oceanogr.*, 19: 1589 - 1603.

Petterssen, S. 1935. Contribution to the theory of Frontogenesis. *Geofys. Pub.* 11, 5 - 27.

Press, W. H.; B. P. Flannery; S. A. Teukolsky and W. T. Vetterling. 1986. *Numerical recipes: The Art of Scientific Computing.* Cambridge University Press, Cambridge, 818 pp.

Ralston, A. and P. Rabinowitz. 1978. *A first course in numerical analysis.* McGraw-Hill Book Company, New York, 556 pp.

Reed, R. K. 1971. An observation of divergence in the Alaskan Stream. *J. Phys. Oceanogr.* 1: 282 - 283.

Richardson, P. L.; R. E. Charney and L. V. Worthington. 1978. A census of Gulf Stream Rings, Spring 1975. *J. Geophys. Res.* 83, 6136 - 6144.

Rott, N. 1958. On the viscous core of a line vortex. *ZAMP,* 96, 534-553.

Rott, N. 1959. On the viscous core of a line vortex. II. *ZAMP,* 10, 73-81.

Sanderson, B. G. 1984. Two-dimensional dispersion of Plankton. *Oceanologica Acta,* 7: 323 - 328.

Sanderson, B. G. 1987. Statistical properties of iceberg motion at the western entrance of Lancaster Sound. *Oceans 1987 Proceedings, IEEE,* 17 - 23.

Sanderson, B. G.; B.K. Pal and A. Goulding. 1988. Calculations of unbiased estimates of the magnitude of residual velocities from a small number of drogue trajectories. *J. Geophys. Res.* 93, C7: 8161 - 8162.

Saucier, W. J. 1953. Horizontal deformation in atmospheric motion. *Trans. American Geophys. Union,* 34, 5: 709 - 719.

Saucier, W. J. 1955. *Principles of meteorological analysis*, The University of Chicago Press, Chicago, 438 pp.

Schertzer, D. and S. Lovejoy. 1989. Generalised Scale Invariance and Multiplicative Processes in the Atmosphere. *PAGEOPH*, 130, 1: 57 - 81.

Stewart, G. W. 1973. *Introduction to matrix computations*. Academic Press, Inc., New York, 441 pp.

Taussky, O. 1950. Note on the condition of matrices. *MTAC*, 4: 111 - 112.

von Neumann, J. and H. H. Goldstein. 1947. Numerical inverting of matrices of high order. *Bull. Amer. Math. Soc.* 53: 1021 - 1099.

Westlake, J. R. 1968. *A handbook of numerical matrix inversion and solution of linear equations*. John Wiley and Sons, Inc., New York, 171 pp.

Wilkinson, J. H. 1963. *Rounding errors in algebraic processes*. Prentice-Hall, Inc. New Jersey, 161 pp.

APPENDIX A

The following programs denoted by 'ok1' and 'ok2' are to be used on obtaining a, b, c of the OK method when $a^2 + b^2 - c^2 \neq 0$ (see equations (2.48), (2.49), (2.50)). The programs are written in MACSYMA.

```
-*- ok1 -*-

dskgc:true;

x:((d*d-2*m2)*u1-u3)/m2*m2;

y:((d*d-2*m2)*v1-v3)/m2*m2;

l:2*d*d-4*m2;

j:4*u1-x*l;

k:4*v1-y*l;

p:2*d*x;

q:2*d*y;

jp:j*q+k*p;

pm:p*p-q*q;

pp:p*p+q*q;

b:(jp-pm*ro)/pp;

a:(j-q*b+q*ro)/p;

ro*ro-a*a-b*b+d*d-4*m2;
```

```
solve(%,ro);

b0:(jp-pm*ro)/pp;

%,d16;

b1:ratsimp(%);

a0:(j-q*b0+q*ro)/p;

%,d16;

a1:ratsimp(%);

r1:ro;

%,d16;

ro1:ratsimp(%);

x*(Γ+2*a1*d)+2*y*d*(b1-ro1)-4*u1;

ratsimp(%);

2*x*d*(b1+ro1)+y*(Γ-2*a1*d)-4*v1;

ratsimp(%);

x*(2*d*d*(a1-d)+Γ*(3*d+a1))+y*(b1-ro1)*(2*d*d+Γ)-8*u2;

e1:ratsimp(%);

x*(b1+ro1)*(2*d*d+Γ)+y*(-2*d*d*(d+a1)+Γ*(3*d-a1))-8*v2;

e2:ratsimp(%);
```

x*(Γ*Γ+4*d*d*(Γ-d*d)+4*a1*d*Γ)+4*y*d*(b1-ro1)* Γ-16*u3;

ratsimp(%);

4*x*d*Γ*(b1+ro1)+y*(Γ*Γ+4*d*d*(Γ-d*d)-4*a1*d *Γ)-16*v3;

ratsimp(%);

store([nilai,mac,DSK,directory],a1,b1,ro1,e1,e2,y,x);

-*- ok2 -*-

dskgc:true$

loadfile(nilai,mac,DSK,directory);

d0:(u1*v3-v1*u3)/(u1*v2-v1*u2);

m20:(u2*v3-u3*v2)/(u1*v2-u2*v1);

e1;

e2;

a1;

b1;

ro1;

x;

y;

ev(d45,d=d0,m2=m20);

```
ratsimp(%);

ev(d46,d=d0,m2=m20);

ratsimp(%);

ev(d47,d=d0,m2=m20);

ak:ratsimp(%);

ev(d48,d=d0,m2=m20);

bk:ratsimp(%);

ev(d49,d=d0,m2=m20);

ck:ratsimp(%);

quit();

-*- executing ok1 and ok2 programs in a batch mode -*-

batch"ok1";

batch"ok2";

exit;
```

APPENDIX B

Using the Eulerian point of view, both the pure stretching and shearing without translating motion can be described in terms of their streamlines patterns.

For pure stretching, the flow field can be written

$$u = \frac{a}{2}x, \; v = -\frac{a}{2}y, \tag{6.1}$$

and, for pure shearing

$$u = \frac{b}{2}x, \; v = \frac{b}{2}y. \tag{6.2}$$

The equation for stt. amlines is

$$\frac{dx}{u} = \frac{dy}{v}. \tag{6.3}$$

Substituting the above flow fields from each case into the equation for streamlines and integrating to give

$$xy = k_1, \quad x^2 - y^2 = k_2 \tag{6.4}$$

for pure stretching and shearing, respectively. The sketch resulting from these equations can be drawn as shown in the following figure. These sketches are in agreement with figure 3.1 and figure 3.6 of sections 3.1 and 3.2 mentioned earlier.

Figure 6.1: The streamlines from pure stretching case (upper) and those from pure shearing (lower).

APPENDIX C

The following program written in MATLAB uses the OK method to obtain the kinematic parameters from a single drifter trajectory.

```
% ok.m - program for calculating the parameters

load dr_6.dat

t=(:,1); x=[dr6(:,2) dr6(:,3)];

xf=ftt(x); xx=xf(:,1); yy=xf(:,2);

dx=df(xf,101,1); dxf=ftt(dx);=dxf(:,1); v=dxf(:,2);

d2x=df(dxf,101,1); d2xf=ftt(d2x); u1=d2xf(:,1); v1=d2xf(:,2);

d3x=df(d2xf,101,1); d3xf=ftt(d3x); u2=d3xf(:,1); v2=d3xf(:,2);

d4x=df(d3xf,101,1); d4xf=ftt(d4x); u3=d4xf(:,1); v3=d4xf(:,2);


t0=u1.*v2-u2.*v1;

a=-(u1.*v3-2*u2.*v2+u3.*v1)./t0;        % stretching deform. rate

b=-(v1.*v3-v2.*v2-u1.*u3+u2.*u2)./t0;% shearing deform. rate

c=-(v1.*v3-v2.*v2+u1.*u3-u2.*u2)./t0; % vorticity

d=(u1.*v3-u3.*v1)./t0;                  % divergence

m2=(u2.*v3-u3.*v2)./t0;

xp=(u1.*(d.*d-2*m2)-u3)./(m2.*m2);
```

```
yp=((d.*d-2*m2).*v1-v3)./(m2.*m2);
us=(.5*(a+d).*xp)+(.5*(b-c).*yp);      % swirl velocity
vs=(.5*(b+c).*xp)+(.5*(d-a).*yp);      % swirl velocity
ut=u-us; vt=v-vs;                      % translation velocity
xs=xx-xp; ys=yy-yp                     % singularity's position

%plotting
xl=['time (hours)'];yld=[' × 10^-4/s'];ylv=['m/s'];
xlp=['position eastward direction (m)'];
ylp=['position northward direction (m)'];
axd=[0, 95, -5, 5];axv=[0, 95, -0.6, 0.6];
axp=[-25000, -8000, -5000, 30000];

clc
clg
axis(axd);
plot(t,a,'-',t,b,'-.',t,c,t,d,':')
gtext('- - - - - a')
```

```
gtext('-.-.- b')

gtext('-- c')

gtext('..... d')

xlabel(xl)

ylabel(yld)

pause

print


clc

clg

axis(axv);

plot(t,ut,t,vt,'- -')

gtext('-- UT")

gtext('- - - - - VT")

xlabel(xl)

ylabel(ylv)

pause

print
```

```
clc
clg
axis(axv);
plot(t,us,t,vs,'- -')
gtext('— us')
gtext('- - - - - - vs')
xlabel(xl)
ylabel(ylv)
pause
print

clc
clg
axis(axp);
axis('square');
plot(xx,yy,xs,ys,'*')
xlabel(xlp)
```

```
ylabel(ylp)

gtext('--- dr.6')

gtext('**** ctr')

axis('normal');

axis;

pause

print

clc

clg

end;


%ft.m - program for low-pass filtering the data

function [f]=ft(x);

xx=x(:,1); yy=x(:,2); .[b,a]=butter(10,0.1);

xf=filtfilt(b,a,xx); yf=filtfilt(b,a,yy);

f=[xf yf];


%df.m - program for time-differentiating the data
```

```
function [d]=df(x,nlines,dt)
 for j=1:2;
  for i=1:3;
   d(i,j)=(-3*x(i,j)+4*x(i+1,j)-x(i+2,j))/(2*dt);
  end;
 end;
 for j=1:2;
  for i=4:nlines-4;
   d(i,j)=(-x(i+2,j)+8*x(i+1,j)-8*x(i-1,j)+x(i-2,j))/(12*dt);
  end;
 end;
 for j=1:2;
  for i=nlines-3:nlines;
   d(i,j)=(3*x(i,j)-4*x(i-1,j)+x(i-2,j))/(2*dt);
  end;
 end;
```

APPENDIX D

The following MATLAB program is used for the HS method on obtaining the kinematic properties from a cluster of 3 drifters.

```
load dr_1.dat

load dr_2.dat

load dr_6.dat

format long;

t1=y1(:,1)-24.25;n=size(t1);n1=n(1,1);s=n1-47;

alpha=zeros(1,s);beta=zeros(1,s);ki=zeros(1,s);pi=zeros(1,s);

as=zeros(1,s);bs=zeros(1,s);cs=zeros(1,s);ds=zeros(1,s);

ut=zeros(1,s);vt=zeros(1,s);xt=zeros(1,s);yt=zeros(1,s);

us=zeros(1,s);vs=zeros(1,s);t0=zeros(1,s);

st=zeros(1,s);sh=zeros(1,s);vor=zeros(1,s);div=zeros(1,s);

sumx=zeros(1,s); sumy=zeros(1,s); sumu=zeros(1,s); sumv=zeros(1,s);

dt=900.;%15minute-time-interval

t=t1(1:1:s,1);

p1=[dr_1(1:1:s,2)*1000. dr_1(1:1:s,3)*1000.];%km-to-meter conversion

p2=[dr_2(1:1:s,2)*1000. dr_2(1:1:s,3)*1000.];

p3=[dr_6(1:1:s,2)*1000. dr_6(1:1:s,3)*1000.];
```

```
x1=ft(p1);x2=ft(p2);x3=ft(p3);%filtering

dx1=df(x1,s,dt);dx2=df(x2,s,dt);dx3=df(x3,s,dt);

u1=ft(dx1);u2=ft(dx2);u3=ft(dx3);

d2x1=df(u1,s,dt);d2x2=df(u2,s,dt);d2x3=df(u3,s,dt);

up1=ft(d2x1);up2=ft(d2x2);up3=ft(d2x3);

pos=[x1(:,1) x1(:,2) x2(:,1) x2(:,2) x3(:,1) x3(:,2)];

vel=[u1(:,1) u1(:,2) u2(:,1) u2(:,2) u3(:,1) u3(:,2)];

acc=[up1(:,1) up1(:,2) up2(:,1) up2(:,2) up3(:,1) up3(:,2)];


for  i=1:s

        mu=vel(i,:);ma=acc(i,:);mx=pos(i,:);

        sumx(i)=mx(1,1)+mx(1,3)+mx(1,5);sumy(i)=mx(1,2)+mx(1,4)+mx(1,6);

        sumu(i)=mu(:,1)+mu(:,3)+mu(:,5);sumv(i)=mu(:,2)+mu(:,4)+mu(:,6);

        um=[ones(1:3)' reshape(mu,2,3)'];am=[reshape(ma,2,3)'];

        g1=um'*um;g2=inv(g1);g3=g2*um';g4=g3*am;g5=um*g4;res=am-g5;

        alpha(i)=g4(1,1);beta(i)=g4(1,2);

        as(i)=g4(2,1);cs(i)=g4(2,2);bs(i)=g4(3,1);ds(i)=g4(3,2);

        ki(i)=(sumu(i)-as(i)*sumx(i)-bs(i)*sumy(i))/3.;%3-drifters
```

```
        pi(i)=(sumv(i)-cs(i)*sumx(i)-ds(i)*sumy(i))/3.;
        t0(i)=bs(i)*cs(i)-as(i)*ds(i);
        ut(i)=(ds(i)*alpha(i)-bs(i)*beta(i))/t0(i);
        vt(i)=(as(i)*beta(i)-cs(i)*alpha(i))/t0(i);
        xt(i)=((vt(i)-pi(i))*bs(i)-(ut(i)-ki(i))*ds(i))/t0(i);
        yt(i)=((ut(i)-ki(i))*cs(i)-(vt(i)-pi(i))*as(i))/t0(i);
        us(i)=as(i)*(mx(1,3)-xt(i))+bs(i)*(mx(1,4)-yt(i));
        vs(i)=cs(i)*(mx(1,3)-xt(i))+ds(i)*(mx(1,4)-yt(i));
        st(i)=10000*(as(i)-ds(i));sh(i)=10000*(cs(i)+bs(i));
        vor(i)=10000*(cs(i)-bs(i));div(i)=10000*(as(i)+ds(i));
end
%plotting
ttl=['dr_1, dr_2, dr_6 - butter(10,1/10)'];
xl=['time (hours)'];yld=['DKP x 10(-4)/s'];ylv=['m/s'];
xlp=['pos. eastward dir. m'];ylp=['pos. northward dir. m'];
axd=[0, 95, -10, 10];axv=[0, 95, -0.6, 0.6];
axp=[-25000, -8000, -5000, 30000];
```

```
clc
clg
axis(axd);
plot(t,st,'-',t,sh,'-.')
title(ttl)
xlabel(xl)
ylabel(yld)
gtext(- - - - a')
gtext(_____ b')
print

clc
clg
axis(axd);
plot(t,vor,':',t,div,'-')
title(ttl)
xlabel(xl)
ylabel(yld)
```

```
gtext('..... c')
gtext('____ d')
print

clc
clg
axis(axv);
plot(t,ut,t,vt,' ')
title(ttl)
xlabel(xl)
ylabel(ylv)
gtext('____ UT')
gtext('- - - - VT')
print

clc
clg
axis(axv);
```

```
plot(t,us,t,vs,' ')
title(ttl)
xlabel(xl)
ylabel(ylv)
gtext('____ us')
gtext('- - - - vs')
print

clc
clg
axis(axp)
plot(x1(:,1),x1(:,2),'-')
hold on
plot(x2(:,1),x2(:,2),' ')
hold on
plot(x3(:,1),x3(:,2),'-',xt,yt,'*')
title(ttl)
xlabel(xlp)
```

```
ylabel(ylp)

gtext('(1)')

gtext('(2)')

gtext('(6)')

gtext('start')

axis

print

hold off

end
```